



**Politecnico
di Torino**



Mittuniversitetet
MID SWEDEN UNIVERSITY

Politecnico di Torino, Italy

Dipartimento di Scienza e Tecnologia Applicata (DISAT)

Mid Sweden University, Sweden

Sports Tech Research Centre, Department of Quality Technology and
Management, Mechanical Engineering and Mathematics

Master of Science in Materials Engineering
Academic Year 2022/2023

3D-Printed Foot Manikin

For Determining Thermal Insulation Of Footwear

Supervisors:

Prof. Ada Ferri (PoliTo)

Prof. Andrey Koptuyug (MiUn)

Prof. Mikael Bäckström (MiUn)

Student:

Simone Demichelis

S297971

Acknowledgments

I would like to express my deepest gratitude to Professor Andrey Koptug, who welcomed me on the day I arrived in Sweden and accompanied me throughout my work, guiding me every step of the way, fulfilling and going far beyond the duties of a supervisor. His practical help and the discussions we had together were instrumental in steering the project in the right direction and achieving satisfactory results within the given time frame. Special thanks to Professor Mikael Bäckström for supervising the entire work and making sure that the other thesis students and I were always at ease in the department.

I am also thankful to Professor Ada Ferri for giving me the opportunity to do this thesis abroad in such an inspiring research environment and to get to know a fascinating culture, as well as wonderful people. Without her support, even from a distance, this project could never have started, nor developed in the best possible way.

I had the pleasure of sharing the office with two companions who quickly became great friends and with whom I engaged in long lunchtime discussions on a wide variety of topics, as well as weekends going out, cooking, and enjoying the scenery offered by Sweden. Thanks to Gianmarco and Giorgia for being an integral part of my experience abroad, and I hope not only that.

I would like to mention my parents Dhebora and Mariano, who together with my sister Alessia were willing to visit me in a place so far from home and have always been by my side since I can remember, and my girlfriend Martina, a constant presence even through the difficulties of a long-distance relationship, to whom I owe much of my personal successes and more.

Thanks to Felicia, Francesca, Leonardo, Marco, Omar, and all my colleagues at PoliTo for helping to brighten every day of class each in their own way. One last thought goes to Luca, Evrim, Yannick, Emely, Frida, Fabienne, Daniel, Johan, Emelie, and all the other people I met during my experience in Sweden and who made even a moment of any day better with a word or a smile. I will carry them with me forever.

Abstract

A thermal foot manikin was developed, 3D printed, and sensorized with the aim of determining the thermal insulation provided by footwear. Compared with existing thermal foot models, the manikin of the present work is cheaper, easier to set up, and simpler in its structure and components. It consists of a selective laser sintered (SLS) polyamide shell equipped with 16 digital temperature sensors and filled with water from the leg opening. The shell was designed in Rhino 3D using a Creative Commons licensed STL file selected from "thingiverse.com" website as the starting model, then printed at AIM Sweden AB. The sensors face the inner wall of the shell, thus in direct contact with the water inside. Data acquisition and processing are handled by a National Instruments interface device on the hardware side and a LabVIEW program on the software side. Instead of being actively heated and kept at a constant temperature during testing through power control (as most existing thermal foot models do), our manikin was initially filled with room temperature water, then exposed to cold while monitoring the cooling of the foot shell at 16 points of interest. The system was tested inside a freezer at $(-40 \pm 1) \text{ }^\circ\text{C}$ in four configurations: (a) bare foot, (b) wearing a liner (a thin sock), (c) wool sock over a liner, and (d) liner and slipper. Configurations (a), (b), and (c) were tested both with the manikin standing on the freezer floor and with the use of wooden spacers that avoided direct contact of the foot sole with the cold surface. The cooling curves of each sensor were plotted on a temperature-time chart for all tests performed. A qualitative interpretation of the general trends was provided, along with an objective analysis of the time it took each sensor to detect a temperature below $15 \text{ }^\circ\text{C}$ (pain threshold) and $7 \text{ }^\circ\text{C}$ (numbness threshold). Insulation values for each part of the foot were formulated using the original approach of relating the time it takes for a sensor to detect a temperature drop of $10 \text{ }^\circ\text{C}$ to the time that must elapse, according to EN ISO 20344 (for the test to be successful), before the insole temperature sensor detects a temperature change of $10 \text{ }^\circ\text{C}$, or 1800 seconds. The results correlate well with the respective "steady-state cooling rates", or the slope of the cooling curves in their linear segment. Further studies are needed to refine the method, redesign the manikin shell to fit shoes and boots, and compare the results with those obtained from tests on human subjects.

Contents

Aims and Objectives	6
1. Introduction.....	8
1.1 Human thermoregulation and thermal comfort	8
1.2 Cold environments	12
1.2.1 Effects of cold on feet	12
1.2.2 Cold-related injuries	14
1.2.3 Protective footwear.....	15
2. Method – General discussion.....	17
2.1 Test methods for determining thermal insulation of footwear.....	17
2.1.1 Tests on human subjects.....	18
2.1.2 Standard test method for footwear (EN ISO 20344)	18
2.1.3 Thermal foot manikins.....	20
2.2 The manikin of the present work	25
2.2.1 3D-printed body part surrogates.....	28
3. Measurement setup	29
3.1 General layout.....	29
3.2 Foot manikin shell.....	29
3.2.1 Design and modeling.....	30
3.2.2 Materials and 3D-printing.....	34
3.3 Electronics.....	37
3.3.1 Sensors placement.....	38
3.3.2 Electronic components.....	42
3.3.2.1 Sensors (Sensirion STS40).....	48
3.3.2.2 Switches (Onsemi NLHV4051)	49
3.3.2.3 Interface device (NI USB-8452)	50
3.3.3 LabVIEW project.....	51

3.3.3.1 Main VI.....	54
3.3.3.2 Comment SubVI.....	57
3.3.3.3 Testing SubVI.....	57
3.3.3.4 Measuring SubVI.....	58
3.3.3.5 Reading SubVI.....	59
3.3.3.6 Comment&Filename SubVI.....	60
3.3.4 Procedures and tests.....	61
3.3.4.1 Heat loss measurements in freezer.....	63
3.3.4.2 Comparison with real foot heat loss.....	65
3.3.4.3 Footwear thermal insulation tests.....	65

4. Results and discussion..... 67

4.1 Cooling rates at different points of the foot manikin.....	67
4.2 Thermal insulation values.....	73
4.3 Time-to-pain, Time-to-numbness and Steady-state cooling speed.....	76
4.4 Personal experience and Future developments.....	80
4.4.1 Tests for manikin-foot comparison.....	82
4.4.2 Water recirculation and Active heaters.....	83

Conclusions..... 85

References..... 86

Aims and Objectives

The ultimate goal of the present work was to construct a 3D printed foot surrogate system that could be used to determine the thermal insulation provided by footwear to different areas of the foot.

To achieve this goal, a number of challenges had to be overcome. The author's prior knowledge of materials science proved extremely useful in defining the preferred properties of the manikin, its desired thermal behavior, and how heat transfer could be monitored during measurements. However, many of the aspects related to the development and construction of a thermal model were initially unknown to the author, including:

- how to properly design a 3D CAD model of the foot manikin;
- how to choose the most suitable additive manufacturing technique and materials for the present project from all available possibilities;
- how to use an FDM (Fused Deposition Modeling) 3D printer to make simple prototypes;
- how to develop and build a measurement system that can acquire data through sensors and manage them in a software environment;
- how to properly perform laboratory tests with the foot manikin system and extract meaningful data from them.

To overcome these obstacles, numerous things were learned along the way. The following pages will describe in detail all the steps of the process and the choices that lead to the construction and testing of the foot surrogate. Most of these steps were handled by the author independently, such as:

- reviewing the literature on thermal comfort, standard test methods for footwear and thermal foot manikins, evaluating the state-of-the-art and its limitations;
- learning how to use Rhino 3D modeling software to design the manikin shell;
- learning how to use LabVIEW graphical software to develop a program that can handle hardware peripherals, acquire signals from sensors and process data;
- learning how to interact with FDM 3D printers to make prototypes of the foot manikin and other various objects;

- setting up and performing laboratory tests with the manikin system, analyzing results, and making critical observations.

Some aspects of the project had to be delegated to improve time efficiency or quality of results, or because of unrealistic skill requirements, which are:

- 3D printing of the final manikin prototype with SLS technology, done by the company "AIM Sweden AB";
- drilling of the manikin shell to accommodate 16 temperature sensors, done by Professor Andrey Koptug at the SportsTech Research Centre;
- wiring, soldering and testing of electronic system for data acquisition and processing, done by Professor Koptug as well.

Lastly, the following goals were initially set but not achieved in this work due to lack of time and resources, or due to unforeseen events that occurred along the way. However, they remain part of potential developments for further studies:

- comparing the results of manikin tests with those from studies conducted on human subjects;
- testing and comparing different shoes and boots in terms of the thermal insulation provided at different areas of the foot;
- integrating self-heating elements into the manikin to make it an actively controlled system.

1. Introduction

1.1 Human thermoregulation and thermal comfort

In a state of thermal equilibrium, the human body is capable of regulating its own temperature around 37°C. This value is not a fixed temperature for all individuals, neither is constant during the day or across multiple days. Upon measuring the body temperature in the morning after a period of rest, the average will typically be around 36.7°C, with a standard deviation of 0.35°C¹. During the day, this value will generally rise (usually by about 0.8°C), reach its peak in the late evening, and decrease again until early morning as a result of the circadian rhythm. Physical exercise also leads to a rise in body temperature, with moderate exercise resulting in body temperatures of around 38°C, and values exceeding 39°C (and occasionally exceeding 40°C, e.g. during a marathon) for heavy exercise¹.

It is important to note that a temporary rise in temperature to 39°C is usually not problematic for the body and should be considered a normal process of thermoregulation. Fever, however, is also associated with an increase in body temperature, but this increase is different from that observed during exercise. While the fever-induced rise is regulated by the body, the exercise-induced rise is not. Therefore, in the presence of a fever of 38.5°C, cooling the body will cause the activation of heat storage mechanisms, such as chills and vasoconstriction, which work to maintain the temperature at that level. During exercise, on the other hand, the body will continue to sweat until the body temperature returns to its neutral level.

Figure 1.1 shows a model of the body's temperature regulation¹, with the body represented by its core and skin temperatures. Afferent signals conveying these temperatures are transmitted to the control centers in the brain, where they are compared to a reference signal, which can be viewed as a single thermostat setpoint or as multiple thresholds that trigger effector responses. Based on the difference between the actual temperature and the reference value (the error signal), different responses can be activated. The primary ones are sweating and vasodilation of skin vessels (if the body temperature is higher than the reference value, i.e., a "positive error") and shivering and vasoconstriction ("negative error"). Sweat evaporation cools the skin, shivering increases heat production and warms the core, while vasodilation and constriction regulate heat transfer between the core and skin. Of course, this is a simplified model, since many different regions of the body are thermosensitive, and a wide range of complex models is possible.

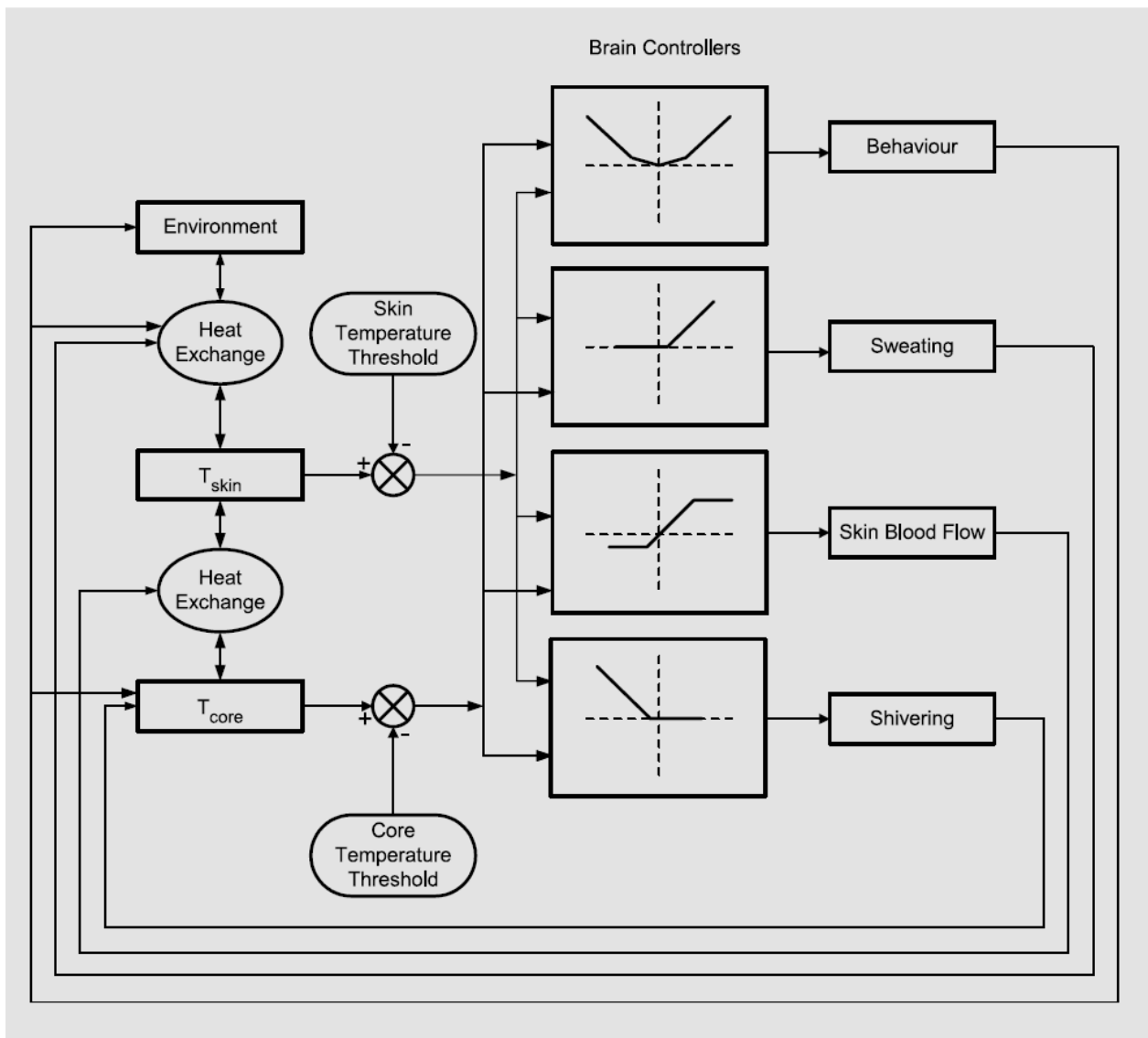


Figure 1.1 Schematic representation of the thermoregulatory control system¹.
 T_{core} = Body core temperature; T_{skin} = mean skin temperature; brain controller graphs show reaction of effector (y-axes) to error signal (x-axes).

Regarding clothing, it can be viewed as an additional, behavioral effector response. We adjust our clothing based on the climate we are in, providing sufficient insulation to enable the other effector responses to function within their optimal range. The primary effect of clothing is its impact on the heat exchange between the skin and the environment. To better understand the phenomena related to human thermoregulation, it is necessary to analyze the heat flows that exist between the body and its environment.

The body maintains a stable temperature when it is not under heat stress, balancing the amounts of heat produced and lost. The rate of heat storage in these cases is close to zero, since the amount of heat produced by metabolic

activity corresponds to the amount of heat lost. During rest, the body's metabolic activity is limited to providing its basic functions, such as respiration and all other organs' function, with oxygen and nutrients for distribution to the body's cells. When the body engages in physical activity, the need for oxygen and nutrients increases, leading to an increase in metabolic activity. When muscles burn nutrients for mechanical activity, some of the energy is released outside the body as external work, but most is released into the muscles as heat. The efficiency with which the body performs work can be defined as the ratio of external work to energy consumed.

For most activities, such as walking on a flat surface, the efficiency is close to zero. Heat released by shoe friction and other external factors is released outside the body, but all other energy used by the muscles ends up as heat inside the body. At lower temperatures, shivering occurs, which produces additional heat, but with zero efficiency. This can increase basal metabolic rate and heat production up to four times and save the body from hypothermia. To lose heat from the body, several routes are available, such as conduction, convection, electromagnetic radiation, and evaporation. The amount of heat transferred by each pathway depends on the driving force, body surface area, and resistance to heat flow.

Conduction plays a minor role, and conductivity becomes a relevant factor only for people working in water or handling cold surfaces, among other special circumstances. Convection is more important for heat loss in situations where cooler air flows along the skin and absorbs its heat, which is then transferred to the environment. Electromagnetic radiation also strongly influences heat transfer: heat is exchanged through radiation when there is a difference between the surface temperature of the body and the surface temperature of the environment. Finally, the body loses heat by evaporation through sweating, where skin moisture evaporates, releasing a considerable amount of heat from the body.

In addition to convective and evaporative heat loss from the skin, the body also loses heat through respiration from the lungs. By heating and moisturizing inhaled air, the body loses heat to exhaled air, which can account for up to 10 percent of total heat production. To maintain a stable body temperature, heat losses must balance heat production (Eq. 1), as any imbalance will cause a change in the body's heat content, resulting in a rise or fall in temperature.

$$S = M - W + E + Ra + C + K + Re \quad (1)$$

S = stored energy

M = metabolic rate

- W = external work
- E = evaporative heat loss
- Ra = radiation heat loss
- C = convection heat loss
- K = conduction heat loss
- Re = respiratory heat loss

It is important to note that heat loss components are negative when heat is transferred from the body to the surrounding environment and positive when heat is gained from the environment. For instance, if surfaces to which the body is exposed are radiating more energy than the body itself, "Ra" will be a positive term.

Continuing to follow this model of human thermoregulation, clothing can be seen as a barrier to heat and moisture transfer between the skin and the environment². It can protect the body from extreme heat and cold, but it can also impede the loss of excess heat during physical activity. Adjusting clothing and activity levels, humans can maintain skin temperature and skin wetness in the proper range. If the environment gets colder, the skin will cool down to uncomfortable (and then painful) levels. An increased metabolic activity might compensate, but if heavy clothing is worn, sweat will start to accumulate between clothes and the skin and the person will begin to feel discomfort.

Skin temperature and skin wetness are two of the most fundamental physiological factors related to comfort. Figure 1.2 lists mean skin temperature values associated with thermal comfort and provides information about skin wetness and skin temperatures related to extreme discomfort.

Body core temperature (°C)	Condition	Mean skin temperature (°C)	Comfort sensation	Skin Wetness (%)	Local Skin temperature (°C)	Condition
44	heat stroke, brain damage		Very Uncomfortable	60	>45	Skinburns, time dependent
41	Fever therapy	36		40	45	Pain
	very heavy exercise	35	Slightly uncomfortable	20		
38	Exercise	34		6	25	Cool
37	Normal resting condition	33	Comfortable		20	Reduced dexterity
36		32	Slightly uncomfortable		15	Pain
35	Shivering	31			7	Numbness
33	Reduced consciousness	30	uncomfortable		-0.5	Frostbite
31	Ventricle fibrillation 'death'					
14	Lowest measured temperature with full recovery					

Figure 1.2 Body temperatures and skin wetness related to comfort and

discomfort¹.

1.2 Cold environments

The area of the body in charge of thermoregulation is the hypothalamus³. The thermoregulatory system works to maintain thermal balance in cold environments. A decrease in blood flow to the surface and a countercurrent heat exchange between arterial and venous blood are used to accomplish this through heat conservation.

When cold receptors are stimulated, in order to maintain the thermal homeostasis of the central body, heat loss must be minimized. This is accomplished by increasing metabolic rate and decreasing peripheral circulation⁴. The amount of heat that needs to be produced by metabolic activity is determined by the temperature-sensitive nerve endings that feed information to the hypothalamus. Skin temperature decreases as a result, and shivering may occur. Vasoconstriction cools down the extremities, lowering muscle strength and performance. It also reduces skin blood flow, which decreases skin sensitivity³.

According to experimental data, even slight thermal stress can have a negative effect on a person's performance. Poorer manual performance is linked to lower hand skin temperature⁵. The electrical activity of the muscle fibers closest to the skin can become less active when it is cooled⁶. As a result of a drop in body temperature, blood viscosity can rise, and muscles can stiffen³. Sensitivity, strength, simple and complex movements, biomechanical processes at the nerve or receptor level, mechanical properties of the skin, and synovial fluid viscosity in the joints can all be negatively impacted by cold. Additionally, discomfort and shivering can cause people to become distracted and change their behavior, which increases the risk of accidents and injuries when using sharp tools or working quickly under pressure⁷.

The risk of both freezing and non-freezing injuries increases as the temperature drops. Pinching pain is the initial sign of freezing injuries, but it goes away before the tissue actually starts freezing because nerve conductivity is lost below +7 °C in the tissue. Later, sensation completely fails. For non-freezing injuries, numbness, paraesthesia, and sleep-disturbing pain may be the first symptoms. The victim of hypothermia might experience apathy, weakness, and a lack of ability to start up their muscles.

1.2.1 Effects of cold on feet

When compared to other sections of the body, the extremities are more affected by exposure to cold. Since the skin temperature in the feet and hands is typically the lowest due to vasoconstriction, if a person feels overall cool, he or she will frequently notice it in those places. Cold feet were found to be a common cause of discomfort in a study on the impact of additional clothing on warmth and comfort in cool settings⁸.

Because hands and feet frequently come into touch with cold surfaces, they are the first body parts to become chilled and are also the areas where the effects are most noticeable⁹. The extremities usually lose heat at fast rates due to their significantly high surface-to-volume ratio¹⁰. Due to their small muscle mass, they generate minimal local metabolic heat, which further decreases as tissue temperature falls. Each foot, for instance, may produce up to 2 W of heat, but at tissue temperatures below 10 °C, heat production can be as low as 0.2 W¹¹.

Warm blood from the body's core provides a significant amount of the heat balance in the extremities. When heat production is moderate or low in the cold, extremity blood flow, which is controlled by thermoregulation, is frequently decreased. In warm weather or during exercise, the blood flow to the foot can generate over 30 W of heat, but in the cold, this number can drop as low as 3 W¹¹. Sweating helps the body cool down more quickly when physical activity is low. Evaporation is a significant element affecting the feet skin temperature, accounting for 27% of the heat lost from the feet in cold environments¹². Toes skin temperature drops quickly when feet are confined inside protective footwear (such as military boots), especially if the wearer is inactive in the cold¹¹. This phenomenon is much intensified if sweating has made the footwear wet. The toes might warm up again if physical exercise is performed, but will quickly cool down again when the movement ceases.

High levels of clothing and boot insulation are required for work that involves prolonged standing in the cold. The balance between heat input from circulatory blood and heat loss is what keeps the feet warm in the cold. Thus, physiological factors as well as the levels of insulation provided by socks and shoes become important. Walking causes the body to produce more heat and improves blood flow to the feet, but sweating and external moisture must be removed since they decrease the insulation of shoes. According to studies¹³, footwear insulation can be reduced by up to 35% after a protracted soak.

With regard to the thermal comfort ranges of feet, they are typically comfortable when relative humidity near the skin is ~ 60% and skin temperature is ~ 33 °C¹¹. Feet begin to feel cold at toe temperatures around 25 °C, while cold discomfort is noted at 20–21 °C¹⁴. Strong cold perception is linked to foot temperatures below 20 °C¹⁵. The sensation of cold or pain is often related to a particular part of the

foot: the toes or sometimes the heel. Since thermal sensation depends mainly on the temperature of the coldest part of the leg, cold protection of the toes is essential for comfort¹⁶.

1.2.2 Cold-related injuries

A person will still feel uncomfortable and could sustain a cold injury if his feet are wet and cold, regardless of how warm the rest of his body is. But even if dangerous levels are not reached, workers' efficiency still remains strongly influenced by their thermal condition. Personal mobility is crucial for many occupations, including those of farmers, loggers, construction and industrial workers, and military personnel. Personal mobility is related to how well the feet and legs are taken care of, which is largely determined by the type of footwear that is worn (that is tied to the working conditions).

Mobile jobs performed in cold climates cause the feet to perspire intensely while working and quickly cool off when inactive, which causes pain due to the high humidity concentration in footwear. When performing standing activities, such as cutting meat, the feet lose heat by conduction, since contact with the ground is constant and blood supply is low. This is especially true if there is no opportunity for foot movement or exercise to warm the feet up.

Exercise may warm up the extremities or reduce cooling, but for the skin temperature of the toes to be affected, the exercise duration should probably be more than 10 minutes¹⁶. Therefore, as it is difficult to warm up the toes, it is essential to pay special attention to protecting them from the cold and preventing them from cooling in the first place.

Looking at other fields, war emerges as an extremely challenging context for cold protection. Soldiers in battle encounter both moving and stationary circumstances. They frequently don't have the chance to remove their boots, dry them or warm them up, which leaves them vulnerable to problems like poor boot performance and foot conditions, as was seen during the Falkland War¹⁷. Since the 18th century, when the military medical staff began taking care of soldiers, information about frostbite on feet, trench foot, and other foot injuries has been documented.

Frostbite happens when the skin temperature drops below 0.6°C, causing tissue to freeze¹⁶. Gangrene and blistering are two easily observable alterations that appear during the healing process. Trench foot, instead, has been documented in settings with ambient temperatures ranging from well below to well above freezing. It is a condition brought on by elements including cold, moisture,

immobility, tight boots, and other factors that hinder normal blood flow. The lack of sensation in the toes is frequently the first sign of trench foot.

Lastly, cold injuries affect every year thousands of mountaineers. An Iranian study¹⁸ concluded that inadequate clothing, lack of or incorrect use of equipment, and lack of knowledge on how to cope with cold and adverse weather conditions are the main causes of frostbite among mountaineers. 36% of them annually reported experiencing cold-related injuries in some parts of the body.

1.2.3 Protective footwear

In 1993, over 43,000 work-related toe/foot injuries were reported in Sweden. The majority of these injuries are intended to be prevented by adding steel reinforcing elements to footwear. However, safety boots are generally heavy, cumbersome, and perceived as being "cold," which discourages individuals from wearing them for many occupations that need for additional toe or shin protection. Steel toe caps can limit adaptability and fitness.

In a questionnaire survey conducted in 1994¹⁹, thermal discomfort from footwear was the most commonly felt problem (57%). Of these, 43% were related to the alleged cooling effect of the steel toe cap and the discomfort and cold feeling associated with it. The research, however, did not conclusively prove any effect of the steel toe cap on the thermal characteristics of footwear²⁰.

Although cold injuries to the heels and toes are a widespread phenomenon, they are not the most frequent issues associated with unsuitable boots for cold environments. Sliding and falling injuries are significantly more common. Therefore, if one wants to prevent them as well as the negative effects of coming into touch with dangerous surfaces (grease, nails, etc.) the shoe sole must be designed in accordance with the usage for which it is intended.

Moving on to mountaineering boots, a compromise between safety and performance must be made. The designs prioritize factors such as thermal insulation, water resistance, durability, traction, and comfort. To achieve these properties, mountaineering boots are made of distinct components, each crafted from materials that meet the specific requirements.

The upper section of the boot, designed to shield against external elements, often incorporates synthetic materials, leather, or a combination of both, chosen for durability and waterproofness. To ensure thermal insulation in subzero conditions, insulating layers or specialized linings are employed. The midsole, responsible for cushioning and shock absorption, typically utilizes EVA (ethylene-vinyl acetate) foam or polyurethane compounds. The outsole, fundamental for traction on varied terrain, is usually made of rubber compounds engineered for

exceptional grip on snow, ice, and rock surfaces. Integrated crampon compatibility can further enhance grip in icy conditions.

Lastly, military boots are designed to address functional requisites specific to combat environments. They prioritize properties similar to those of mountaineering boots, while adding the requirements of extreme wear resistance and adaptability to varying terrains. Toe caps and ankle support are frequently incorporated, as well as specialized inserts that enhance comfort and mitigate foot-related afflictions.

2. Method – General discussion

2.1 Test methods for determining thermal insulation of footwear

The insulation level of clothing can be assessed using a variety of techniques. One method involves measuring the textiles heat and vapor transfer properties, as specified in EN 31092 standard, and then inferring insulation and evaporative resistance of clothing with mathematical equations. However, the standard applies to 2D materials, which are not a good representation of the final insulating properties of clothing (which also depend on the shape of the garment ensemble).

Another option is to measure the temperature variation inside a product after shifting it from one environmental condition to another, as done in the current standard test method for footwear (EN ISO 20344, 2021) using Ø 5 mm steel balls. A similar approach was followed by a former Soviet footwear testing standard (GOST-12.4.104-81, 1981) which determined shoe insulation by monitoring the temperature change of water-filled rubber balloons that were formed like footwear manufacturing lasts. The footwear insulation value was derived from the time needed to cool the water by 5 °C through the use of empirical formulas. The thermal insulation of individual clothing pieces or garment ensembles can be measured on human subjects, as described in the Russian standard GOST-12.4.185-96 (1996) and in the more recent ISO 9920:2007, in which heat loss and skin temperature are recorded at various points of the body while the person is at thermal comfort. This information is later utilized to determine each garment's insulation value.

Similar measurement techniques are applied to the evaluation of gloves (EN 511, 1993) and clothes (ENV 342, 1997) when testing apparel on thermal models or manikins. According to various mathematical and predictive models (outlined in ISO 11079:2007), the acquired insulation values are compared to the required ones for certain weather conditions and, if they are sufficient, the recommended exposure time in the cold can be derived. For evaluating weather and apparel, a number of whole-body manikins are available²¹, including replicas of certain body parts such the head, hand, and foot. Some thermal manikins are used to assess the effects of air velocity and motion on insulation, and a number of them can simulate sweating. However, there are occasionally differences between the results of experiments conducted on humans and manikins, and it is still unknown why.

2.1.1 Tests on human subjects

Understanding how people construct their sense of comfort is a complex process. Foot pressure and sensibility²², shock absorption, individual foot shape, and internal shoe microclimate are the primary factors that affect comfort when wearing shoes²³.

Assessing the performance and comfort of clothing and footwear becomes a major challenge when carried out with humans. A test protocol can be created, a group of subjects can be chosen, fitted with test garments, and then sent outside to undergo an outdoor test. Then, the subjects respond to individual questionnaires and the results are examined with the goal of deriving generalizations.

In these cases, attempting to isolate a single comfort aspect, like thermal comfort, can be a tricky challenge²⁴. Personal perception can be significantly influenced by additional factors such as the shoe ergonomics²⁵ and the materials used, rather than being limited to thermal parameters alone. Differences in environmental conditions during and between test sessions can hide trends and impact evaluation results. Although the use of climate chambers improves the reproducibility of test conditions, performing tests indoors still retains some subjective elements related to human subjects²⁶. For this reason, human studies typically have significant biases and require a large number of subjects to mitigate the effects of individual variability. This makes both climatic chamber and field tests expensive and time-consuming, not forgetting that each individual must be monitored closely to avert the risk of cold injuries during testing.

However, although preliminary testing with models can greatly improve a particular shoe design, comfort is primarily determined by user evaluation. Therefore, subjective human evaluation is often required, in addition to objective measurements of parameters such as foot skin temperature and moisture retention²⁷ through electronic sensors placed directly on the body. This has a significant impact on the ability to objectively compare the comfort and performance of footwear and clothing, especially those produced by other manufacturers.

2.1.2 Standard test method for footwear (EN ISO 20344)

EN ISO 20344 (2021) describes the current standard test methods for protective shoes, including the one used for assessing insulation of whole footwear against cold. The minimum number of samples to be tested in this specific case is two,

and they must differ in size. All items must be conditioned in a standard environment of $(23 \pm 2) ^\circ\text{C}$ and $(50 \pm 5) \% \text{RH}$ for at least 24 hours prior to testing. The maximum amount of time that may pass between leaving the conditioned environment and the start of testing must not exceed 10 minutes.

Test equipment includes:

- **insulated cold box**, the internal air temperature of which can be regulated to $(-17 \pm 2) ^\circ\text{C}$ (Figure 2.1);
- **thermal transfer medium**, stainless steel balls with $\varnothing 5 \text{ mm}$ and a total mass of $(4 \pm 0,1) \text{ kg}$ that shall conform to ISO 3290-1 (2014) requirements;
- **temperature probe**, with an accuracy of $\pm 0,5 ^\circ\text{C}$, soldered to a copper disc $(2 \pm 0,1) \text{ mm}$ thick and $(15 \pm 1) \text{ mm}$ diameter;
- **temperature measuring device**, with a compensator, suitable for use with the temperature probe.
- **copper plate**, of length $(350 \pm 5) \text{ mm}$, width $(150 \pm 1) \text{ mm}$ and thickness $(5 \pm 0,1) \text{ mm}$, supporting the shoe as illustrated in Figure 2.1.

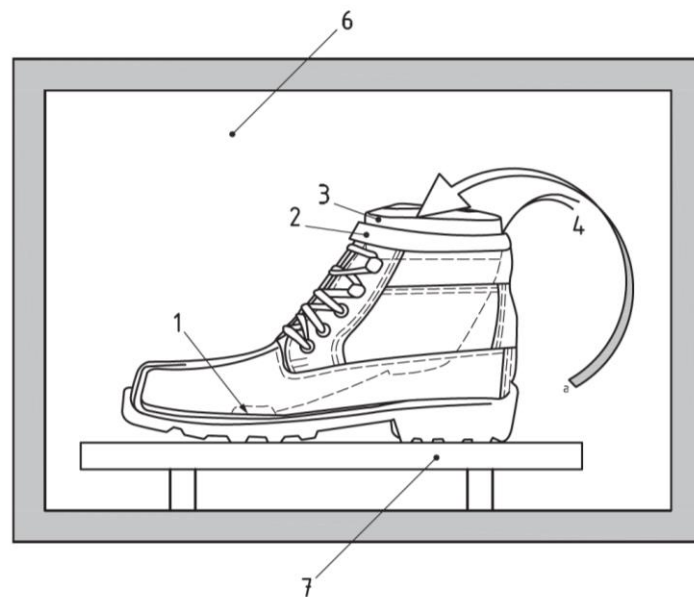


Figure 2.1 Cold insulation test apparatus: 1) point to measure temperature, 2) tape, 3) closing plug, 4) wires to thermocouple, 6) cold box, 7) copper plate, a) steel ball filling, not shown here. From EN ISO 20344.

The procedure mandates the use of the intact footwear item as the designated test specimen. First, the temperature probe must be securely fixed to the insole or insock, if present, in order to measure the temperature in the forepart of the footwear directly above the area where the outsole contacts the support platen. Then, the steel balls can be placed inside the footwear and the upper top opening

be carefully closed with a suitable plug, made up from semi-rigid polymer foam of not less than 25 mm thickness. The plug is fixed to the collar or its prolongation by adhesive tape or other suitable means.

To start the test, the temperature of the cold box is set to (-17 ± 2) °C and maintained constant through the entire duration of the measurements. The test piece is placed on the support platen and the temperature measuring device is connected to the temperature probe to acquire data from the insole/insock right in the beginning and after approximately 30 minutes. The test is considered passed if the detected temperature change within 30 minutes is less than 10 °C. This standard test is quite simple and straightforward, low-cost, easy to perform and highly repeatable. However, it does not provide sufficient feedback on the weak points in the footwear construction to the manufacturers, and the criterion for passing the test happens to be too bland. Even moderately insulated shoes, not intended for technical use in cold climates, can meet the requirements of EN ISO 20344¹⁶, and this makes performing such tests on protective footwear relatively insignificant. Additionally, the recommendations for use in various cold climates should be determined by precise footwear performance, i.e., derived from insulation values. Over the past 30 years, researchers have been trying to find an alternative test method that could provide more detailed and extensive information on the thermal properties of footwear, culminating in the development of thermal foot manikins.

2.1.3 Thermal foot manikins

Compared to human trials, a thermal manikin is considered to be a more quick, reliable, accurate, and reproducible tool to determine clothing properties²⁸. Additionally, these manikin tests are user-friendly for operators and pose no risk or moral dilemmas²¹.

Manikins are primarily used to analyze the effects of thermal conditions on human health and to determine the heat and mass transfer characteristics of garments²⁸. A thermal manikin measures convective, radiative, and conductive heat losses in all directions over the entire surface or a specified local surface area, in the shape of a human body. The accuracy can be significantly increased by increasing the number of manikin segments.

The thermal manikins can currently simulate the head, hand, arm, torso, leg, and foot. Baby, toddler, and adult manikins are included in the full-scale manikin. Both male and female adult manikins exist. Adult male manikins have predominated until recently²¹. To simulate the body movement and walking condition, both mechanical and pneumatic motion systems have been incorporated (Figure 2.2).

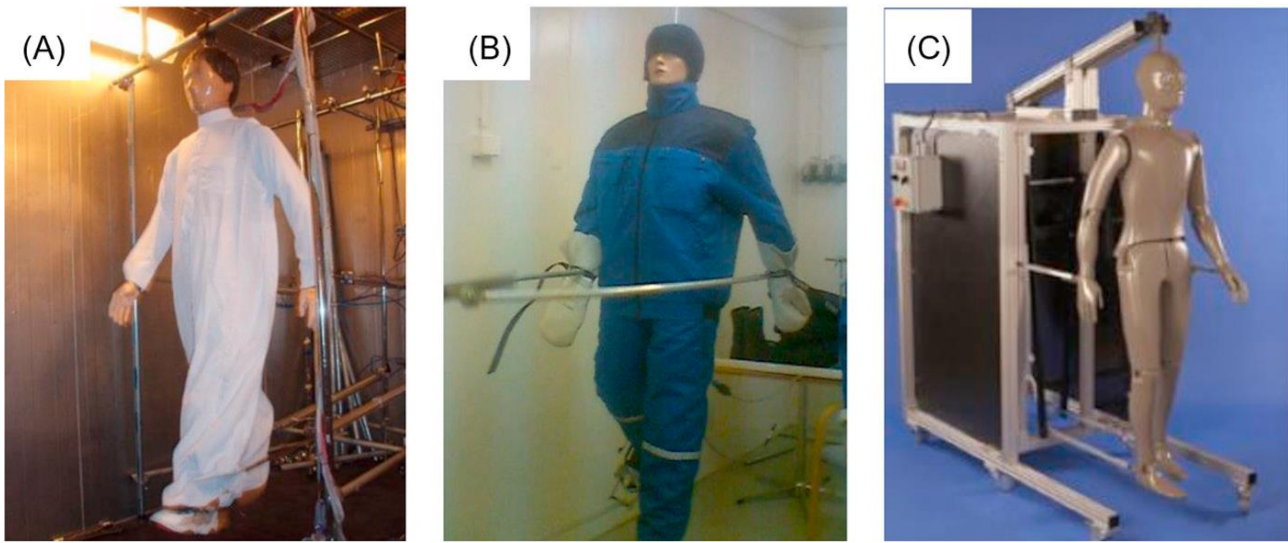


Figure 2.2 Tore walking at Lund University, Sweden, is driven by pneumatic system (A), Pernille type manikin walking at Sintef, Trondheim, Norway (B), and Newton type manikin (C) by mechanical system²¹.

Thermal manikins can be used for both dry and wet studies to evaluate the characteristics of clothes that contribute to thermal comfort. The wet tests can further identify both heat and mass transfer qualities (i.e., clothing evaporative resistance) while the dry tests are used to determine the dry heat transfer capabilities of the clothing ensembles (i.e., clothing thermal insulation). To gather the necessary data, temperature and humidity sensors are built into every part of the manikin. Additionally, the manikin can be constructed with a breathing system for testing in indoor environments²⁹.

With the advancement of modern technology, sweating manikins can be combined with a thermoregulatory model, which can predict the dynamic heat and moisture transfer between a person's body and their surroundings and examine the effects of thermal environments and clothing on a person's body, particularly in extreme environments²¹.

The most common approach^{16,20,30} to the heat and moisture transfer problem from which thermal and evaporative resistance can be derived is the following. Heat flux P through the manikin shell is directly proportional to the surface area A and to the temperature difference between the inner wall of the shell and the air boundary layer ($T_{s,i} - T_A$). The proportional factor is an indicator of how well heat is transferred from the shell to the environment, i.e., a measure of the thermal transmittance T [W/m^2K]. Further, it is possible to write $T = 1/I_T$ where I_T is the thermal resistance, or thermal insulation. The final equation for I_T is (Eq. 2):

$$I_T = \frac{A(T_{S,i} - T_A)}{P} \quad (2)$$

I_T comprises both the thermal resistances of the shell and the air boundary layer, under the hypothesis that air velocity $v < 0.15 \text{ m/s}$ ³¹. At constant temperature, the heat flux P is equal to the power input H_T to the heaters that are typically embedded under the surface of the manikin shell. I_T can be referred to the whole surface of the manikin (and total power input H_T) or to each specific segment (and segment power input $H_{T,i}$) for the computation of total/local thermal insulation.

Regarding wet tests, evaporative resistance per unit of surface can be defined as (Eq. 3):

$$I_E = \frac{A(p_S - p_A)}{H_E} \quad (3)$$

Where p_S is the partial water vapor pressure on the shell surface (in saturation), p_A is the ambient partial vapor pressure, and H_E is the power input to the corresponding heaters. p_S is derived from empirical equations and p_A is subsequently calculated from p_S (Eq. 4). Similar to thermal insulation, evaporative resistance can be calculated for the entire manikin or for each specific segment.

$$p_A = p_S(T_A) \cdot (RH_A/100) \quad (4)$$

To summarize, the basic principles of manikin testing are to maintain certain variables, such as the model's surface temperature and the ambient temperature, constant, and to change other parameters, such as clothing, to measure the difference in third parameters, i.e., power input. The power input is proportional to the heat loss, and further calculations provide footwear insulation values. To ensure a temperature gradient and heat losses significant enough to lessen the measuring error, the ambient temperature should be set to be at least 20 °C (often more than 30 °C) lower than the surface temperature of the model¹⁶. Compared to EN ISO 20344 test method, thermal foot manikins are a more sophisticated technique. They allow for an assessment of the footwear as a whole and provide companies with input on both the footwear's overall design and individual components. Additionally, they give customers helpful information, and the findings can be included in prediction models and user recommendations. Thermal foot measurements of insulation values show a strong correlation with insulation measures taken on human individuals, even stronger when the subjects are at thermal comfort³². However, various factors can affect the results,

leading to higher insulation readings on human subjects than on a thermal model, if the need for total and local thermal comfort is not satisfied³³.

Extremities' insulating value is more significantly impacted, likely as a result of their fast cooling. The presence of moisture/sweat in liquid form near and under a heat flux sensor, i.e., on the skin's surface and under clothing, may be a factor causing this effect. Another one might be related to the fact that highly conductive surfaces are known to increase measuring error³⁴. One more source of inaccuracies can be an uneven contact surface, typically found in human tests on hands and feet. Because of the decreased water vapor pressure and the local cooling of the extremities (especially toes and heels), these regions are more susceptible to condensation. This can increase the user's risk by overestimating insulation in the extremities when testing cold-weather protective equipment on humans.

Measured insulation has a good correlation with feet thermal sensation and cold-related pain³⁵. Compared to footwear without a particular insulation layer, boots with high insulation reduce thermal stress. Foot skin temperatures are closely related to thermal and pain sensations (Figure 2.3). The style or material of the boot does not seem to influence the cold sensation, while the latter is definitely related to the skin temperature of the foot (Figure 2.4). Lastly, the thermal threshold for cold and pain in the toes is lower than that for the entire foot. It is, therefore, important to consider local skin temperatures as a criterion for limiting exposure.

Toe skin temperature is about 5°C lower than the mean foot surface temperature during an intense cold experience, despite the fact that thermal neutrality and heat feelings correspond to similar temperature levels in both the toes and the entire foot. The effect is even more pronounced when it comes to feelings of discomfort: while no pain is experienced when temperatures are above 25°C, the first symptoms begin to occur when toe temperatures drop to 15°C. The action of pain receptors appears to override the activity of cold receptors at temperatures below 15°C, but the cold is likely still felt because other foot regions are warmer. From then on, pain sensation increases quickly without any significant decrease in skin temperature, and it might be unbearable even before reaching the temperature of 10°C^{34,36,37}.

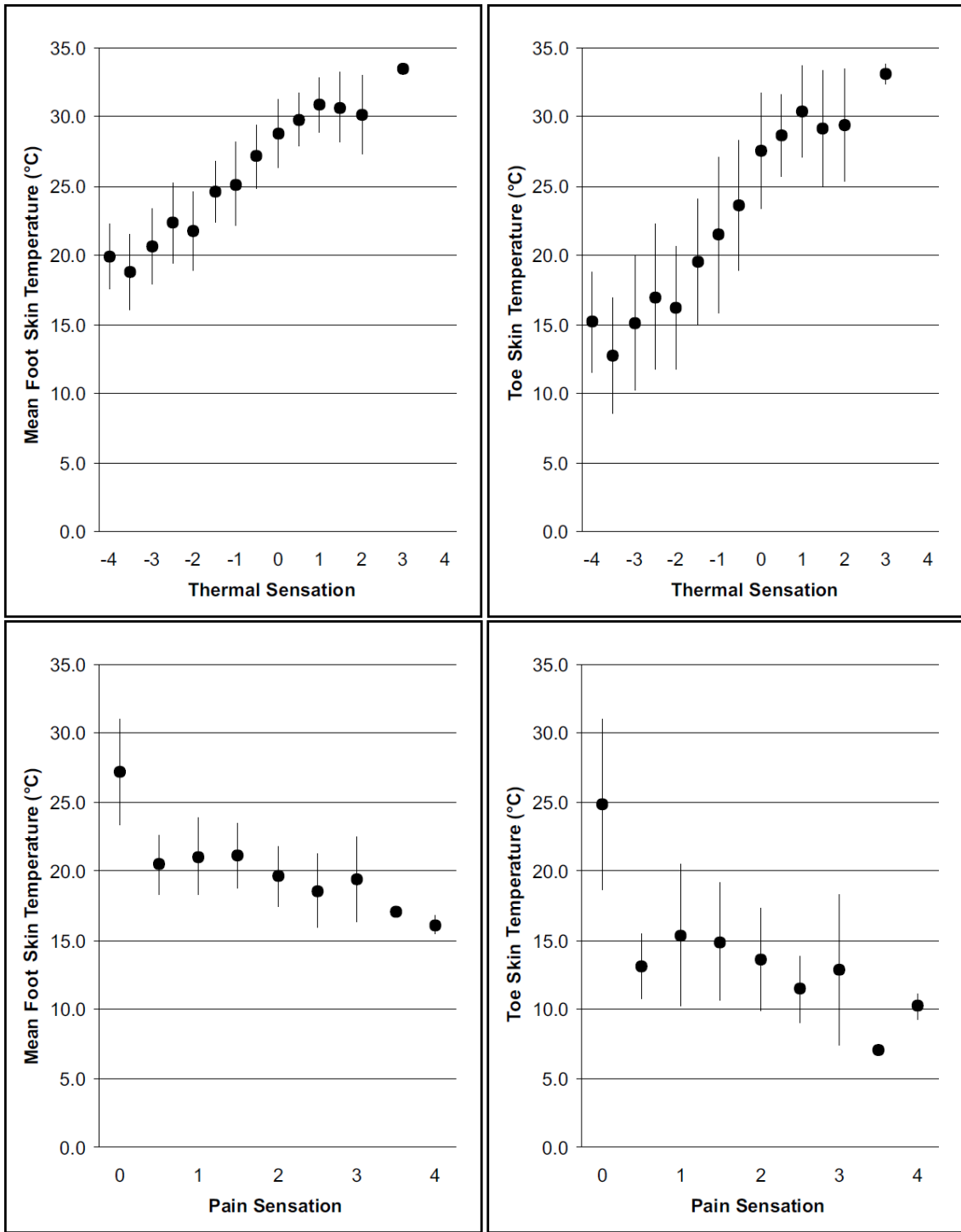


Figure 2.3 Relationship between thermal and pain sensations and mean foot and toe skin temperatures. The values include ratings during cold exposure, intermittent activity and warm up³⁵.

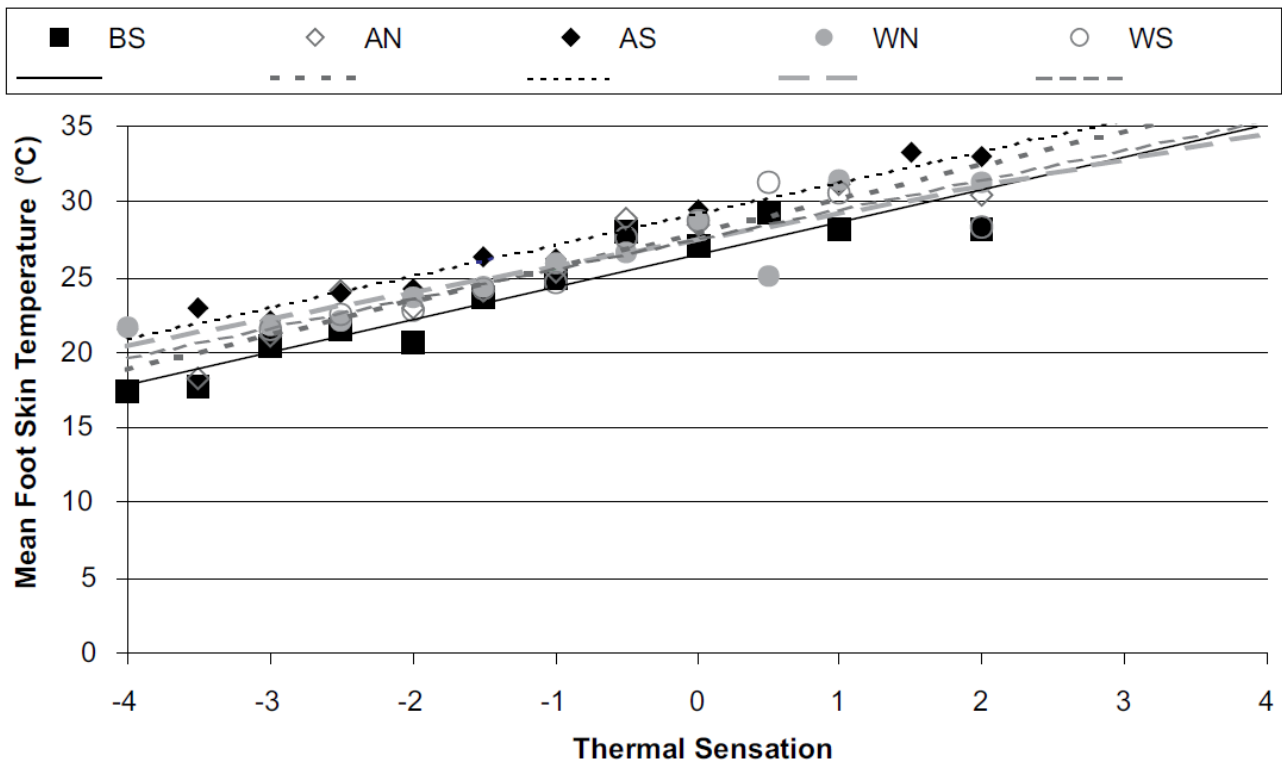


Figure 2.4 Thermal sensation as a function of mean foot skin temperature for various boots at -12°C and their linear trendlines. BS: rubber boot without lining; AN, AS: leather boots without lining; WN, WS: winter boots³⁵.

2.2 The manikin of the present work

Currently existing thermal manikins are definitely a step forward in measuring thermal insulation and evaporative resistance of footwear, compared to EN ISO 20344 standard test method. Results are more detailed and relevant, and the tests as a whole are more reliable and reproducible. However, they do not come without constraints.

One primary challenge lies in replicating the full complexity of the human foot's heat distribution and perspiration patterns accurately. At the current state of technology, the human body is too complex to be artificially replicated with 100% accuracy. The number of different tissues and their partially unexplained interactions, combined with dynamic elements (e.g. blood flow and sweat regulation, muscles contraction) make the properties of the body extremely heterogeneous and unpredictable. Variations in individual foot anatomy and physiology are not comprehensively captured, which can limit the manikins' ability to represent the diversity of human users. Moreover, the fixed geometry of manikins poses limitations in simulating the dynamic movements and changes in pressure that a real foot undergoes during walking or other activities. This lack of dynamic simulation can impact the realism of the obtained thermal data.

Furthermore, while environmental conditions can be controlled to some extent, replicating all real-world scenarios remains a challenge. Factors such as wind, moisture, and varying levels of activity are difficult to accurately reproduce in controlled laboratory settings.

Previous studies have tried to investigate some of the foot properties, mainly interested in deepening the knowledge on diabetic foot and similar pathologies that cause variation in tissue temperature, following various approaches.

A Chinese research team^{38,39} tried to estimate the foot arterial blood flow using the temperature distribution and an artificial neural network. To quantify the relationship between the blood flow and the temperature distribution, a bioheat transfer model of a voxel-meshed foot tissue with discrete blood vessels was established based on computed tomography (CT) sequential images and the anatomical information of the vascular structure. Analytical data was then used for training a neural network which was able to determine the foot arterial blood flow with an accuracy higher than 90%.

Numerous studies⁴⁰⁻⁴² used Digital Infrared Thermal Imaging (DITI) or Infrared Thermography (which is a noninvasive, noncontact, and harmless technique for measuring and recording the skin temperature in the form of a thermogram or thermal image) along with tools and methods for segmenting the plantar foot and identifying anomalies in the skin temperature distribution. For example, a 2017 study⁴⁰ developed a semi-automatic algorithm in MATLAB to segment the foot from images taken with the Fluke TiX560 thermal imaging camera, overcoming challenges related to the presence of the ankle bones in the images and the small temperature difference between the background and the foot, which is a main cause of interference. Another study⁴¹ aimed at finding the best deep learning method for segmenting plantar foot thermal images among three candidates: the Fully Convolutional Networks (FCN), SegNet and U-Net. SegNet outperformed the other methods with a Dice Similarity Coefficient (DSC) equal to 97.26%.

A good number of researchers also applied numerical methods such as finite differences, finite elements, finite volumes, boundary elements, spectral methods, etc. to solve the Pennes bioheat transfer equation for the human body⁴³. One study⁴⁴ focused only on modeling the bare human foot, with qualitatively acceptable results.

Sweat distribution has been thoroughly investigated in a 2013 article⁴⁴ using two independent research approaches: one lab monitored running at two different speeds in males and females and measured sweat with tampons placed inside the footwear, while the other used ventilated sweat pods on a bare, passive foot, evaluating sweat production during passive warm-up and increasing workout to

fatigue. They found that males produced more than twice the volume of sweat than females at the same relative work rate. The highest local sweating rates were observed in the medial ankles, and it was observed that the dorsal foot sweated substantially more than the plantar areas.

Ultimately, the scientific literature is teeming with biological and biomechanical studies of the human foot which, being the present work mainly focused on thermal properties, were of minimal use.

In summary, although thermal foot manikins offer valuable insights, their limitations in accurately emulating human foot dynamics, sweating and different real-world conditions underscore the need for refinement and integration with complementary testing methods. Not to mention that building a thermal manikin system with active heating and sweating capabilities is an extremely complex and expensive project. In fact, there are only a few examples of such systems worldwide, some developed by research laboratories^{34,45} and others made and marketed by private companies such as UCS and Thermetrics. Their cost can easily be in the hundreds of thousands of euros.

With these limitations in mind, the present work aimed to develop and realize a foot manikin following an alternative approach. Instead of fabricating it from metal plates and incorporating active heaters inside, 3D printing was chosen as the process for fabricating a hollow shell (inside which hot water was poured, which became a passive heat source). Temperature sensors were placed on the outer wall of the shell to record foot cooling at 16 points during tests in cold environment. Humidity sensors were not employed because the manikin had no sweating function and therefore wet tests could not be performed. Only dry heat loss tests were carried out, and total and local insulation parameters were extracted from the derivatives of the temperature-time curves of each sensor.

Ideally, once the preliminary tests are completed, the foot manikin should always wear a sock, with known properties, to protect the sensor wires from friction with the inner parts of the footwear being tested. The most suitable sock would be a liner, so that wool socks can also be tested for thermal insulation evaluation (since the liner is usually worn under the wool sock in real cold environments).

As will be discussed later, the lack of active heaters and sweating capabilities, while a major limitation in terms of the type of tests that can be performed and the amount of information that can be acquired, contributed greatly to containing the cost and complexity of the system. Moreover, 3D printing enabled a rapid and inexpensive prototyping, orders of magnitude less than traditional thermal foot manikins. To better understand why additive manufacturing technology was employed, a brief discussion on the most recent developments regarding body part surrogates is needed.

2.2.1 3D-printed body part surrogates

Developing physical models of human body parts with improved biofidelity is one of the fast-developing trends rapidly widening possible application areas. Additive manufacturing and modern sensor application are the main enabling elements in such developments.

Modern additive manufacturing (AM) techniques, often known as 3D printing, make it possible to produce surrogates of body parts with a high degree of precision in both 3D geometry and features. When combined with an array of embedded sensors, they serve as the basis for effective configurations and platforms for device research and development.

Physical surrogates experiments can be implemented together with mathematical and computer modeling to cross-validate both methodologies and fundamental concepts. Physical and computer modeling of body parts can use the exact same 3D shape representation with the use of additive manufacturing. Physical models use synthetic materials, the qualities of which are known or can be accurately tested empirically. Computer models can easily adopt the same settings and parameters for "virtual experiments" that are used for real materials and test conditions with surrogates, making it easier to compare results.

Surrogate body parts produced by 3D printing successfully exploit the well-known advantages of the process, including: the extreme flexibility of the 3D shapes created; the ease with which the dimensions of body parts can be linked using 3D medical image data; the ability to work with a variety of materials; the cost-effective production of unique parts and small batches; the well-controlled modification of existing designs; and the ease with which production files can be shared with manufacturers worldwide²⁶. The thin-walled shell of surrogates can be produced additively in the form of the corresponding body part (that was previously scanned and digitalized as a 3D CAD model) using a variety of possible materials ranging from polymers (e.g. ABS) to metals (Ti-6Al-4V is one of the most common titanium alloys for additive manufacturing).

3. Measurement setup

3.1 General layout

The measurement setup required for the present work consisted of four fundamental parts (Figure 3.1):

1. the 3D-printed foot manikin shell filled with warm water;
2. hardware for data acquisition, comprising temperature sensors (16), wires, switches (2) and interface device;
3. software for managing data acquisition and processing (LabVIEW);
4. refrigerator for testing in a cold, stable and reproducible environment.

The following will describe in detail all parts of the setup and the rationale behind each choice that was made during the course of the work.

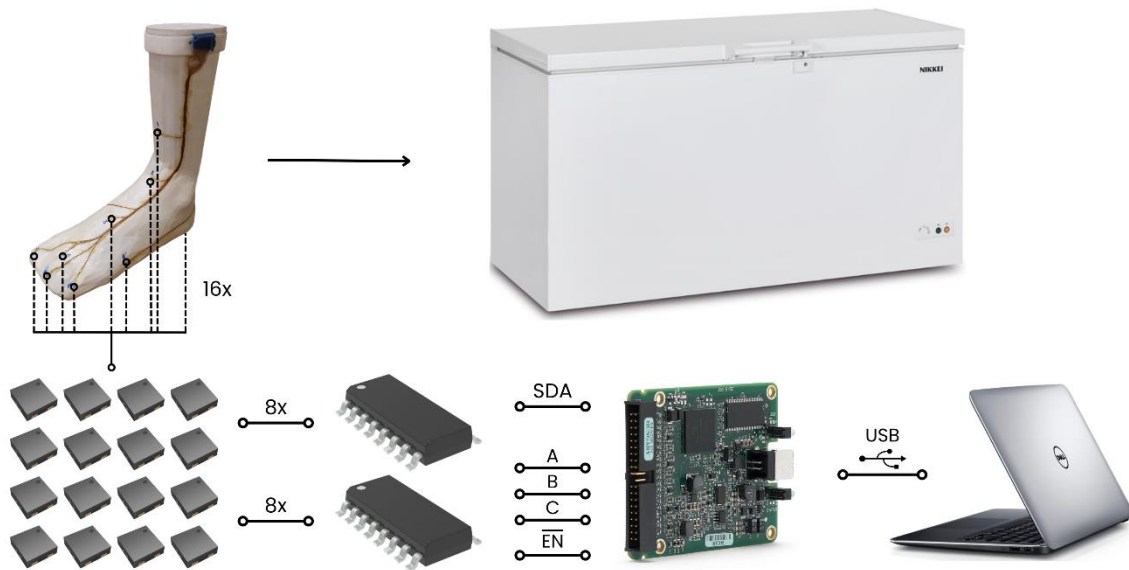


Figure 3.1 General layout of the measurement setup. Arrows and lines indicate how the parts are connected to each other.

3.2 Foot manikin shell

As a result of the literature review, it was decided that the foot manikin would behave like a simplified version of a human foot only from the heat transfer point of view. Sweat production would be neglected, despite being one of the most influent variables on foot thermal comfort^{16,31}. The main reasons for that were: a)

dry heat loss is generally studied before introducing the relative humidity variable, following the simple-to-complex approach, and b) the cheap and simple “dry-heat-loss” version of the 3D-printed manikin might be an accurate enough representation of the human foot for small research studies or commercial purposes.

In other words, the manikin of the present work was “iteration zero” of what could be a new line of research that still has to develop. It is difficult to expect that a first model will be all-encompassing and cover all conceivable cases and circumstances. All models must, by their very nature, make some approximations of actual systems and their processes. Proper modeling always starts with relatively simple and large approximations that represent the most important features of the system. When the most significant attributes are sufficiently depicted, “second order of importance” features are added to strengthen the model. Contrary to the most obvious assumptions, it is generally known that excessive model complexity can limit its applicability by obscuring links, making conclusions hard to grasp, and hiding trends under an immense amount of information²⁶.

3.2.1 Design and modeling

Keeping simplicity as a priority, the manikin structure was the first aspect to be defined. Looking at scientific literature on foot surrogates, the most advanced solutions^{45,46} contemplate a self-heating system with multiple power-controlled heating elements, one for each area of interest. This configuration eliminates almost any construction or material constraint from the inner part of the manikin. The only requirements for it are, then, to be stiff and tough enough to withstand the relatively mild mechanical stresses during the tests. For this reason, the inner part of this kind of manikins can be made of virtually any material. On the outside, a self-heating system requires the use of heat conducting plates which, therefore, must be made of metal. The most common choices are aluminum and silver alloys^{45,46} because of their lightness, good workability and excellent heat conduction.

The downsides of a self-heating structure have already been discussed. Above all are the cost and complexity of such systems. On the other side, it’s the only currently existing solution for determining thermal insulation of footwear through objective steady-state heat loss tests. Additionally, it well resembles what happens with human blood flow adjustments for thermoregulation. But since the present work aimed at finding a much cheaper and more easily reproducible alternative for testing footwear, the active heating had to be abandoned in favor

of a passive heating system. This meant that the manikin would have been tested in a continuous cooling condition, instead of being kept at an equilibrium temperature. The thermal insulation values would then be extracted from the cooling curves (as a derivative value on the temperature–time chart relative to a specific foot area) instead of being obtained from the power required to maintain constant temperature in the same specific area of the foot.

Having made this simplification, the next step was to define how the manikin would be heated before being put in the cold environment for the test. Two approaches were considered:

1. Heating an entire solid manikin, placing it inside the footwear to test and then put everything in the cold.
2. Fill a hollow-shell manikin (already placed inside the footwear to test) with a warm fluid, then put everything in the cold.

Four reasons guided the choice towards the second option: a) the human body is ~70% made of water, so having H₂O as a “core” in combination with an outer shell would be a better approximation of a human foot than any other material in terms of overall properties; b) it would be easier, faster and cheaper to 3D-print the shell only, instead of a solid manikin; c) the core-shell system could be upgraded to a steady-state heat loss system with a water recirculation unit keeping it at constant temperature; d) it would be easier to install sensors measuring the exact “skin” temperature (the skin is represented by the water layer at contact with the inner wall of the shell) without any influence from the environment. Moreover, the core-shell idea had already been tested in a former Soviet standard test for footwear (GOST-12.4.104-81, 1981)¹⁶.

That being said, the foot manikin design was clear enough for the modeling phase to begin. A Creative Commons licensed STL model was selected from the website “thingiverse.com”, called “Lella’s Foot” (Figure 3.2). It was a suitable choice, in the author’s opinion, because the foot had been scanned in a relaxed position, unlike many other models which were in elongated position.

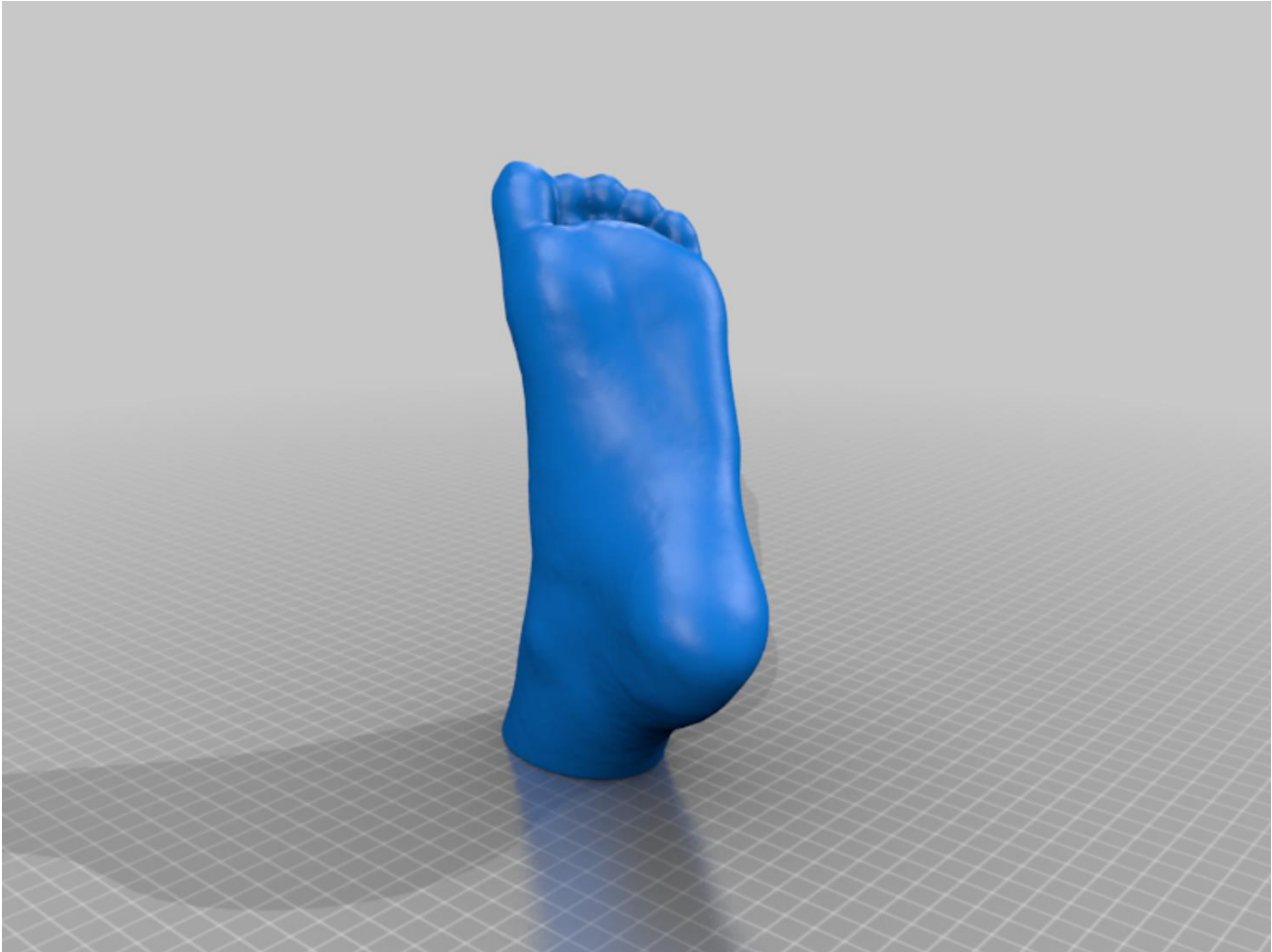


Figure 3.2 The original STL foot model⁴⁷.

Since the foot manikin had to be the best representation possible of a human foot, it was decided to scale it to the average male shoe size dimensions, shown in Table 3.1.

Property	Heel-to-Toe length (mm)	Total height (mm)	Width, tarsal (mm)	Width, heel (mm)
Value	265*	325	103	67

Table 3.1 Foot model scaled dimensions. (*Equivalent to Nike 42.5 EU⁴⁸)

During this process, carried forward in “Rhinoceros 5” CAD modeling software, many characteristics of the foot model were changed (Figure 3.3). First, the STL file was converted into a “polysurface” type of object. From there, it was manipulated to extend the leg length and scale the foot size to the defined dimensions. The sole was flattened in an attempt to simulate the compressed state in which the foot is when forced into a shoe. In that same scenario, the toes are pressed against each other, so it was decided to fuse them all together and

simplify the model even more. Then, a 1.5 mm surface offset was performed for setting the shell thickness to be 3D-printed and a solid plug was designed for closing the hollow foot from the top with a 0.25 mm tolerance. It would later be pierced with a drill press to allow water filling and submerged water temperature measurement. The last modeling step aimed at resizing the overall object dimensions to fit inside a 194x242x325 mm bounding box. These were the maximum dimensions allowed by the EOS Formiga P 110® 3D-printer used at AIM Sweden AB (it has a 200x250x330 mm chamber but, considering the shrinking that the object undergoes during printing, the maximum theoretical dimensions must be approximately 3% smaller). To reach that goal, the leg had to be cut to a 325 mm height and slightly tilted to the front.

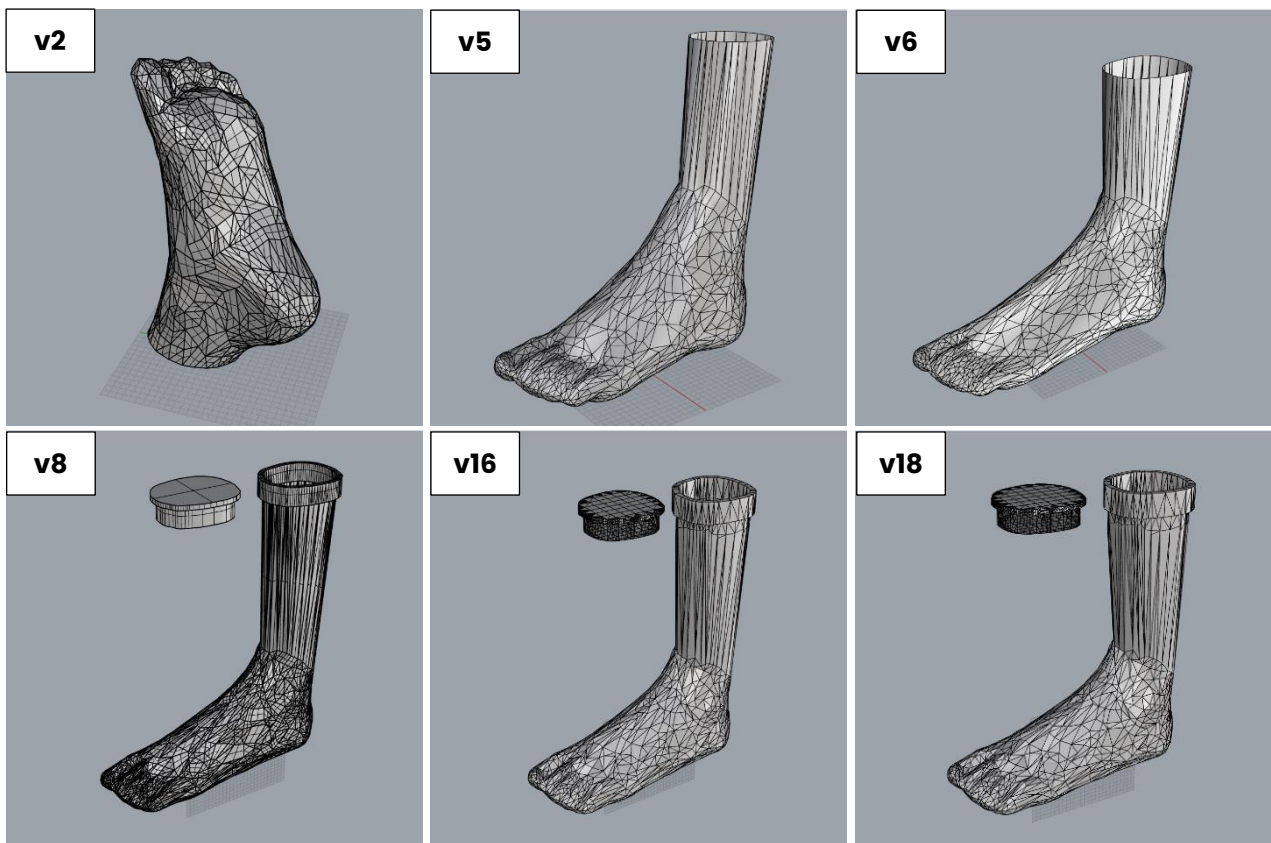


Figure 3.3 Progression of the modeling phase. Going from upper left to lower right: (v2) First mesh, (v5) Extended leg, (v6) Extended foot, (v8) Added cap, (v16) Widened foot, (v18) Final sizing.

Before being printed, the manikin model was reinforced by 3 internal supports: a 5x3 mm rib on the upper foot and two horizontal cylindrical supports (\varnothing 5 mm) at the ankle and mid-leg heights (Figure 3.4). For technical reasons, the printed foot would actually have two more horizontal cylindrical supports (perpendicular to

the first two) replacing the rib. Table 3.2 shows all the final specifications of the foot manikin model.

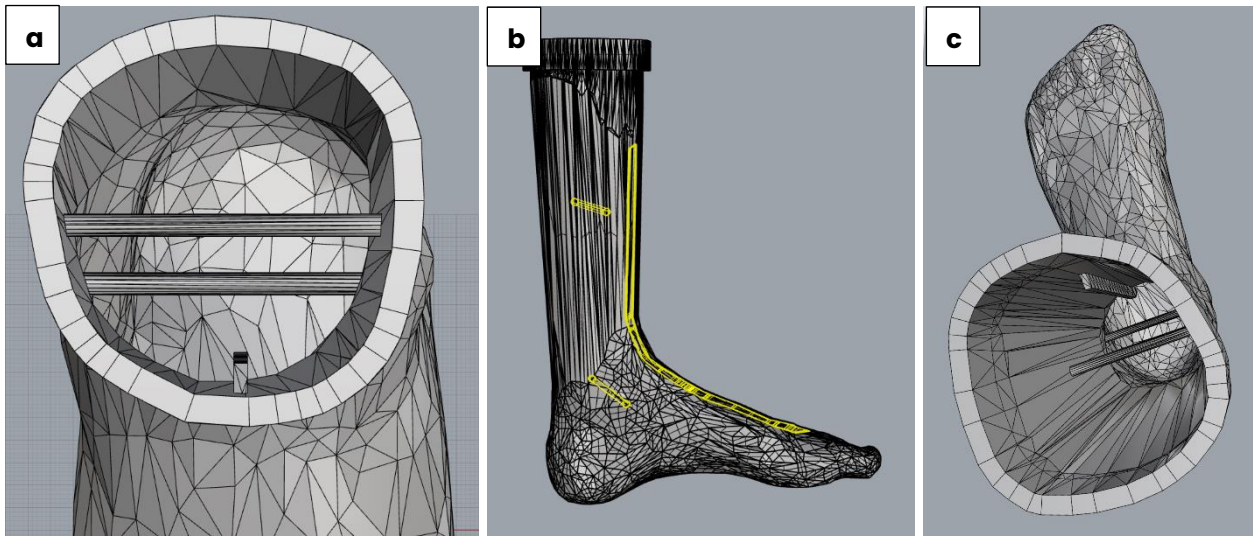


Figure 3.4 Highlights of the internal supports: rib and two cylinders. (a) Top view of the leg, all three supports visible, (b) Ghost view with all supports highlighted, (c) Perspective view of the supports.

Printing method	SLS
Material	PA2200
Layer thickness	0.05 mm
Shell thickness	1.5 mm
Total height	325 mm
Heel-to-Toe length	265 mm
Width (tarsal)	103 mm
Width (heel)	67 mm
Inner volume	1800 cm ³

Table 3.2 Final specifications of the 3D-printed manikin shell.

3.2.2 Materials and 3D-printing

As previously discussed, most existing thermal foot manikins use an active heating system to regulate the temperature and keeping it at a constant value during the entire test. In particular, the “skin” temperature must be held constant since the temperature sensors are usually acquiring data at that level. For that reason, the outer layers of this kind of manikin must be made of a conducting material. This constraint narrows the choice of the material to metals only, hindering the possibility of using cheaper, lighter and easily 3D-printable

polymers, for example.

Following, instead, a passive-heated core-shell approach, the variety of suitable materials for the outer layer is much broader. There is no need for the shell to transfer heat rapidly since the system is not focused on maintaining constant temperature by power input modulation and, therefore, the response in temperature change of the material doesn't have to be fast. Working in a continuous cooling fashion allows to neglect the differences in thermal properties among various materials and makes polymers a suitable class to pick from. The shell only has to satisfy the mechanical requirements of stiffness and toughness to resist the mild stresses during tests – and be waterproof.

Regarding the possibility of using a multilayer shell, it was not taken into account because of increased complexity, but it could be an option for further studies, if considered useful. The same goes for thickness variations of the shell (being thicker in some areas of the foot to simulate tissue with a greater heat transfer resistance) and surface treatments.

That being said, the choice of the shell material fell on the most readily available and less expensive solution that could guarantee a waterproof structure through 3D-printing. The company AIM Sweden AB⁴⁹, a Mid Sweden University commercial spin-off, had three possible options (Figure 3.5):

1. **uPrint SE Plus**[®], a 3D-printer that uses FDM (Fused Deposition Modeling) technology to build in real ABS plus thermoplastic, creating models and functional prototypes that are durable, stable and pinpoint accurate.
2. **EOS Formiga P 110**[®], a flexible, cost-efficient and highly productive additive manufacturing system of polymer parts with SLS (Selective Laser Sintering) technology for small series production, customized products with complex geometries and rapid prototyping applications. Material: PA2200 (polyamide).
3. **Arcam EBM Q10plus/Q20plus**[®], new generation EBM (Electronic Beam Melting) machines designed specifically for cost-efficient production of orthopedic implants and aerospace components made of Ti6Al4V alloy.

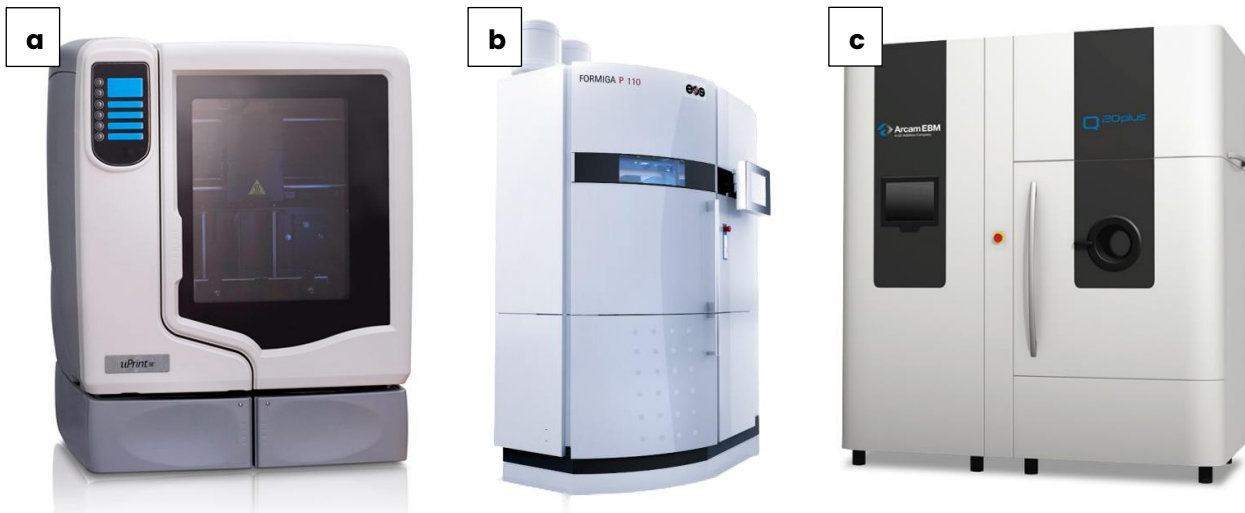


Figure 3.5 Available solutions for additive manufacturing offered by AIM Sweden. (a) uPrint SE Plus®, (b) EOS Formiga P 110®, (c) Arcam EBM Q10plus/Q20plus®.

The SportsTech Research Centre hosted four uPrint SE Plus® printers as well, but it was clear that their chamber was too small to accommodate a real size human foot model (build box dimensions were 203x203x152 mm). Also, these machines had been previously used for creating prototypes and it was found that they were not waterproof. On the other side, a metal additive manufacturing system was substantially more expensive and the titanium alloy had unnecessarily excellent mechanical properties. For these reasons, it was decided that the best-suited choice for the foot manikin 3D-printing was selective laser sintered polyamide. SLS technology has a multitude of benefits. It can be used to produce manufactures of any geometry, thanks to the non-fused powder bed as a support. The objects have no undercut constraints, which are one of the main limitations of FDM products. Multiple parts can be printed at the same time and can be arranged freely within the print volume. The absence of supports allows greater productivity and reduced post-process costs. The resolution is five times higher, compared to an FDM machine (0.05 mm against 0.254 mm layer thickness) and the mechanical properties of the product are more isotropic and better overall. Lastly, SLS manufactures are waterproof.

Upon receiving it from the company, the foot manikin shell was briefly cleaned with water from the residual powder inside, especially in the toes region (Figure 3.5a). Water was also used to measure the free volume inside the shell, which happened to be 1800 cm³. After that, the plug was polished with sandpaper with decreasing grain size to ensure a smooth coupling with the shell inner walls. A drill press was used to perform three M8 holes through the plug (Figures 3.5b and 3.5c), later tapped. The utility of these holes would be to accommodate wires for

submerged sensors and simultaneously allow for water filling and/or recirculation. In the present work, only one hole was left open to allow for water filling, while the other mentioned functionalities should be deferred to future studies. Also, the plug will eventually be glued to the shell to guarantee complete waterproofness.



Figure 3.6 Details of the manikin cleaning and drilling. (a) Dust particles inside the toes, (b) Drilling the plug, (c) The plug with holes and 3D-printed bolts.

3.3 Electronics

All thermal foot manikins are equipped with a sophisticated electronic system capable of acquiring data through sensors and processing it. The ones with active elements (e.g. heaters, sweat nozzles) are also able to modulate the power input based on the feedback received from those sensors.

As previously stated, the manikin of the present project was much simpler. It was passively heated, so there were no heating elements, and it was a dry-heat-loss system, which means that sweat simulating nozzles were not required. In terms of sensors, only temperature ones were needed on the manikin since humidity should have always been controlled by the environment and possibly kept constant across multiple tests. The absence of power regulation feedback loops made the programming simple enough to be performed in LabVIEW with a basic level of knowledge of the software. Before going into the details of electronics and programming, it shall be briefly discussed the logical process that led to the final choice regarding sensors' positioning.

3.3.1 Sensors placement

The scientific literature on thermal foot manikins provides a variety of possible configurations for partitioning the total foot area in a certain number of regions²¹. Lund University's manikin^{32,34} developed by Kalev Kuklane had 8 independently heated zones: toes, midsole, heel, midfoot, ankle, lower calf, midcalf, and guard. The Josef Stefan Institute's manikin⁴⁵ had 10: big toe, remaining toes, sole, heel, medial foot, lateral foot, instep, anterior ankle, posterior ankle and midcalf. The foot manikin made by the company Thermetrics had 12 zones, and the one from UCS had 13. Figure 3.7 shows all the mentioned manikins.

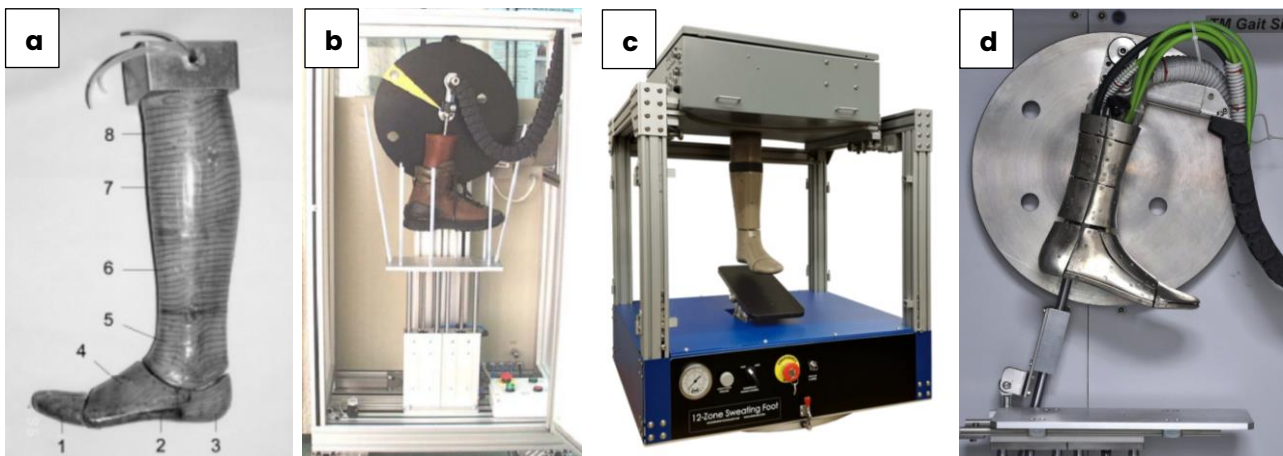


Figure 3.7 Thermal foot models. (a) Lund University, (b) Josef Stefan Institute, (c) Thermetrics, (d) UCS. Courtesy of Kuklane (1999), Mekjavic et al. (2005), Thermetrics, UCS.

It must be said that most of the publications in which these manikins are presented lack any dissertation on how the authors had come up with the chosen foot area partition and, consequently, sensors position and numerosity. One

could hypothesize that they went for the minimum number of zones that could still highlight the differences in thermal properties of the various foot parts, keeping an eye on the symmetries of the foot itself. However, the preliminary research or tests that were carried out to get to the final choice remain unknown. Trying to fill this knowledge gap, the present work aimed at giving the reader a clear idea of the criteria on which decisions about sensors placement were made for the current project.

The starting point was foot anatomy. To investigate the structure in detail, the online resource "Human Studio"⁵⁰ was consulted. This website provides a 3D representation of the human body with specific models for certain regions. The one of interest was, of course, the lower limb. As shown in Figure 3.8, the human foot consists of multiple tissues (skin, muscles, bones, tendons, nerves, blood and lymphatic vessels) that intersect and interact with each other in a complex manner. It should not be forgotten that these images represent an average male's anatomy and can vary widely among individuals.



Figure 3.8 Human foot 3D model from different points of view⁵⁰.

What can be noticed with a certain degree of precision (see also Figure 3.9) is that, in line with the cuneiform bones, the plantar aponeurosis ligament, plantar nerves and all the main blood vessels branch out. That is, ideally, a region of interest of the foot because at that point the anatomy changes significantly.

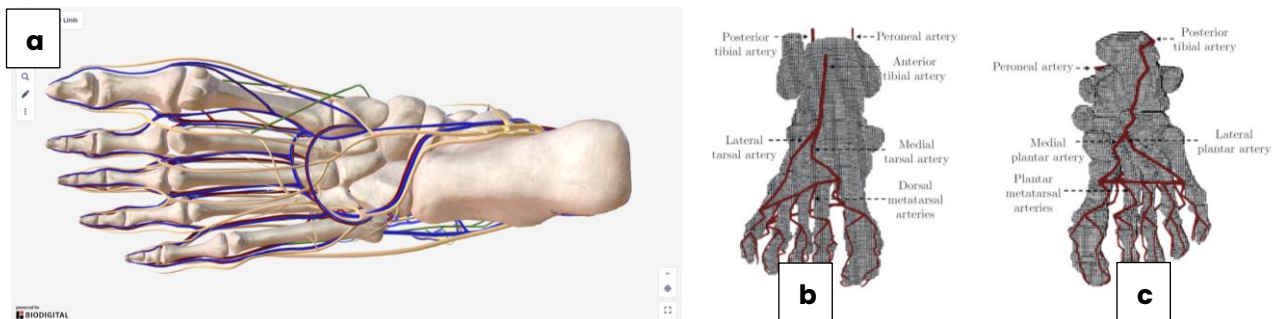


Figure 3.9 Structure of the embedded arteries from (a) plantar⁵⁰ (b) dorsal³⁸ and (c) plantar³⁸ views.

If a frontal section was performed at that level, it would have no lines of symmetry. Therefore, it should be reasonable to have at least four sensors measuring the temperature of (what from now on will be called) the “mid-foot” at the top, bottom, medial and lateral points. The distance between the mid-foot plane and the end of the heel was set to 143 mm and the height from the sole at which the lateral and medial sensors were placed was 25 mm.

Moving approximately 80 mm from the top mid-foot point in both directions of a line inclined 24° with respect to the sagittal axis, two other points of interest can be found on the upper foot skin: one is in line with the base of the middle toe, while the other lands on the inferior extensor retinaculum. The former is where anatomy changes significantly again, from a whole piece of body to five separated parts (i.e. the toes). The latter is in line with the fulcrum of the ankle. That way, a three-points line of sensors was ready to measure the upper foot temperature.

Regarding the toes, the decision about the sensors number and position relied on the results and modus operandi taken from previous studies on cold. The literature suggests that in cold environments the first part of the foot that cools down to a critical temperature value is the big toe. In other words, it is the first part to feel painful¹⁶ (when its skin temperature goes below 15 °C) and to go numb⁵¹ (when its skin temperature goes below 7 °C). Not surprisingly, most of cold injuries start from the big toe and then spread to the other parts of the foot.

That being said, the manikin of the present work had all toes “fused” together, so there was no real reason to have a sensor for each individual toe. In addition to the sensor on the big toe, the best compromise was to place one also on the little toe, which is equally exposed to the cold as the big toe, and one approximately in

the middle to measure the average temperature of the inner toes. Looking at previous studies^{45,52}, the number of sensors was doubled: three of them were placed on the upper toes and other three on the lower toes, all about 5mm from the fingertip.

The last region of the foot that had to be considered was the heel. The minimum number of sensors for that part was thought to be two: one in the middle of the lower calcaneus, at contact with the ground or shoe sole, and the second one on the posterior calcaneus, at contact with air or shoe counter. A different environment surrounding the two heel parts could justify a difference in cooling speed and, therefore, having two separate sensors instead of one.

At this point, the total number of sensors was 14. They covered all the regions of interest and might have been enough to highlight which parts of the foot were more susceptible to cold. As will be discussed in detail in the next paragraph, two 1-to-8 analog switches were employed to connect the sensors to the interface device. This system allowed for two more sensors to be added, so they were placed onto the leg of the manikin: one in the front and one in the back, at a height of 190 mm from the ground.

The final configuration consisted of 16 sensors connected to the two switches through two eight-wires bundles. As shown in Figure 3.10, the wires had been glued to the outer manikin shell to prevent damages during tests and bring a more stable signal from the sensors. One thing to notice is that the sensors were positioned at contact with the water inside the shell, rather than facing outwards. That was made possible by drilling a hole for each sensor to be hosted in it, then sealing it with glue from the outer side. Measuring temperature at the water level makes any influence from the shell almost negligible. As a matter of fact, if the location from where data is acquired is considered as the manikin "skin", then the outermost water layer (at contact with the inner shell walls) plays that role instead of the shell itself.

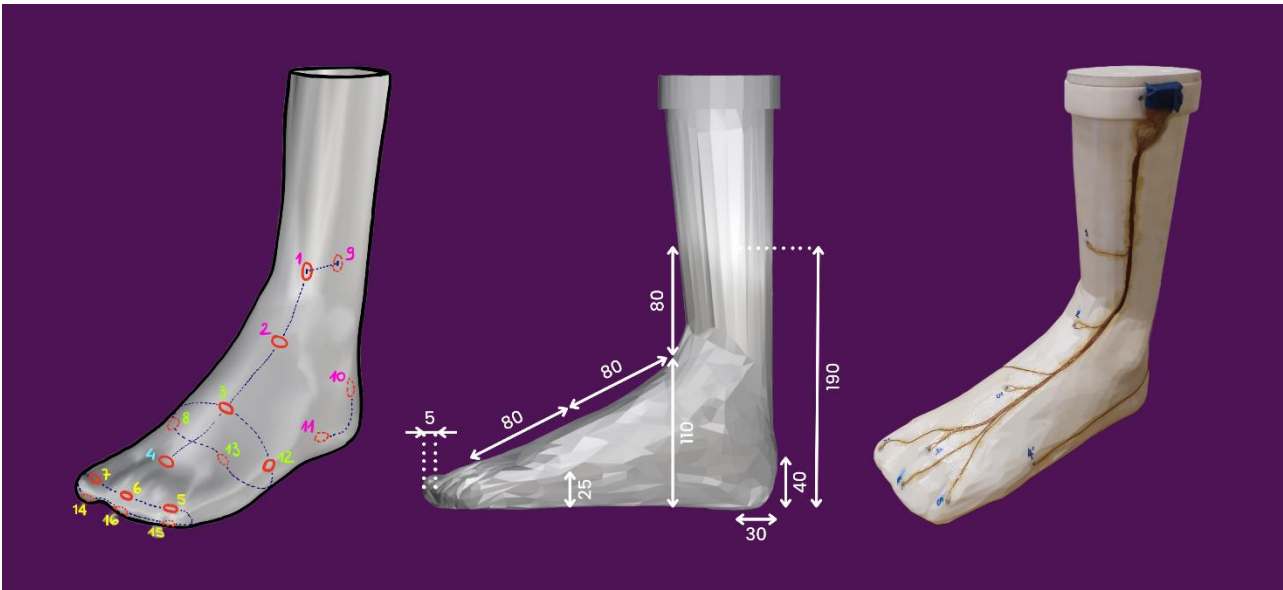


Figure 3.10 From left to right: sensors' positioning and numbers; sizing and dimensions; photo of the real manikin. A bigger version of the picture with sensors' positioning is given in "4. Results and Discussion".

3.3.2 Electronic components

Building an electronic system is a process that starts with the choice of the most appropriate set of components. That includes sensors, actuators, interfaces and other intermediate devices (e.g. switches). To properly do so, it had to be taken first into account the final goal of the system, which was to acquire data from 16 temperature sensors with a relatively low sampling frequency (around 1 Hz) on an hour or longer time frame. Temperature gradients between manikin and environment during footwear tests are small enough to guarantee a slow heat transfer, and therefore a slow and steady cooling of the foot. Temperature variations are then slow enough to be caught with excellent resolution also when using very low sampling frequencies, which means that long duration tests can be performed without the risk of accumulating enormous amount of data.

Keeping an eye on the aforementioned goal, there was no need to include actuators in the system. Being a passive-heated manikin, only data acquisition and processing were required. Moreover, working with a low sampling frequency allowed for using digital type of sensors instead of analog ones.

Both analog and digital sensors can measure physical quantities from the surrounding environment. The fundamental distinctions between these two types of sensors are the different underlying operating principles and the nature of their output signals. Analog sensors, relying on continuous measurements, possess a unique ability to capture a wide range of real-world values with remarkable precision (higher than digital ones). They convert a physical quantity (analog

signal) into corresponding electrical voltage levels. This analog representation offers a smooth and uninterrupted flow of data, making them particularly well-suited for applications that demand fine-grained sensitivity and high accuracy. Analog temperature sensors are ideal in climate control systems, for example, ensuring precise monitoring and regulation of indoor temperatures to enhance comfort and energy efficiency. However, the journey of analog signals from the sensor to the destination may encounter some obstacles. As the electrical signals travel through various components and over long distances, they become susceptible to noise and interference. External electromagnetic fields, signal losses and other factors can introduce disturbances that might degrade the data quality. To address this problem, engineers employ signal conditioning techniques and shield the sensor and its transmission paths to minimize interference and preserve the integrity of the analog data.

On the other side, digital sensors provide a more robust and noise-resistant approach to data capture. Instead of representing data as continuous voltage levels, digital sensors generate discrete outputs, typically in binary form, based on a series of on-off switches. This binary representation simplifies data processing, transmission, and storage by electronic devices. It also diminishes the influence of noise and interference, making digital sensors well-suited for applications in environments where electromagnetic disturbances are prevalent. Communication systems is a field of application that heavily rely on digital sensors, since data is transmitted over various channels, often spanning vast distances. By representing information in a binary format, these sensors can accurately reconstruct the transmitted data, mitigating the effects of noise and ensuring reliable communication. Similar goes for the manikin of the present work: 16 temperature sensors required an equal number of channels, which meant there would be high risk of interference between the wires, although the distance to the interface was not that long. That, together with the need to sample at low frequencies, prompted the decision to use digital sensors instead of analog ones.

Moving on to the type of interface, two serial communication protocols were considered: SPI (Serial Peripheral Interface) and I2C (Inter-Integrated Circuit).

SPI is a widely adopted and time-tested communication protocol in modern electronics, whose origin dates back to the 1980s. At that time, Motorola (now Freescale Semiconductor, a division of NXP Semiconductors) patented a simple yet effective solution for short distance wired communication between electronic devices. Throughout the decades, SPI firmly established itself as a de facto standard, offering a low-power reliable means of data exchange between a "master" device and multiple peripheral or "slave" devices.

At the core of SPI's functionality lies a simple yet robust "master-slave" architecture (Figure 3.11). The communication process hinges on four lines, each serving a specific role: Master In Slave Out (MISO), Master Out Slave In (MOSI), Serial Clock (SCK), and a distinct Chip Select (CS) line for every connected slave device. The master device, often a microcontroller or FPGA (Field Programmable Gate Array), orchestrates data transmission and reception with the interconnected slave devices.

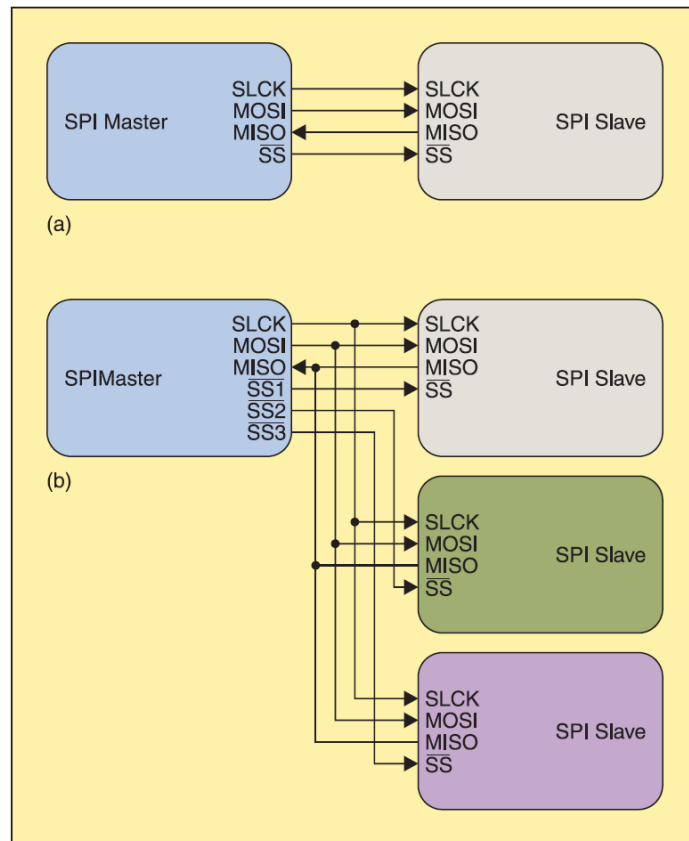


Figure 3.11 Two SPI bus topologies. (a) An SPI master connected to a single slave (point-to-point topology), (b) An SPI master connected to multiple slaves⁵³.

To initiate communication, the master selects a specific slave device through the reduction of its Chip Select (CS) line. It's important to note that the CS line is indicated with an overbar, signifying an active low signal, wherein a low voltage signifies "selected," and a high voltage indicates "not selected." Throughout each clock cycle within the SPI protocol, a full-duplex transmission of a single bit takes place. The master transmits a bit via the MOSI line, while the slave transmits a bit through the MISO line, after which both read their respective received bits. This sequence remains consistent even when data transfer is intended in a single direction.

For data transmission using a solitary slave device, a particular configuration

(Figure 3.12) involves the presence of a shift register in both the main and the sub, each with a designated word size, often 8 bits. These shift registers are interconnected in a virtual ring topology.

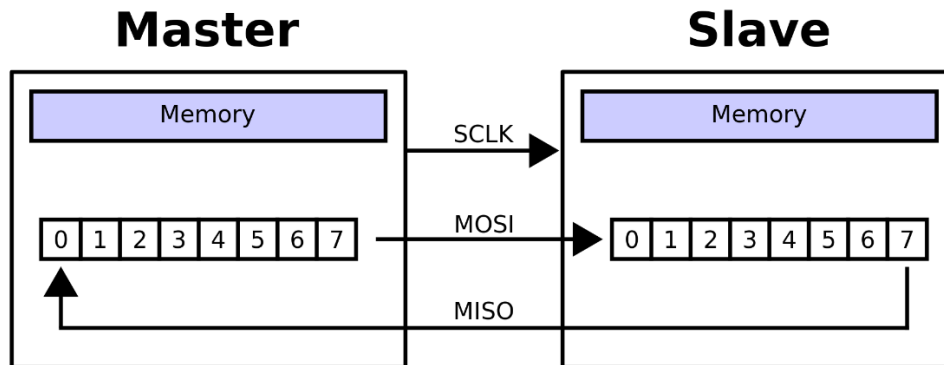


Figure 3.12 Master-Slave architecture with SPI configuration. Courtesy of Wikipedia.

The usual approach is to shift out data with the most significant bit (MSB) leading. As the clock edge occurs, both master and slave shift out a bit to their counterpart. Subsequently, at the next clock edge, each recipient samples the transmitted bit and stores it within the shift register as the new least significant bit. This process repeats until all bits have been transmitted in both directions, culminating in an exchange of register values between the master and the slave. If additional data requires transmission, the shift registers are reloaded, and the sequence recommences. This iterative process can continue for any number of clock cycles. Upon completion, the master ceases clock signal toggling and typically deselects the sub.

In the SPI context, all non-selected slaves must disregard input clock and MOSI signals, and to prevent contention on the MISO line, non-selected slaves must employ tristate output. Devices lacking this functionality will require external tristate buffers to ensure adherence to this principle.

Among SPI's numerous advantages is its high data transfer speed. It stands out in applications that require real-time data processing, swift information flow and prompt responsiveness. Furthermore, SPI's support for full-duplex communication significantly enhances its efficacy. By enabling both the master and slaves to engage in simultaneous data transmission and reception, SPI overcomes the inherent latency problems of half-duplex communication protocols. This makes SPI an attractive choice when immediate feedback and interactivity between devices are paramount.

SPI's implementation and configuration in both hardware and software are relatively straightforward. Its direct hardware control mechanism further

augments its user-friendliness, eliminating the need for complex addressing schemes (required by the I2C protocol, instead). Exhibiting outstanding performance within the bounds of a single printed circuit board (PCB) or where signal degradation and noise remain minimal, SPI emerges as a preferred communication solution for an extensive array of applications: flash memory storage, precision analog-to-digital converters (ADCs), digital-to-analog converters (DACs), real-time clocks, and various sensor interfacing tasks.

Despite its numerous merits, SPI is not without constraints. Notably, the number of slave devices a master can accommodate is inherently contingent on the availability of chip select (CS) lines. In systems integrating multiple peripherals, that could contribute to a higher pin count and increased complexity of PCB layout and design. Scaling a system to include a large number of peripheral devices demands careful strategic planning. Another downside of SPI is that avoiding a standardized addressing scheme may complicate interoperability between devices produced by different manufacturers. Comparing the negative aspects of SPI to those of I2C, the decision of the best-suited interface for the present project tilted towards the latter.

The Inter-Integrated Circuit (I2C) protocol was conceptualized and developed by Philips (now NXP Semiconductors) in the early 1980s. At its core, I2C boasts an essential architecture consisting of two bidirectional lines: the Serial Data Line (SDA) and the Serial Clock Line (SCL). This minimalist design allows for multiple devices to coexist on the same bus, giving rise to a master-slave communication paradigm (Figure 3.13).

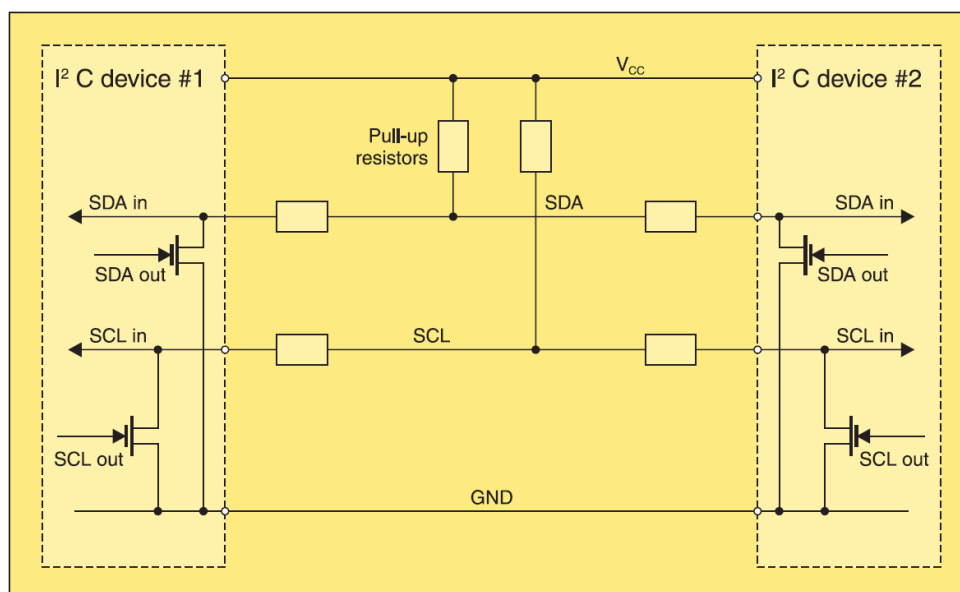


Figure 3.13 I2C bus with two devices connected. SDA and SCL are connected to VCC through pull-up resistors. Each device controls the bus lines outputs with open drain buffers⁵³.

I2C communication between a master and a slave device follows a structured sequence (Figure 3.14). The master sends a “START” condition, then transmits a 7-bit sequence corresponding to the manufacturer-chosen slave address, along with a “Write” bit to indicate a write operation. The addressed slave responds with an ACK (“Acknowledged”) bit if present. Next, the master transmits data bytes to the slave, with each byte followed by an ACK or NACK bit from the receiver. To terminate the transmission or change the addressed slave, the master may send a “Repeated Start” or “STOP” condition. For read operations, the master transmits the slave address with a “Read” bit, and the slave responds with an ACK. Data transmission from the slave to the master follows, with the receiver sending ACK/NACK bits after each byte. The communication ends with a “STOP” condition.

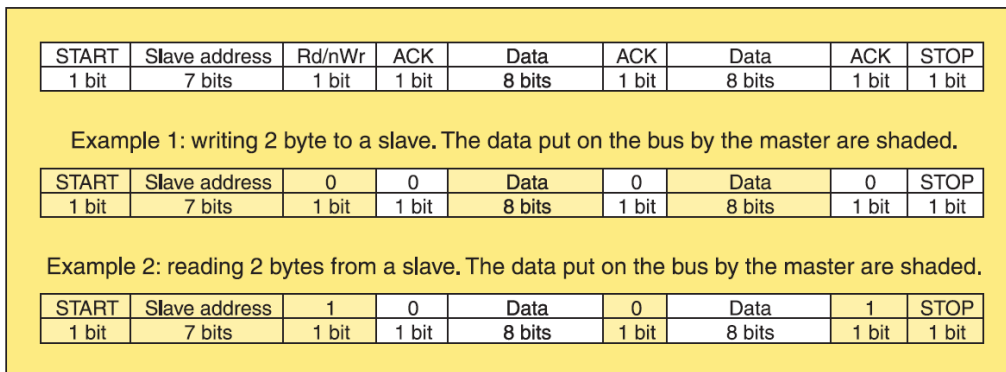


Figure 3.14 Typical I2C transfer, with 2 bytes of data⁵³.

The versatility of I2C is at the heart of its widespread application. Its ability to accommodate multiple devices without requiring an excessive number of pins makes it an ideal choice for systems with many peripherals. This attribute is particularly beneficial when resource efficiency is an absolute priority. Other advantages are its innate simplicity, which facilitates implementation and integration in various hardware and software environments, and a flexible addressing system that allows for selective communication with specific slave devices. The ACK/NACK mechanism ensures data integrity and addresses verification.

The main limitation of I2C is its restricted data transfer rate, which makes it less suitable for applications that demand high-speed data exchange. SPI outperforms I2C in this regard, but the present project worked with a very low sample rate, so the choice of I2C was not compromised. One more thing to keep in mind is that I2C protocol lacks a built-in error-checking mechanism. It relies, instead, on external error-checking resources, such as parity bits or cyclic redundancy checks (CRC) to safeguard data integrity. While these

supplementary measures are effective in detecting and correcting errors, they do introduce additional complexity, which must be weighed against the specific requirements of a given application. In the current case, that additional complexity was a “lesser evil” compared to the need of having multiple CS-SPI lines.

In summary, I2C interface was chosen over SPI because of its simpler architecture, considering the number of sensors to be managed (despite the lower achievable data transfer rate which, as previously discussed, was not a priority in the present work). Having identified the best-suited type of sensors and communication protocol, the specific models of electronic components had to be chosen and connected through switches. That is because all the sensors would have the same I2C address and, therefore, they could not be connected in series to the same line.

3.3.2.1 Sensors (Sensirion STS40)

Among all the possibilities, the Sensirion STS40 (Figure 3.15) digital temperature sensor was considered the best available option by the author. This sensor can achieve a resolution of 0.01°C and its temperature range spans from -40°C to +125°C. Such a wide range allows it to operate effectively in diverse and demanding environments, including the freezing temperatures at which footwear tests must be performed. STS40 has a response time of just 5 ms, which is ideal for real-time data acquisition. Complementing its remarkable performance is the sensor’s compact and robust form factor, measuring only 1.5 mm x 1.5 mm, and a temperature drift of merely $\pm 0.02^\circ\text{C}$ per year.

STS40 operates on a digital I2C interface, meaning that communication starts when a master device sends a signal containing the sensor’s address. As previously stated, all the sensors were identical, therefore a switch system was employed.



Figure 3.15 Sensirion STS40. Courtesy of Sensirion.

3.3.2.2 Switches (Onsemi NLHV4051)

The Onsemi NLHV4051 (Figure 3.16) is an advanced solution for signal routing within electronic circuits. As a member of the HV4051 series developed by On Semiconductor, this switch offers eight channels and is capable of handling both analog and digital signals. Its low ON-state resistance, rated at typically 20 Ω , ensures minimal signal distortion and attenuation. The switch's wide voltage range is another notable characteristic, going from -15V to +15V, more than enough to meet the requirements for low power consumption sensors like the Sensirion STS40.

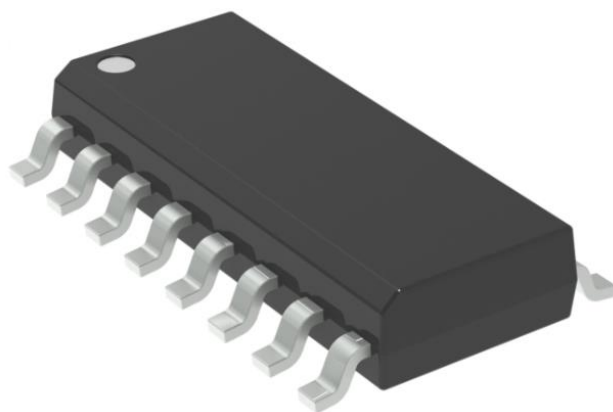


Figure 3.16 Onsemi NLHV4051. Courtesy of Onsemi.

Performance-wise, the NLHV4051 demonstrates impressive speed, with a turn-on time of 5 ns and turn-off time of 1 ns. Additionally, it has remarkable crosstalk isolation between channels: the crosstalk rejection ratio typically reaches -105 dB at 1 MHz. With a bandwidth extending up to 100 MHz, it can handle high-frequency signals with ease.

As previously discussed, the foot manikin of the present work was equipped with 16 identical temperature sensors, therefore requiring the use of two eight-channel switches. Each sensor had a dedicated SDA line connected to a pin of one of the two switches, while SCL (clock), VDD (power supply) and GND (ground) were shared among all the sensors. The role of the switches was the following: upon receiving a 4-bit signal from the master (interface device) indicating which output line had to be selected (0 to 15 in decimals), enable the connection between SDA-IN and SDA-OUT of the proper sensor, then wait until a new command was sent from the master. This simple configuration allowed for a direct and undisturbed communication between the master and one sensor at a time.

3.3.2.3 Interface device (NI USB-8452)

The USB-8452 from National Instruments (Figure 3.17) is a serial interface device tailored to precision data acquisition and control applications. It incorporates 24-bit analog-to-digital converters (ADCs), which provide high resolution and accurate measurements in a wide variety of scenarios. Its simultaneous sampling mode across all channels enables seamless synchronization and the correlation of data from multiple sources. The device is equipped with eight differential analog input channels and two analog output channels that boast a 16-bit digital-to-analog converter (DAC). This allows for a controlled modulation of analog signals, generation of dynamic output waveforms and delivery of precise voltage outputs to external devices.

Additionally, the USB-8452 has comprehensive digital I/O capabilities, featuring eight digital input and eight digital output channels, and it is equipped with a USB interface which ensures compatibility across a wide range of computers and operating systems. Its “plug-and-play” nature allows users to integrate it into their existing systems and workflows without the need for complex setup procedures.

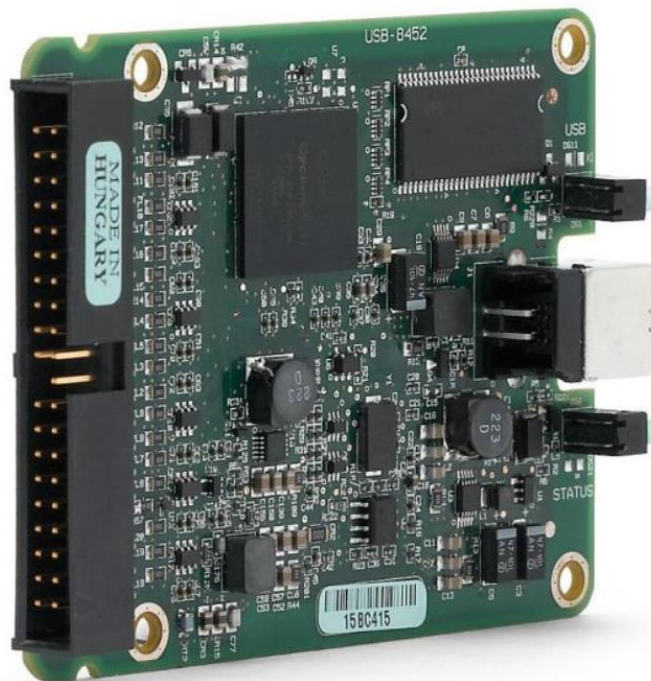


Figure 3.17 NI USB-8452 interface device. Courtesy of National Instruments.

This specific device was chosen for the present work for several reasons. First, it is

fully compatible with the user-friendly LabVIEW® graphical programming environment, being National Instruments the company behind both products. That was crucial in the early stages of the work, during which many electronics concepts still had to be fully understood by the author. Ease of learning, intuitive language and direct connectivity were the priorities for choosing the software to use, and the match between USB-8452 and LabVIEW could provide all these features. Moreover, the device supports both SPI and I2C configurations, it operates on low power consumption rates (given the 5.25 V maximum input voltage and 250 mA typical working mode current) and, lastly, it was readily available at the SportsTech Research Centre at the time of the present work.

3.3.3 LabVIEW project

LabVIEW® is a software solution developed by National Instruments. It has garnered widespread recognition for its distinctive graphical programming paradigm, which addresses the needs of system design and automation. This approach was conceived as a response to the complex demands of connecting engineers, scientists, and intricate instrumentation systems in an accessible manner. Having its roots in traditional text-based coding while at the same time introducing a graphical interface has allowed users, regardless of their programming backgrounds, to construct programs by visually connecting nodes or icons that represent data and logic pathways. This approach simplifies the programming process and accelerates prototyping, facilitating iterative development cycles.

Programming in LabVIEW centers on Virtual Instruments (VIs), modular software representations of real-world instruments or functions. A VI has two essential components: the front panel and the block diagram. The front panel provides the interface for user interaction, presenting controls and indicators, while the block diagram is the graphical depiction of the program's logic and functionality. LabVIEW offers an extensive library of predefined functions and tools that empower users to create intricate systems with basic programming knowledge, ranging from basic arithmetic operations to advanced signal processing algorithms. By dragging and connecting icons, users establish the flow of data, perform calculations, and control mechanisms. This modular, visual approach not only boosts developments but also enhances collaboration between programmers and domain experts.

In the context of the present work, LabVIEW was approached with the novice's eye. After an initial learning phase, followed by experimentation with simple test programs, the actual project started to take shape. It was defined how the

software would go through the different stages of the data acquisition process, such as: interface configuration, sensors testing, writing and reading cycles, saving to memory, etc. A flat sequence structure was chosen for containing all the portions of the program and ensuring the right timing for subsequent operations. SubVIs for each “function” of the program were created for modularization purposes. Figure 3.18 shows the front panel with all the controls and indicators the user can interact with during test measurements. The final main VI is shown in Figure 3.19, along with a three-parts enlargement (Figure 3.20) and a simplified diagram representation (Figure 3.21) for better clarity.

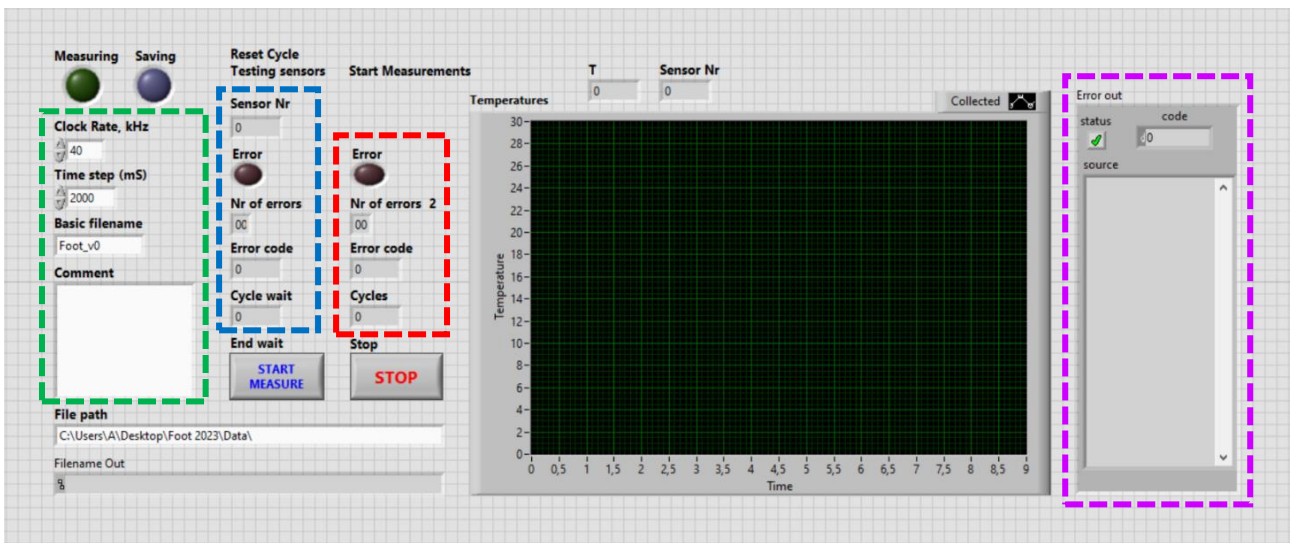


Figure 3.18 The front panel of the LabVIEW program that handles data acquisition. The green rectangle contains the input controls that must be set up before running the program. The blue rectangle contains indicators that provide information during the sensors’ testing phase. The red rectangle provides information about errors occurring during measurements. The violet rectangle on the right contains the error details window and shows a brief description of the errors that have occurred when the program was running.

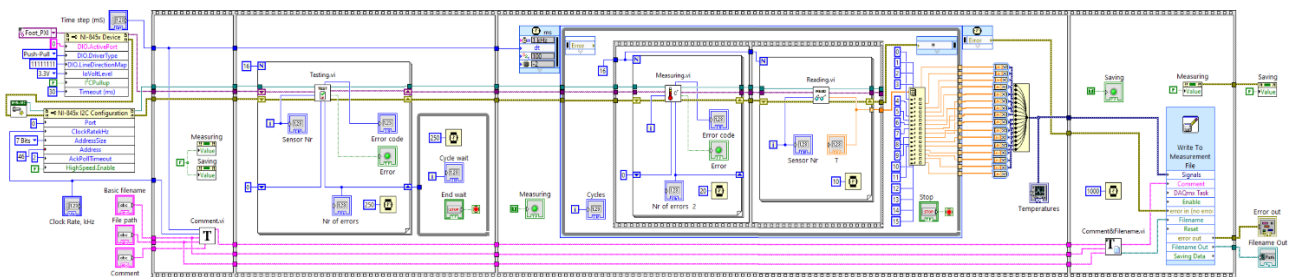


Figure 3.19 The whole block diagram of the LabVIEW program.

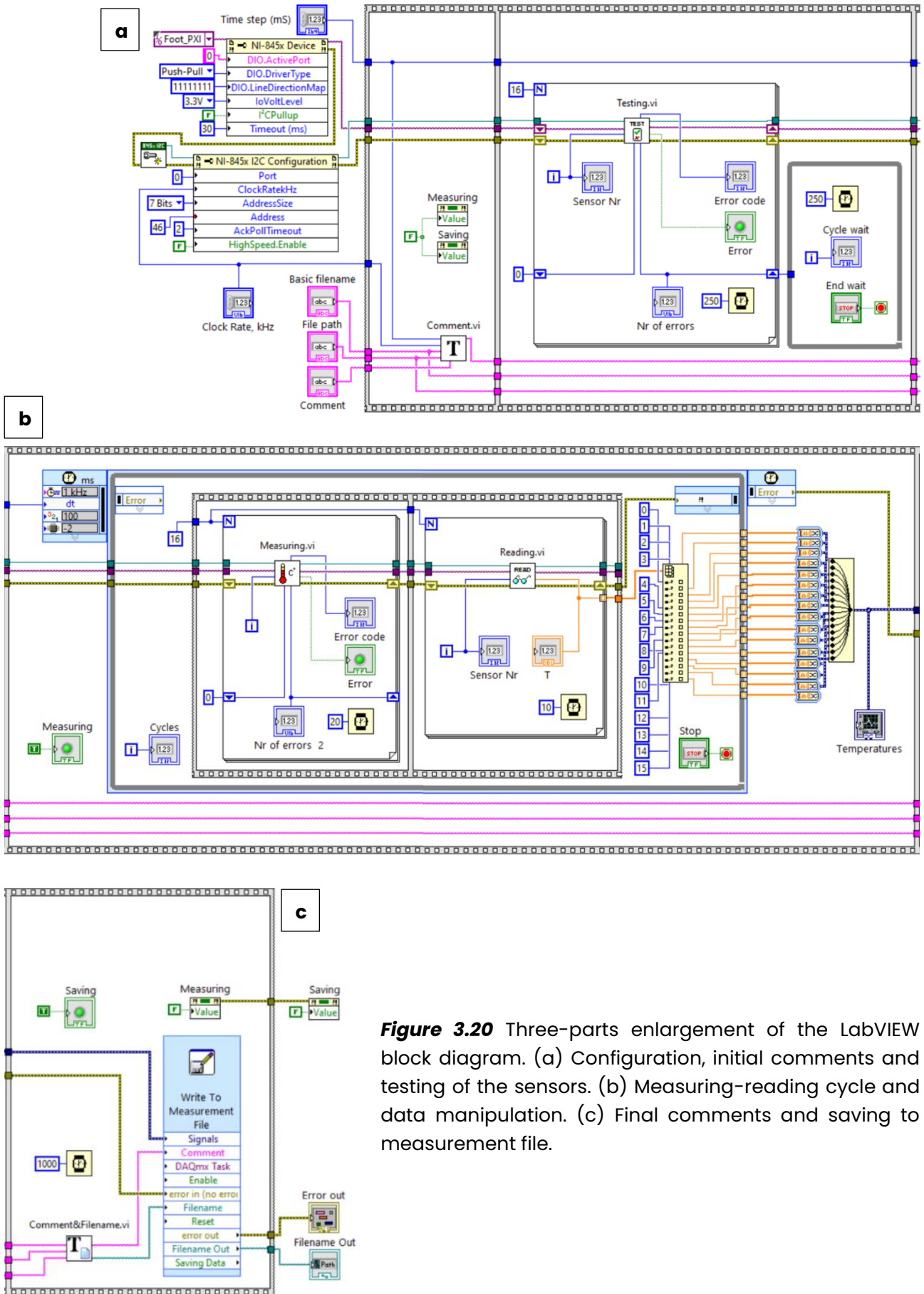


Figure 3.20 Three-parts enlargement of the LabVIEW block diagram. (a) Configuration, initial comments and testing of the sensors. (b) Measuring-reading cycle and data manipulation. (c) Final comments and saving to measurement file.

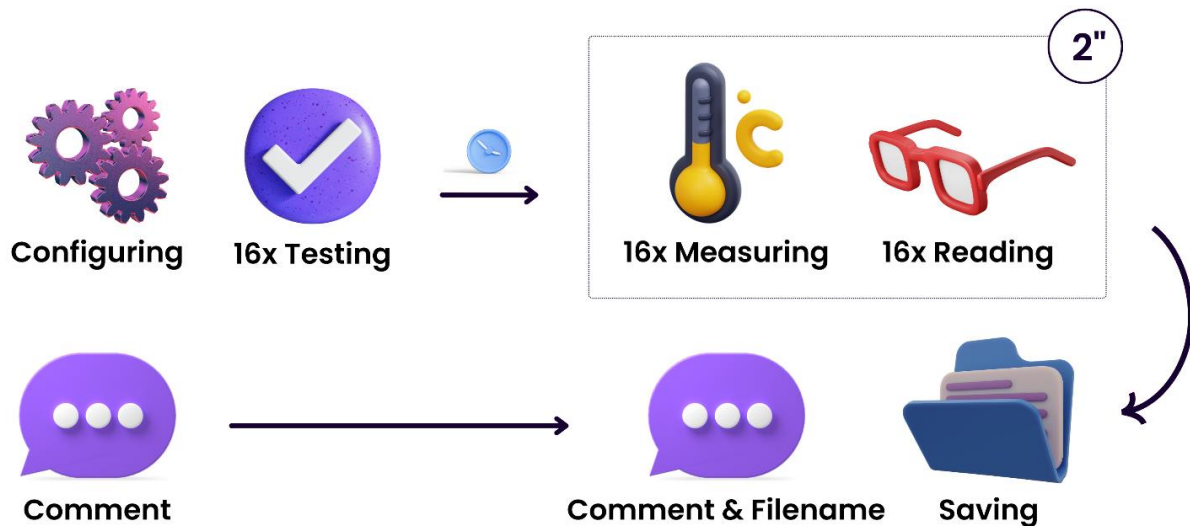


Figure 3.21 Simplified diagram of the LabVIEW program functionalities.

3.3.3.1 Main VI

The first thing to notice is that the main program has two branches that run in parallel: one manages the data acquisition process, while the other oversees building the data file and saving it. In the simplified diagram, the upper line represents the former and the lower line the latter.

The program starts with the configuration of both the interface device (USB-8452) and the selected communication protocol (I2C). Key parameters are defined in this phase:

- **DIO:Active Port:** the number of the DIO (Digital I/O) port to be activated.
- **DIO:Driver Type:** the driver type of that port, open-drain or push-pull.
- **DIO:Line Direction Map:** a set of bits that specifies the function of each individual line within the port, "1" being output and "0" being input.
- **I/O Voltage Level:** the board voltage for SPI, I2C and DIO.
- **I2C Pullup:** enables/disables the internal pullup resistors to SDA and SCL.
- **Timeout (ms):** the maximum number of milliseconds an I2C, SPI, or DIO operation is allowed to complete.
- **Port:** the I2C port that this configuration communicates across.
- **ClockRatekHz:** the I2C communication clock rate.
- **AddressSize:** the addressing scheme to use when addressing the I2C slave device related to this configuration (7 or 10 bits).
- **Address:** the I2C slave device address, given by the manufacturer.
- **AckPollTimeout:** the I2C ACK poll timeout in milliseconds.

Note that all the parameters are set to constant values except for the clock rate, which is adjustable through its corresponding control element in the front panel. Same goes for the time step of the “measuring-reading” cycle (i.e. the data acquisition sampling rate) that will be discussed later, and for:

- **Basic filename:** the initial string from which the file name will be built.
- **File path:** the position on the computer where the data file will be saved.
- **Comment:** the user’s notes that will be added to the comment section of the data file.

The program then continues by entering the first frame of the flat sequence. At this level, virtual LEDs called “Measuring” and “Saving” are turned off and the initial comment section of the data file is built using string concatenations (see more details in 3.3.3.2 *Comment SubVI*). It will be retrieved in the last frame of the sequence for adding the final comments.

The second time frame hosts a FOR cycle (N=16) responsible for checking if all the 16 sensors work properly. Every iteration, it selects one sensor to test and sends a request to acquire data. If the sensor does not acknowledge the command, the error status is set on TRUE, error counter is increased by one, “Error” virtual LED is turned on and the corresponding error code is shown. A delay of 250 ms is set between each iteration of the test cycle and, at the end of it, the program goes into a waiting WHILE cycle until the “End wait” button (labeled “START MEASURE” in the front panel) is pressed.

Moving on to the third time frame, the virtual LED “Measuring” is turned on. In fact, the timed loop inside this frame represents the data acquisition phase and contains two subsequent FOR cycles (N=16) that, respectively:

- send a measurement request to each of the 16 sensors;
- read the temperature detected by each of the 16 sensors.

This timed loop, which was earlier called “measuring-reading cycle”, has an iteration duration equal to the time step set at the beginning of the program, and goes on until the “Stop” button is pressed. Note that there is a 20 ms delay between each iteration of the measuring cycle and a 10 ms delay between each iteration of the reading cycle. Those delays allow the switches to change connections from one sensor to another without the risk of interfering with data signals and give the sensors enough time to acquire and store temperature values before reading them. Also, notice that the measuring cycle has an error checking system analogue to the test cycle’s one (more details in 3.3.3.4

Measuring SubVI).

After being converted from a raw 16-bit binary sequence to a decimal value in Celsius scale (see 3.3.3.5 *Reading SubVI*), temperature data from each of the 16 sensors is stored separately in 16 indexed arrays. That is realized using the “Index Array” function, which extracts all T values from the 16-elements array generated every iteration of the timed loop, and the “Indexing” tunnel mode, which saves each T value in the i-th position of a corresponding array. A visual representation of the data storage process is given in Figure 3.22.

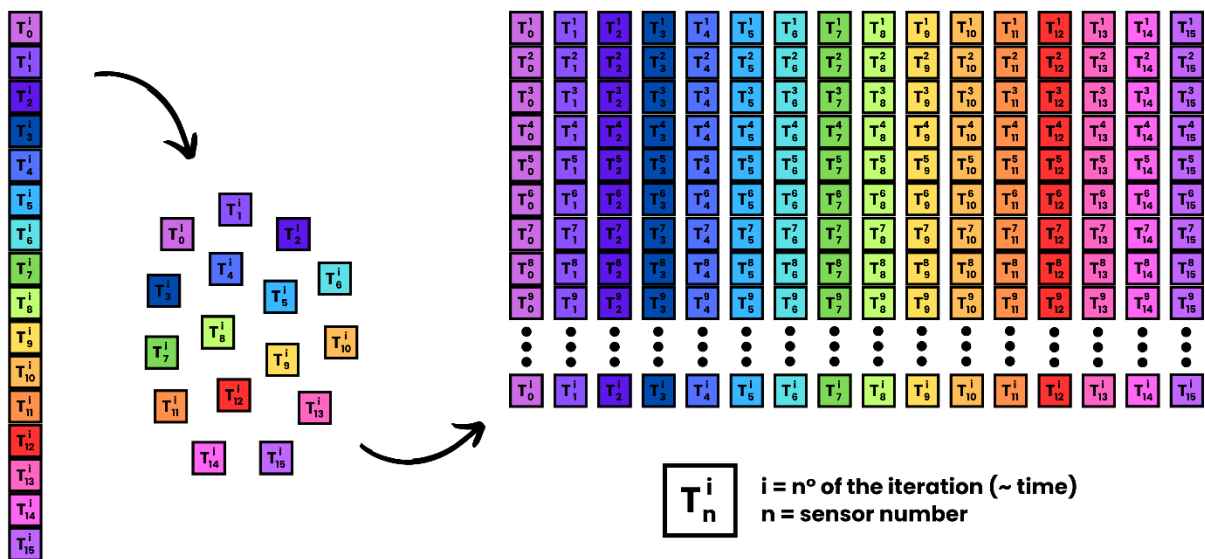


Figure 3.22 Reorganization of data for storage and saving.

When the “Stop” button is pressed, the timed loop ends, and all the data arrays will have a size equal to the number of performed iterations (N). The 16 1D-signals are then merged into a (16xN) dynamic data matrix and plotted as 16 curves on a single temperature–iterations waveform graph. Put simply, this graph is a visual representation of the temperature variations that have occurred to each sensor during the measurement. Information on heat loss in different parts of the foot is derived from this graph. The time to reach a certain temperature and the derivative of the temperature–time curve of each sensor will be indicators of the level of thermal insulation provided in the corresponding region of the foot.

The time sequence’s last frame hosts the saving elements of the program. First, the LED called “Saving” is turned on and “Measuring” is turned off. Final comments are added to the data file and its path, which will be the location of the file on the computer, is built (see 3.3.3.6 *Comment&Filename SubVI*). Using the “Write to Measurement File” Express VI, the data file is finally assembled and saved as LVM. The “LabVIEW Measurement” (.lvm) format is a text-based file format for one-

dimensional data used with the “Read/Write to Measurement File” Express VIs. When imported into a text editor such as Notepad or a spreadsheet tool such as Microsoft Excel, the LVM file is designed to be easy to analyze and understand. It facilitates adding new data sets to existing files, as well as grouping and combining data sets. Like all text-based formats, LVM is not intended for high performance or very large data collections. Because saving can be almost instantaneous, the program waits 1000 ms before turning the “Saving” LED off and displaying the full file name on the front panel to check for errors.

3.3.3.2 Comment SubVI

This SubVI (Figure 3.23) builds through concatenation an initial comment string that will be added to the data file. Automatically added information are starting time, time step of the timed loop, I2C clock rate. Time is taken from the computer’s internal clock. Manually added information are the basic file name, its computer path and a free comment of the user.

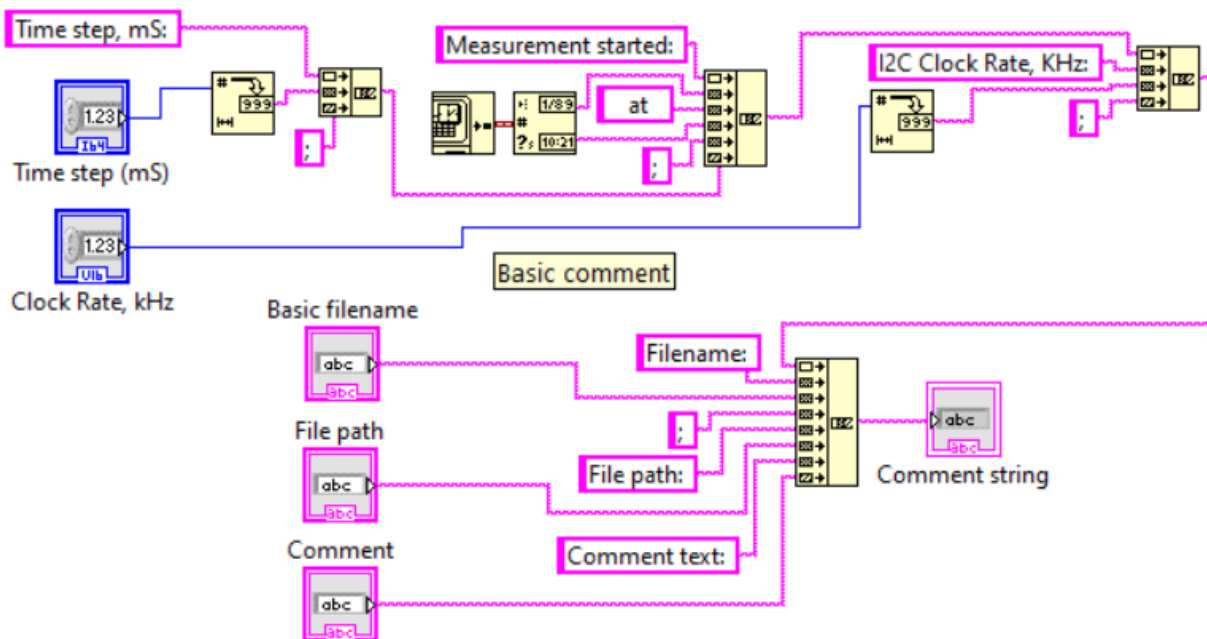


Figure 3.23 LabVIEW block diagram of the “Comment” SubVI.

3.3.3.3 Testing SubVI

First, this SubVI (Figure 3.24) writes an 8-bit sequence to DIO port number (0) of the USB-8452. The three most significant bits of this sequence are associated with the color of a LED on the device (**100** = Blue, **010** = Red, **001** = Green), the fourth bit

is always 0 and the last four digits represent the number of the channel that must be activated by the switches (from **0** to **15** in decimals). The role of the “DIO Write Port” function is, therefore, to establish a communication with one specific sensor. Being iterated 16 times, this portion of the program will always select a different sensor, since the “Counter” variable is connected to the cycle counter index in the Main VI.

The second part of this SubVI is responsible for asking the sensor to acquire a test measure. As written in the datasheet of the Sensirion STS40⁵⁴, hex command “F6” corresponds to “measure T with medium precision (medium repeatability)”, which is more than sufficient for testing if the sensor is working. This signal is sent to the sensor through the function “I2C Write” which also requires, as an input, information regarding the I2C configuration.

As for the outputs, this SubVI must be able to tell if something is wrong with the sensor and, in that case, give more details about the errors that have occurred. Therefore, both the error status and code must be displayed on the front panel. Additionally, if an error has been encountered, a variable called “Err counter” (shown on the front panel as well) is increased by one.

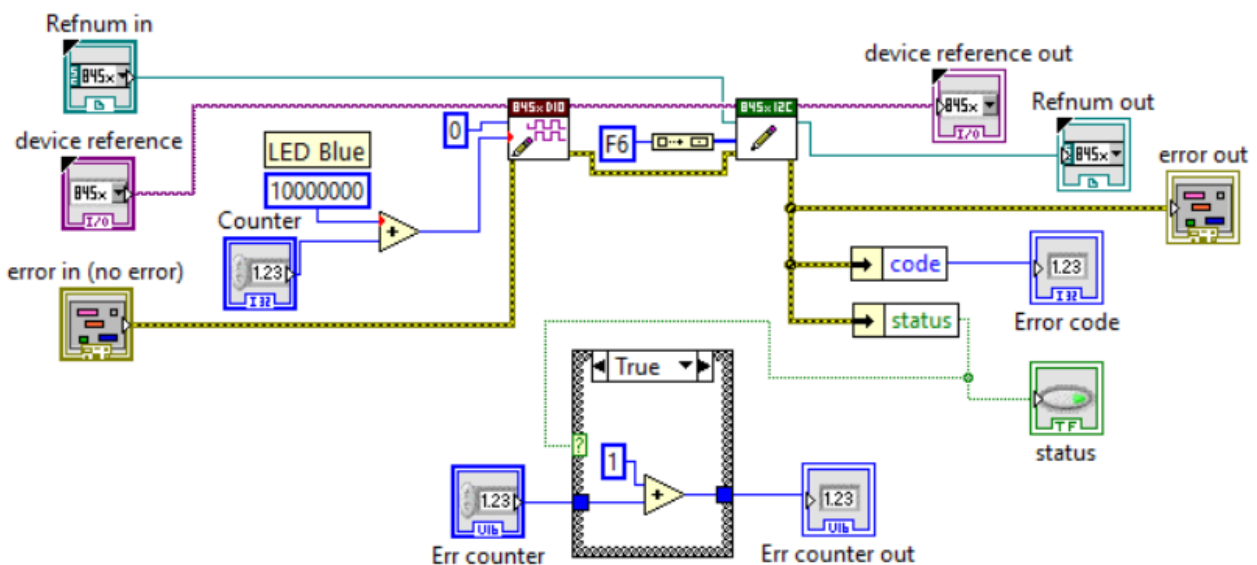


Figure 3.24 LabVIEW block diagram of the “Testing” SubVI.

3.3.3.4 Measuring SubVI

This SubVI (Figure 3.25) is conceptually analogue to the previous one, “Testing”. In fact, it establishes a connection with the *i*-th sensor and sends a request for acquiring temperature measure, both actions using the same functions as before. The only differences are the following:

- the LED on USB-8452 is turned on green instead of blue, to distinguish between testing phase and actual measurements;
- the sensor is asked to measure temperature with high precision (“FD”, see specifications⁵⁴) instead of medium precision.

Outputs shown on the front panel are analogue to the testing ones. In this way, errors during measurement can be identified and distinguished from test errors.

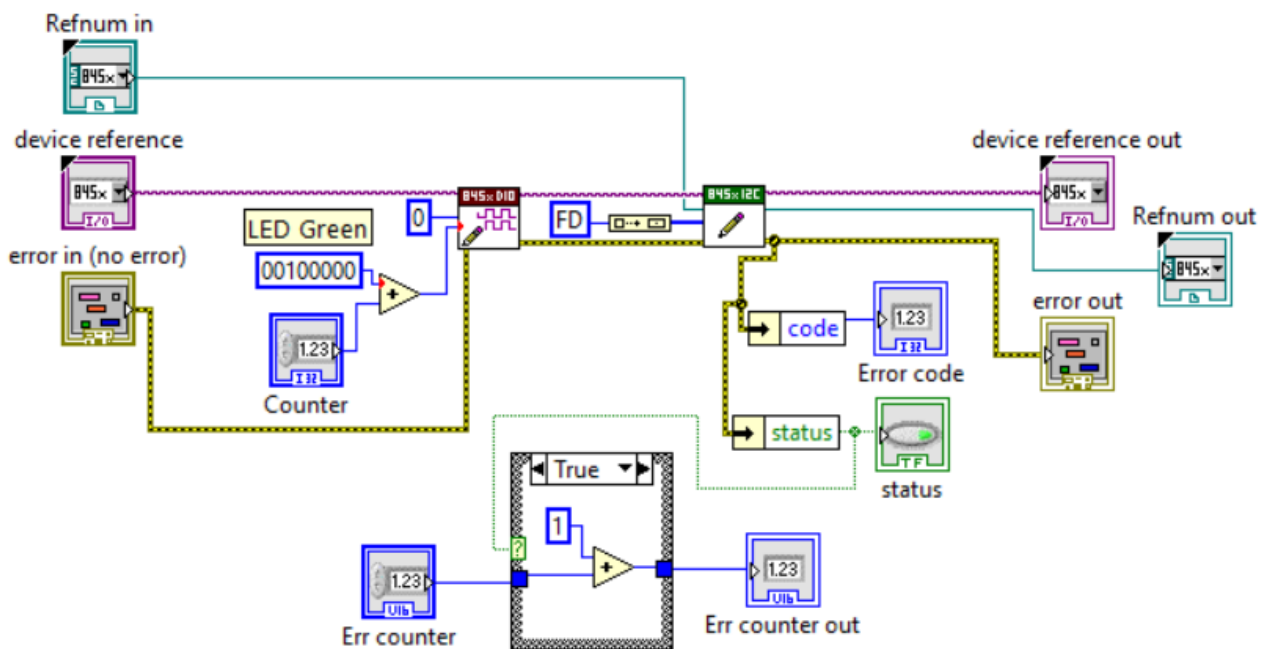


Figure 3.25 LabVIEW block diagram of the “Measuring” SubVI.

3.3.3.5 Reading SubVI

This SubVI (Figure 3.26) starts with sensor selection, in the same way already seen in “Testing” and “Measuring” SubVIs. This time, LED on the USB-8452 is turned on red. The second part revolves around the “I2C Read” function, which is responsible for reading an array of data from the sensor. The constant input “3” indicates the number of bytes that must be read from the sensor, in fact:

- two bytes represent the temperature value;
- one byte is the checksum (CRC, “Cycle Redundancy Check”).

The 3-bytes sequence read from the sensor is then mathematically converted to a decimal value expressed in Celsius degrees (see Eq. 1 in chapter “4.5 Conversion of Signal Output” of the sensors’ datasheet⁵⁴) and transferred to the next stages of the program.

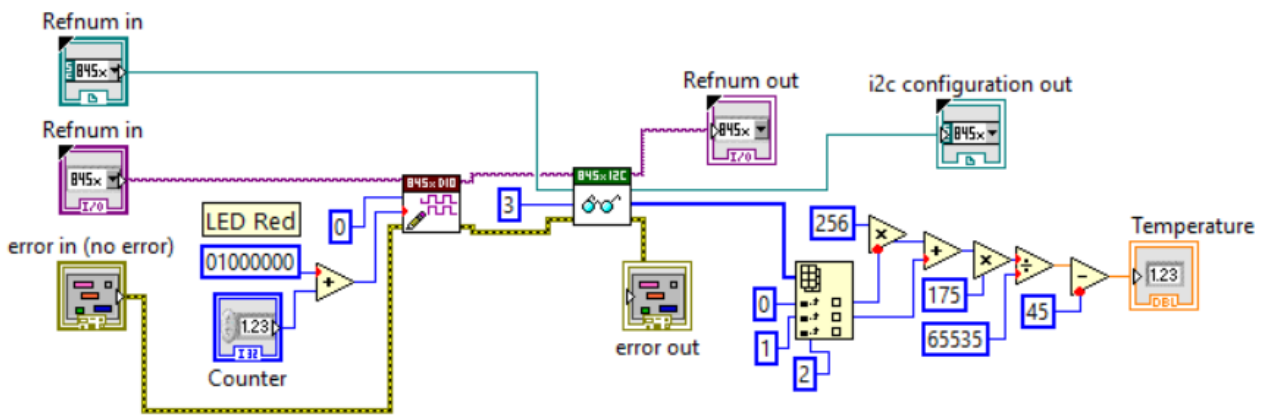


Figure 3.26 LabVIEW block diagram of the “Reading” SubVI.

3.3.3.6 Comment&Filename SubVI

This SubVI (Figure 3.27) takes as inputs the initial comment string created in “Comment” SubVI, the basic file name and the computer path and outputs the final comment string and a path element that will be used by “Write To Measurement File” Express VI to save the data file in the proper position. Automatically added information are the finishing time taken from the computer internal clock and the data structure of the file. An example of the output raw data file is given in Figure 3.28, along with an enlargement focused on the header of the file. Unfortunately, the comments are written on a single line coming out of the window on the right, so they are not visible in the image.

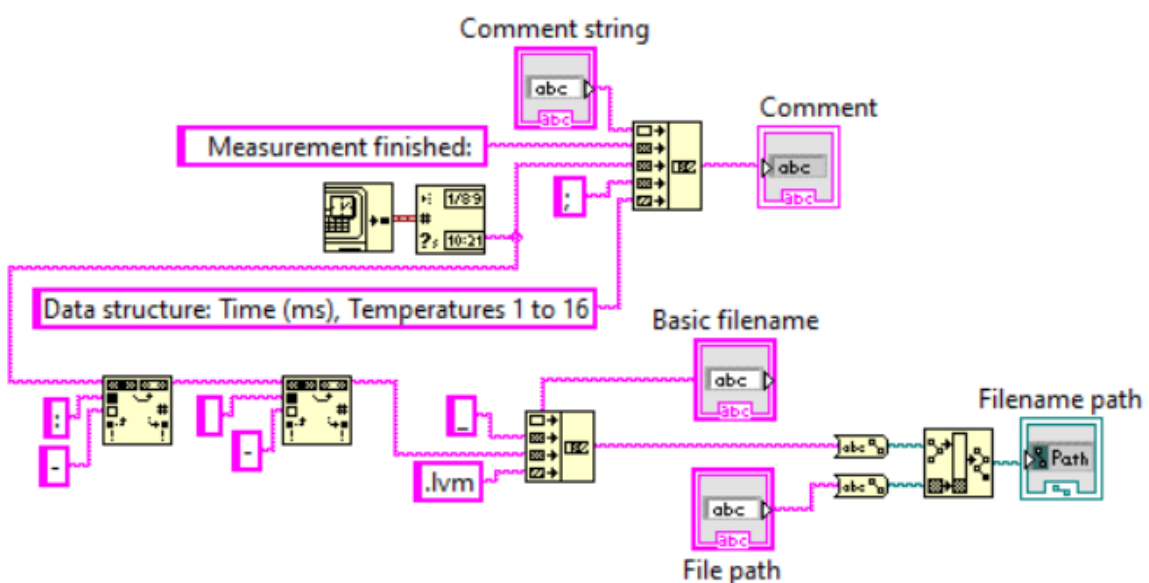


Figure 3.27 LabVIEW block diagram of the “Comment&Filename” SubVI.

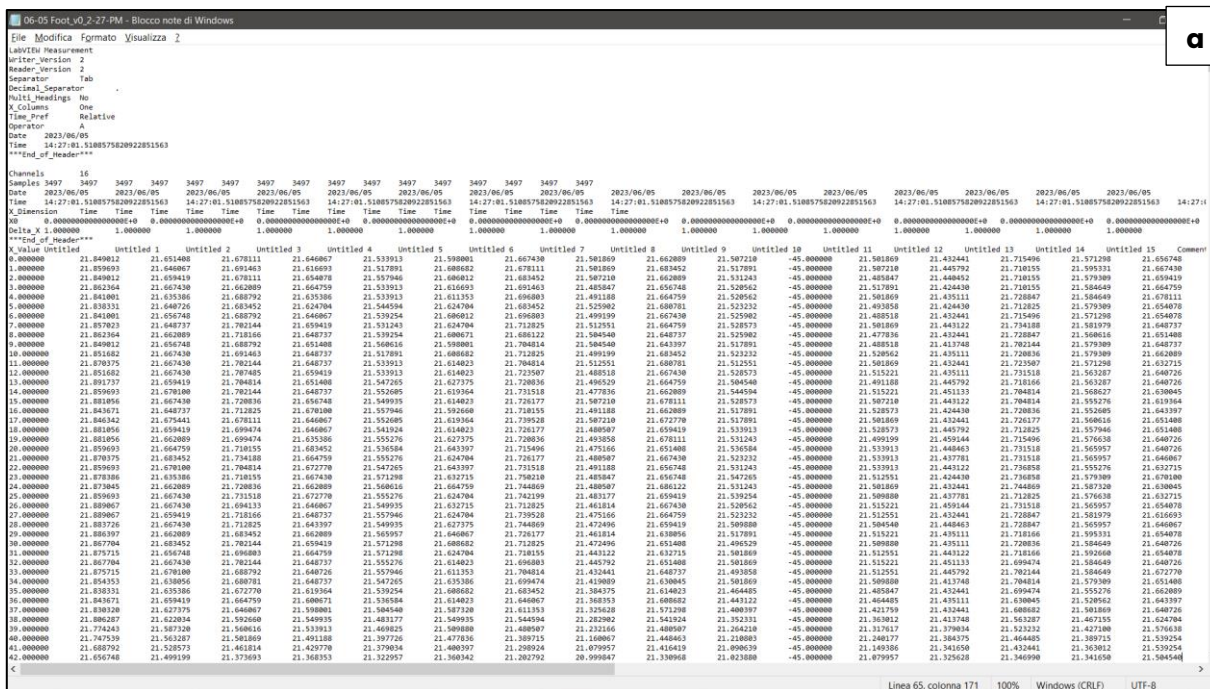


Figure 3.28 Example of file containing the output raw data.
(a) Original, (b) Enlargement on the header section.

3.3.4 Procedures and tests

Once the foot shell was 3D-printed and the electronic system was built, the manikin was finally ready for being tested. The exact test procedure had to be defined, including the following parameters:

- initial core temperature of the manikin;
- environment (temperature, humidity, air velocity);
- time of exposure/temperature to reach;

- eventual “default” layer (i.e. sock);
- contact with floor and walls.

As previously discussed, most thermal manikins described in scientific literature are actively heated up to 34 °C and the tests are performed at constant temperature, while the manikin of the present work is only passively heated and tested in continuous cooling condition. The literature also provides some information on the typical thermal thresholds of the foot:

- $T_{\text{skin}} \sim 33 \text{ °C}$: comfortable¹¹
- $T_{\text{skin}} \sim 25 \text{ °C}$: cold feeling¹⁴
- $T_{\text{skin}} \sim 20 \text{ °C}$: cold discomfort¹⁴
- $T_{\text{skin}} \sim 15 \text{ °C}$: pain⁵⁵
- $T_{\text{skin}} \sim 7 \text{ °C}$: numbness⁵¹

Additionally, EN ISO 20344 standard for protective footwear testing states, as a general guideline on conditioning before and during tests, that “all test pieces shall be conditioned in a standard atmosphere of $(23 \pm 2) \text{ °C}$ and $(50 \pm 5) \text{ \% RH}$ for a minimum of 24 h before testing, unless otherwise stated in the test method.” It then specifies that “where the testing in conditioned atmosphere is required, the maximum time which shall elapse between removal from the conditioning atmosphere and the start of testing shall not be greater than 10 minutes, unless otherwise stated in the test method.”

Given all these premises, it was decided to carry out the first tests with the manikin shell filled with water at room temperature. They would return no information about the comfortable–cold feeling region but, more interestingly, would investigate what happens at lower temperatures of the foot, where discomfort and pain emerge. Also, for the purpose of understanding which parts of the foot cool down faster, the initial core temperature is a relatively insignificant variable since what matters is only the relative comparison between different foot regions’ cooling rates.

Regarding the environment, consistent parameters had to be maintained across multiple tests if the aim was comparing footwear with different levels of thermal insulation. As will be seen later in the discussion, only freezer tests were performed although other possibilities were also considered. This limited the variety of data to analyze and prevented the possibility of conducting similar tests with human subjects to compare the results of the two. However, using a freezer environment allowed for keeping constant temperature at $(-40 \pm 1) \text{ °C}$ and negligible air velocity and absolute humidity (since the amount of water vapour air can retain

decades exponentially as temperature decreases). It was further hypothesized that the freezer was large enough to be unaffected by any temperature change. To make sure that meaningful data was acquired, the tests had to be long enough to ensure that each part of the foot manikin went “numb” ($< 7\text{ }^{\circ}\text{C}$). The graph on LabVIEW only appeared after ending the measurements, so the temperature numerical indicator on the front panel was monitored instead. The tests were ended when all sensors detected $T < 1\text{ }^{\circ}\text{C}$.

The addition of a “default” layer around the foot shell was deeply discussed. That would be, in its simplest form, a liner or a thin sock put on the manikin and never taken off. This layer would ensure wires protection during the insertion of the foot into a shoe or from direct contact with cold surfaces. However, it would be an impediment when testing shoes that require the use of specific socks. Ultimately, it was decided not to use a default sock but to test the manikin as needed with the sock chosen for a specific shoe and then subtract the thermal insulation contribution of the sock from the “sock plus shoe” test results.

Contact with cold surfaces was considered a significant variable to investigate, so freezer tests were performed in both the following conditions:

- a. Sole of the foot manikin at contact with freezer floor (direct contact or separated by sock/shoe sole depending on what garment was tested);
- b. Sole of the foot manikin standing on wooden spacers (not done if footwear was being tested).

Following this approach, it was possible to evaluate the effects of conductive heat transfer from the foot sole area to the ground.

3.3.4.1 Heat loss measurements in freezer

The procedure for freezer tests started with putting the proper garments on the foot manikin. In the present work, four configurations were tested:

- **“Bare”**: manikin without any add-on layers;
- **“Liner”**: manikin with a thin sock, usually wore under a wool sock in boots;
- **“Liner + Sock”**: manikin with a liner and, on top of that, a wool sock;
- **“Liner + Slipper”**: manikin with a liner, wearing a slipper.

Specifications of liner and wool sock used in the tests are described in Table 3.3, while the socks themselves and the slipper are visible in Figure 3.29.

Sock type	Liner knee-high	Wool sock knee-high
Weight	175 g/m ²	450 g/m ²
Weaving	Plain knit	Terry loop knit
Gauge (mesh density)	24 loops/in	36 loops /in
Material composition	60% wool 35% polyamide 5% Elastane	64% wool 35% polyamide 1% Elastane

Table 3.3 Socks specifications from the manufacturer.



Figure 3.29 The foot manikin in four different configurations. From left to right: barefoot, wearing a liner, wearing a sock on top of a liner, wearing a liner and a slipper.

As stated earlier, if the manikin did not wear any footwear, it would have been tested both at contact with the freezer floor and with wooden spacers (Figure 3.30). Therefore, the tested conditions were seven in total, and are shown in Table 3.4. No shoes were tested because, as will be better discussed later, the manikin shell was designed with a relaxed forefoot that could not fit any normal-sized closed footwear.



Figure 3.30 Wooden spacers used in the tests. Approximate dimensions 100x60x35 mm.

	Contact with freezer	Wooden spacers
Bare	Yes	Yes
Liner	Yes	Yes
Liner + Sock	Yes	Yes
Liner + Slipper	Yes	No

Table 3.4. Configurations tested (Yes) and not tested (No).

Once the manikin was properly dressed, water was poured into the empty foot shell until the entire available volume (1800 cm³, see 3.2.2 *Materials and 3D-Printing*) was filled. Then, the opening was sealed and the manikin was left in the laboratory overnight to reach equilibrium temperature with the room.

The day after, the electronics were connected to a laptop from which the LabVIEW program was launched. After checking that all the sensors were working, the “START MEASURE” button was pressed. The manikin was shortly thereafter placed inside the freezer and, from then on, its temperature was monitored. At the end of the test, the data file was saved, the manikin was removed from the freezer, let defrost and emptied of the water contained within it.

3.3.4.2 Comparison with real foot heat loss

Freezer tests should have been followed by a series of field tests aimed at comparing cooling rates of the manikin with cooling rates of a real human foot in the same environmental conditions. The results of these tests would have shed light on the differences between a passively heated model and an actively thermoregulated piece of the human body, with guidance on how to modify the manikin to better replicate the local properties of the foot.

These tests were not performed for the following reasons: the sensorized sock that was intended to be used for the purpose was not ready at the time of the present work, and the weather conditions were far from the freezing temperatures needed for the tests. However, they remain part of future developments, therefore the dedicated section of this work (4.4 *Personal experience and Future developments*) contains some suggestions on the procedure that could be followed.

3.3.4.3 Footwear thermal insulation tests

The final goal of the present work was to build a foot manikin system able to

determine the level of thermal insulation of any kind of footwear. The first candidates for testing were two mountaineering boots for cold environments: the MEINDL® Dovre Extreme MFS and the SCARPA® Phantom Tech (Figure 3.31). Other useful candidates for thermal insulation tests would have been found among safety shoes and military boots.



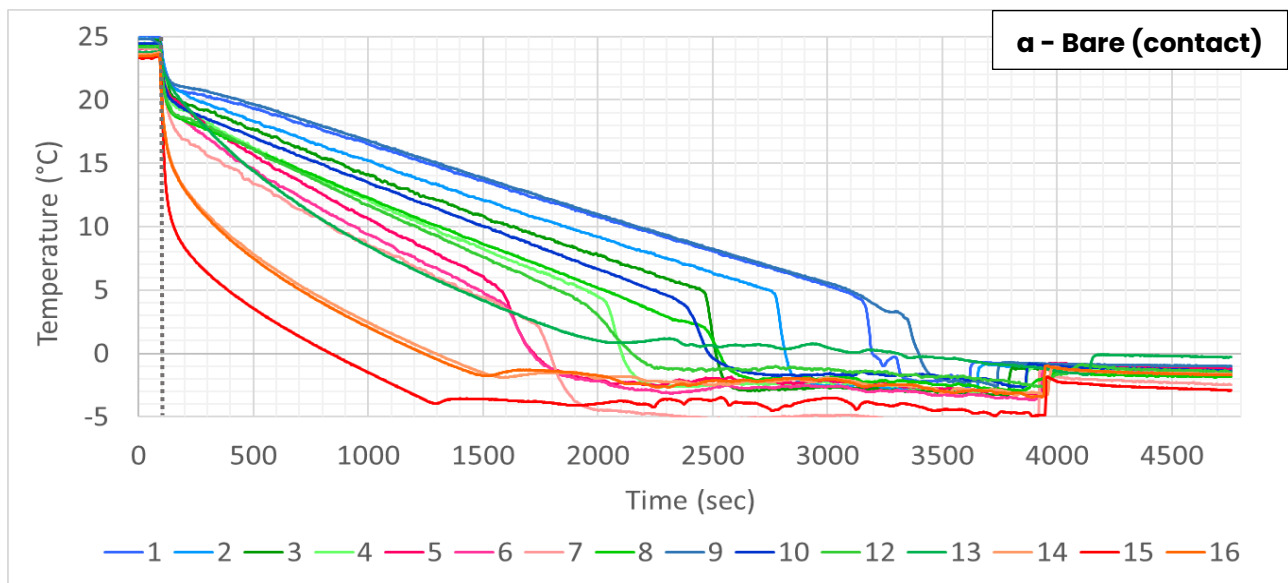
Figure 3.31 Footwear candidates for future tests. SCARPA® Phantom Tech on the left, and MEINDL® Dovre Extreme MFS on the right.

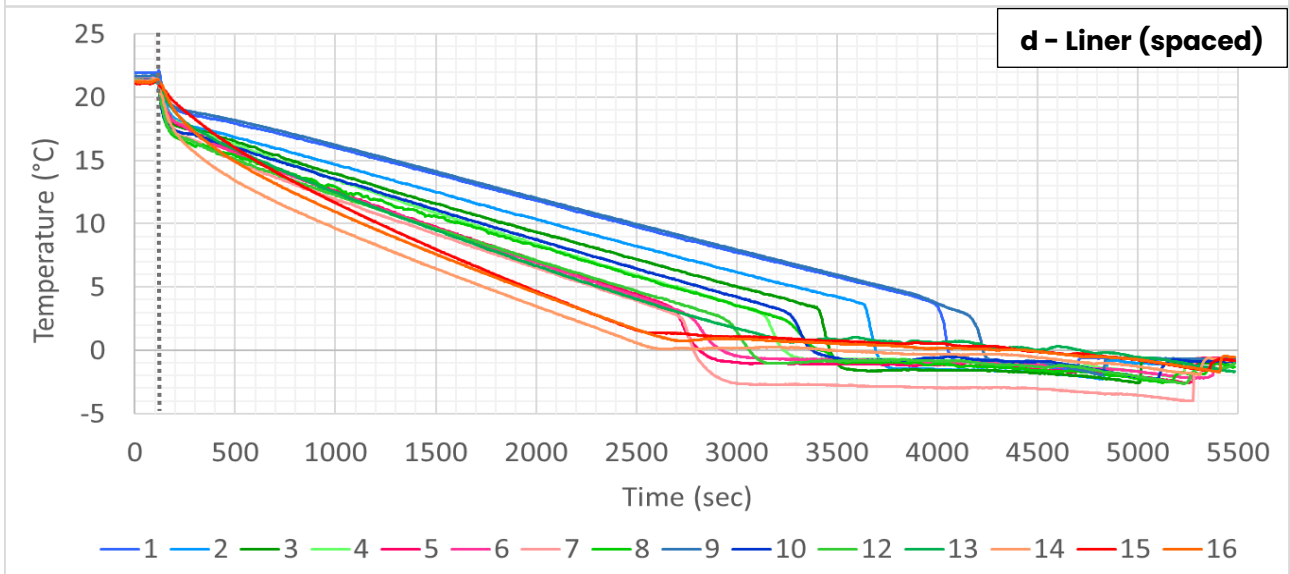
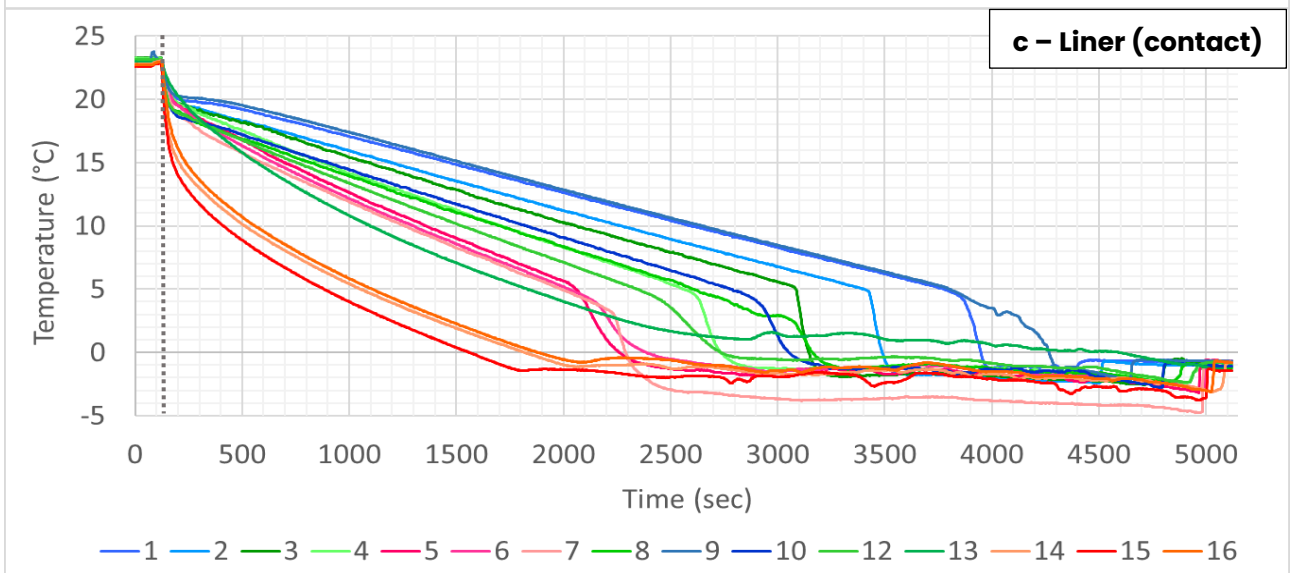
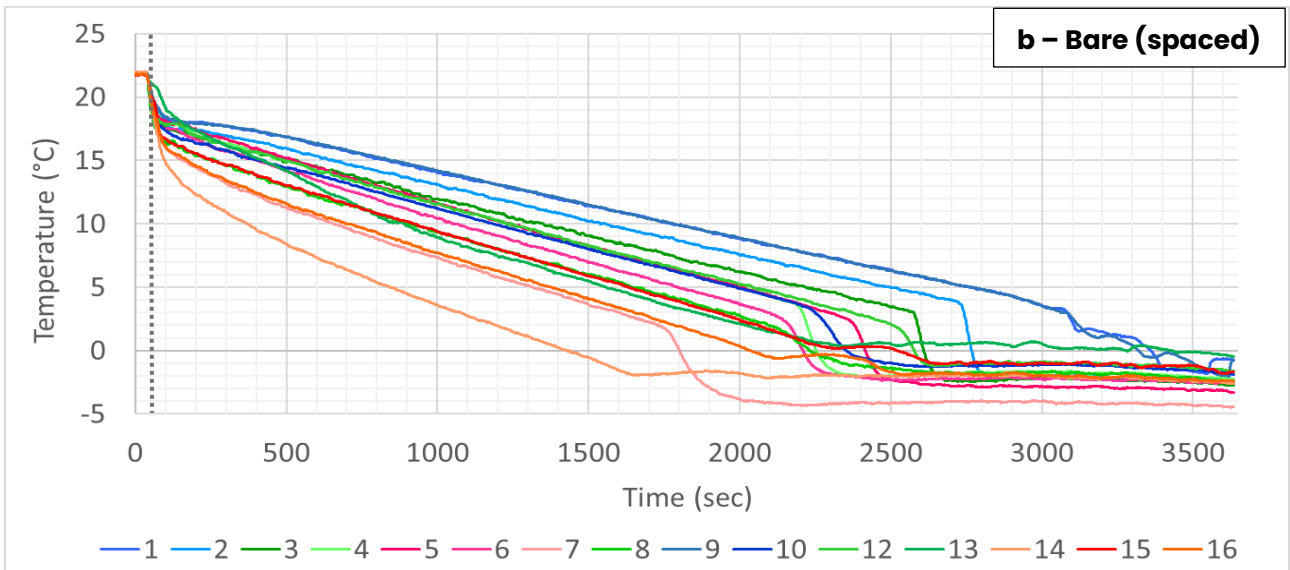
Unfortunately, being the first iteration of this kind of project, the manikin was sized in such a way that it was nearly impossible to fit inside a closed footwear without damaging the shoe or the shell itself. The forefoot was too large compared to that of a human foot when compressed inside a shoe, and the polyamide is too stiff to accommodate for such large deformations. Needless to say, the only way to overcome this problem is through a redesign of the manikin shell (4.4 *Personal experience and Future developments*) that shall take into account the compact form human feet adopt when inserted into shoes.

4. Results and discussion

4.1 Cooling rates at different points of the foot manikin

Figures 4.1a to 4.1g show the temperature-time plots corresponding to the seven experiments performed in this work. Each curve (color) represents the cooling detected by a sensor, whose number corresponds to a specific point on the foot shell (shown in Figure 4.3). Shades of red indicate the sensors on the toes (n. 5-6-7-14-15-16), shades of green the middle foot (n. 3-4-8-12-13), and shades of blue the ankle and leg area (n. 1-2-9-10). Notice that sensor number 11 (bottom heel) was never included in any result because the device stopped working during the first test. The dashed vertical gray line defines the start time of the experiment, that is, the time when the foot was placed in the freezer. Figure 4.2 is a compact representation of the first six experiments (excluding "Liner + Slipper" test) to qualitatively appreciate the differences between the various socks configurations. On the y-axis is the temperature ($^{\circ}\text{C}$) and on the x-axis is the time in seconds. The temperature sampling rate was always kept at 0.5 Hz. Data were extracted from the LVM files created through the "Write to Measurement File" Express VI, imported into Microsoft Excel and then plotted as seven separate temperature-time graphs.





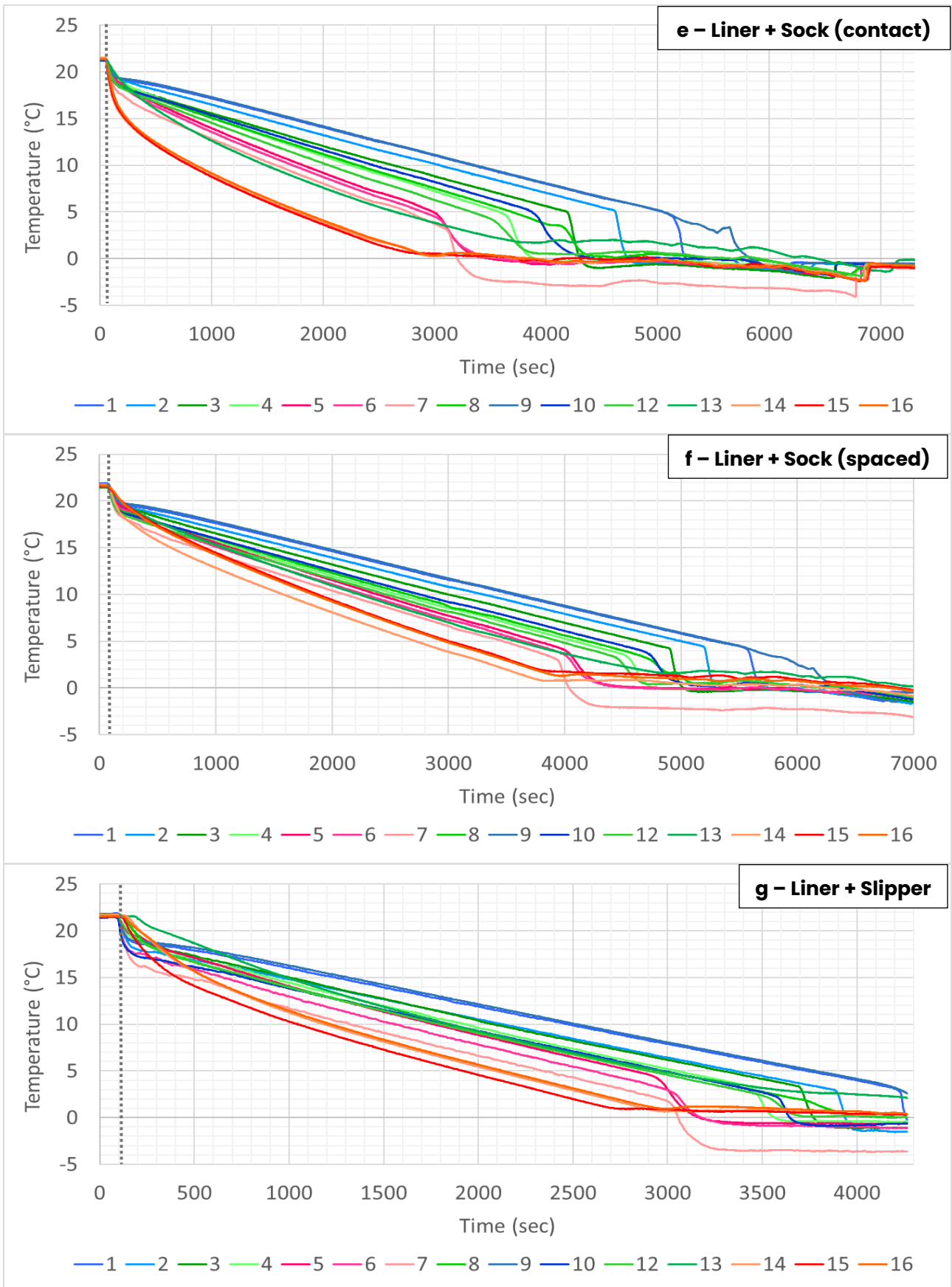


Figure 4.1 Temperature-time graphs corresponding to each configuration tested. Notice the different time scale on the x-axis and the sensors numbers from 1 to 16, missing n. 11 due to technical failure.

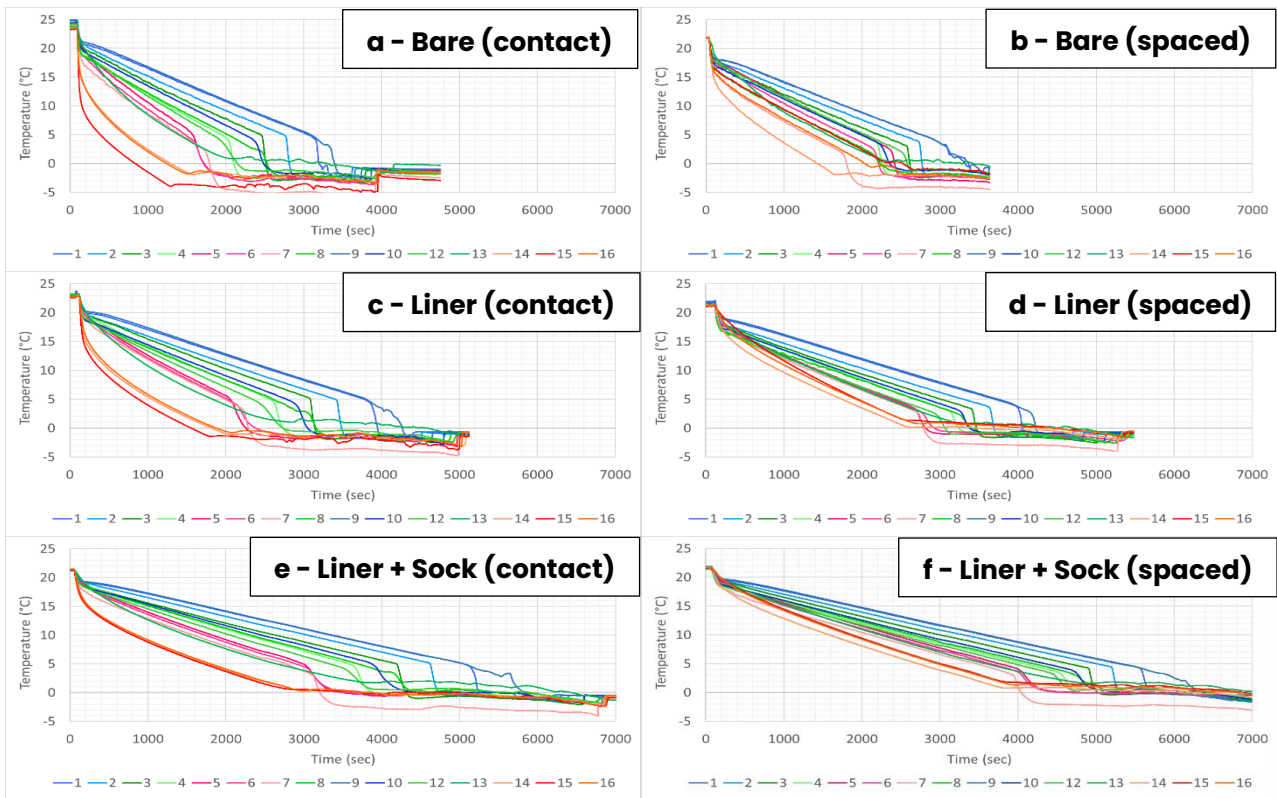


Figure 4.2 Compact representation of bare and socks configurations for an easy qualitative comparison. Time scale on the x-axis has been standardized.

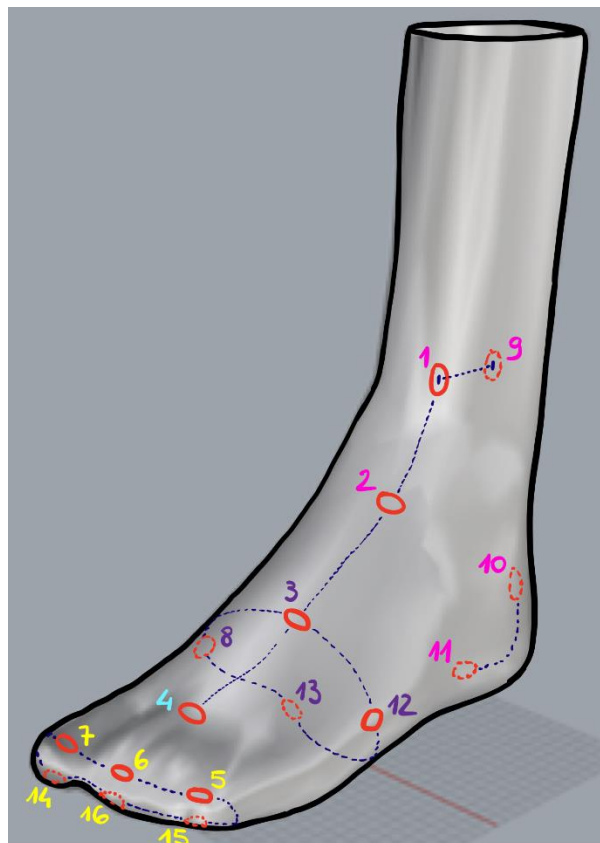


Figure 4.3 Sensors' positioning and numbers.

One important thing to point out about the above graphs is that they show that the temperature acquisition system was sensitive enough to discriminate between different foot areas and levels of thermal insulation of the manikin, i.e., bare foot, liner, and liner plus wool sock. Going from the worst cold-protective configuration to the best one, the cooling curves qualitatively move to the right, i.e., to longer cooling times, for each sensor. Their slope decreases, symbolizing a slower cooling speed, and this effect is more pronounced in the sensors placed on the foot sole than the other ones. This achievement shows that the components of the measurement system and the parameters set (temperature gradient, sampling rate, etc.) worked in good synergy to provide meaningful data. For the “bare foot” configuration, it is worth noting that the average initial temperature of the test in contact configuration was 24.1 °C, while the test with wooden spacers started with an approximate temperature of 21.7 °C. This explains why the curves in Figure 4.2b, despite having a smaller slope than the ones in Figure 4.2a, reach freezing temperatures after a similar amount of time (as will be shown in more detail in *4.2 Thermal insulation values*).

Each cooling curve can be interpreted by considering three segments:

- I. **Acclimation**, a quasi-instantaneous drop of ~4 °C from initial room temperature to a temporary stable value (although some sensors show a regular change in slope, making it difficult to demarcate the end of this first stage). Heat loss from the outer shell in this phase is extremely high because the polyamide from which the manikin shell is made has a low specific heat capacity ($\sim 1.7 \text{ J g}^{-1} \text{ K}^{-1}$), so it must dissipate little energy to decrease its own temperature by one unit.
- II. **Steady-state cooling**, a linear temperature change from the acclimatized value to the onset of freezing. In this stage, heat is transferred from the water to the surrounding environment through the manikin shell at a constant rate. If the sensor is placed on the foot sole, in contact with the freezer floor, this phase is absent, and heat dissipates rapidly following an exponential trend. Conversely, if wooden spacers are used, the sensors on the foot sole behave more similarly to those in other zones. Water has a high specific heat capacity ($4.186 \text{ J g}^{-1} \text{ K}^{-1}$), so steady-state cooling is relatively slow compared with the acclimation phase. This property of water is extremely useful for the human body to avoid temperature swings in cold (or uncomfortably hot) environments.
- I. **Freezing of water**, occurring at ~0 °C but preceded by a sudden drop in temperature from about 4 °C. This might be explained by the fact that

water at 4 °C has the lowest density. As cooling continues below 4°C, the water molecules start forming a hexagonal lattice structure in preparation for freezing into ice. This hexagonal structure has more open space than the liquid structure, causing volume expansion as the rearrangement of molecules proceeds. Ice is known to have four times the thermal conductivity of water (~2.23 against ~0.6 W m⁻¹ K⁻¹) therefore, if the hexagonal lattice begins to appear between 4 and 0 °C, the heat loss from the manikin may be more like that of ice than that of water, resulting in a steeper segment of the cooling curve. In addition, it can be seen that most of the cooling curves stabilize at a temperature value of a few degrees below zero before suddenly shifting to ~0 °C and remaining constant from then on. This effect is described in the literature as the water going into a supercooled state, followed by an incubation period that ends with instantaneous nucleation and temperature adjustment to 0 °C (return to thermodynamic equilibrium) before ice crystal growth can occur⁵⁶. The phenomenon unfolds as follows: the water temperature is lowered until the thermodynamic driving force for the phase change is strong enough to allow the metastable hydrogen bonds to alternately form and break. This occurs at a temperature below zero, which remains constant as the energy removed from the water is used to power the process. After an incubation time, a cluster of critical size will form (Figure 4.4, "B", nucleation point) releasing latent heat at a rate greater than the rate of heat removal, bringing the system temperature to 0°C (restoring thermodynamic equilibrium) and allowing ice crystal growth to begin^{56,57}. During ice growth, the temperature will remain constant because the energy removed from the water is used to break the hydrogen bonds between the molecules and reorganize them into the more ordered structure of the ice. In no test was the manikin allowed to freeze completely, so the cooling curves ended with this horizontal segment. If freezing was completed, the temperature would begin to decrease again.

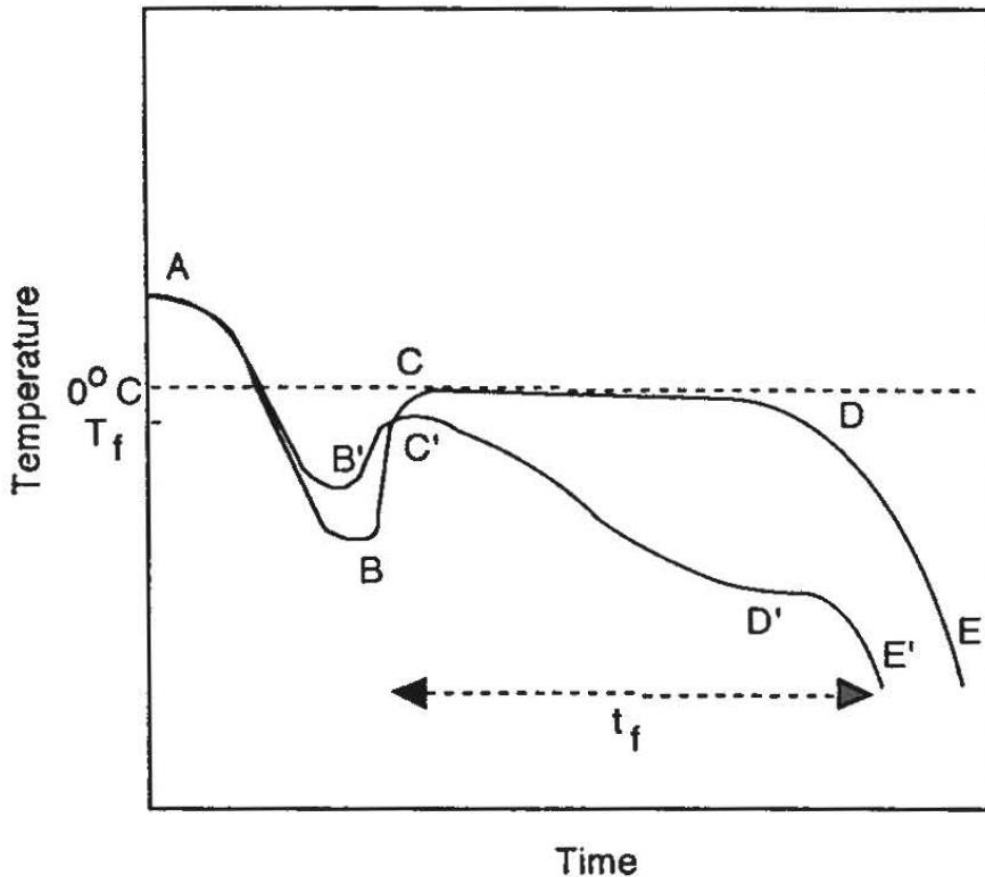


Figure 4.4 A temperature-time curve of water (ABCDE) and an aqueous solution, e.g., 20% sugar (A'B'C'D'E') during freezing. T_f represents the initial freezing point of the solution, and t_f represents the freezing time as determined by such an experiment⁵⁸.

4.2 Thermal insulation values

The EN ISO 20344 standard test is considered passed if the detected temperature change within 30 minutes is less than 10 °C. In the context of the present work, an initial manikin core temperature of (23 ± 2) °C, equal to the room temperature, was used instead of adhering to the standard of (33 ± 2) °C. However, the freezer temperature was set to (-40 ± 1) °C instead of following the guidelines of EN ISO 20344, which require an initial cold box temperature of (-17 ± 2) °C. Since heat transfer depends on the temperature gradient between two regions, i.e., the manikin's surface and the surrounding environment, the conditions of the experiment were reasonably coherent with the ones described in the international standard ($\Delta T_{in}(exp) = 63$ °C, $\Delta T_{in}(std) = 50$ °C), thus allowing similar "pass/fail" criteria to be adopted while also providing more detailed information on the precise level of thermal insulation at different points of the foot.

A simple but effective way to express the local thermal insulation values $I_{T,i}$ (Eq. 5)

obtained from manikin tests would be to use the time it takes for a sensor to detect a temperature drop of 10 °C from the start of the experiment ($t_{10,i}$, in seconds) and divide it by 1800 seconds (30 minutes), which, according to EN ISO 20344, is the minimum time that must elapse before the insole temperature sensor detects a temperature change of 10 °C for the test to be successful.

$$I_{T,i} = \frac{t_{10,i}}{1800} \quad (5)$$

This way, one could not only know which parts of the footwear satisfy the cold protection requirements given by the standard, but also quantitatively determine the goodness of thermal insulation in that specific region. The closer $I_{T,i}$ is to zero, the worse the thermal insulation provided in the corresponding area will be, because the cooling of that part of the foot will have been extremely rapid. Conversely, the more $I_{T,i}$ increases above 1, the better is the cold protection in that zone. A value close to 1 indicates that the thermal insulation would be just sufficient to meet the requirements of EN ISO 20344 standard, which, as mentioned earlier, the literature has revealed as relatively mild.

Table 4.1 highlights the thermal insulation values $I_{T,i}$ corresponding to each part of the foot across the various experimental conditions of the present work. These values underestimate the actual thermal resistance of each foot area because the temperature gradient used in the tests was 26% higher than that of the international standard method, resulting in faster cooling and lower $t_{10,i}$. Figure 4.5 also provides a visual representation of the same insulation values, clearly showing that the more layers of clothing are added to the foot, the higher the protection from the cold, even though no configuration tested was able to return all 15 values above 1.

Sensor n°	1	2	3	4	5	6	7	8	9	10	12	13	14	15	16
Bare (contact)	0.65	0.54	0.46	0.35	0.32	0.25	0.20	0.36	0.73	0.45	0.35	0.25	0.05	0.01	0.05
Bare (spaced)	0.77	0.68	0.57	0.52	0.52	0.44	0.22	0.34	0.78	0.48	0.52	0.37	0.12	0.37	0.26
Liner (contact)	0.99	0.83	0.74	0.59	0.47	0.43	0.41	0.62	1.06	0.69	0.55	0.36	0.12	0.09	0.13
Liner (spaced)	1.00	0.87	0.78	0.71	0.62	0.60	0.55	0.71	1.12	0.79	0.60	0.61	0.37	0.53	0.46
Liner + Sock (contact)	1.58	1.41	1.19	1.02	0.82	0.77	0.69	1.09	1.64	1.15	0.94	0.65	0.32	0.32	0.34
Liner + Sock (spaced)	1.57	1.48	1.33	1.13	1.07	0.99	0.90	1.22	1.65	1.25	1.11	1.00	0.65	0.83	0.79
Liner + Slipper	1.06	0.91	0.89	0.81	0.75	0.64	0.51	0.78	1.16	0.83	0.76	0.81	0.47	0.41	0.49

Table 4.1 Thermal insulation values for each sensor position across all tests. Dynamic background coloring highlights which are the highest (more saturated green) and lowest (more saturated red) values.

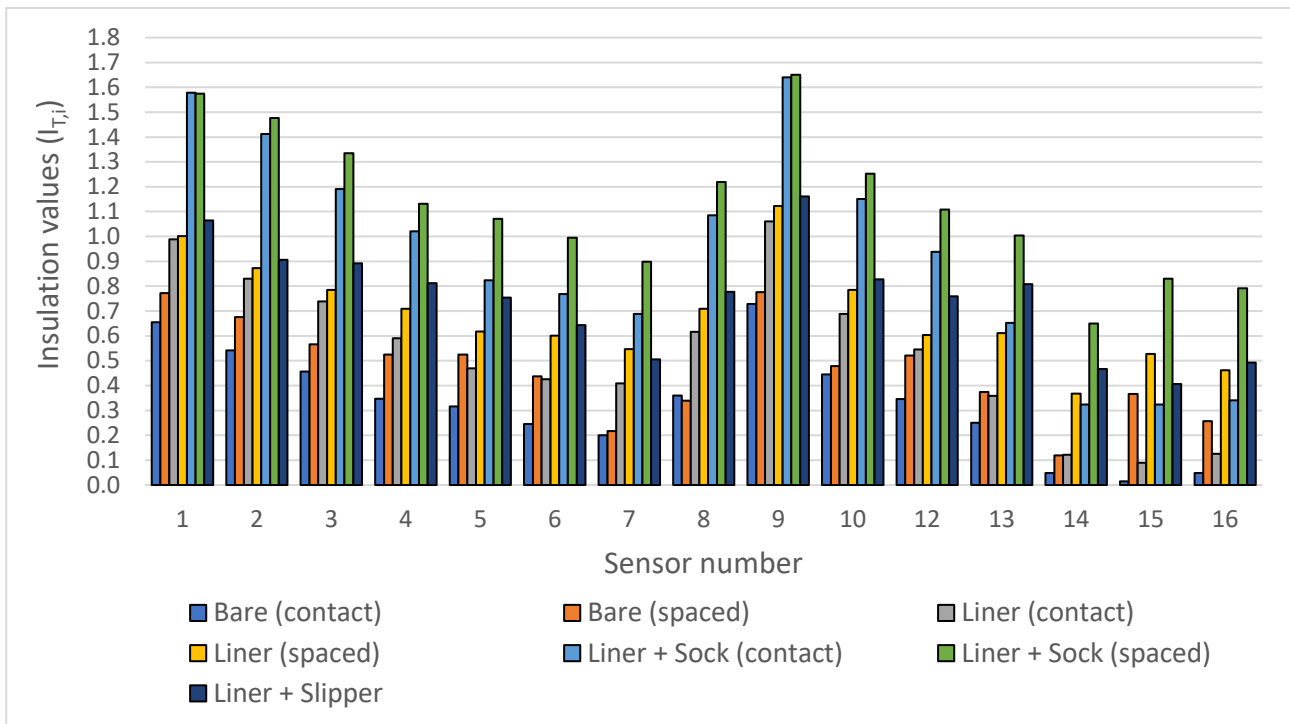


Figure 4.5 Thermal insulation values (visual representation).

It can be clearly deduced from the graph above that the parts of the foot most exposed to cold are the toes. Sensors n. 5-6-7 and n. 14-15-16, representing these areas, record the lowest insulation values in all tests. Sensor n. 13, located in the middle area of the foot sole, also shows high sensitivity to cold, and similar results would be expected from sensor n. 11 (lower heel), as the two devices are in close proximity to the source of cold, i.e., the freezer floor. Presumably for the same reason, sensors n. 14-15-16 (lower toes) show slightly lower insulation values than n. 5-6-7 (upper toes).

Of all the toes, the big toe appears to be the least able to retain heat (sensors n. 7 and n. 14). This is consistent with the results of previous studies that have found the big toe to be the quickest to cool and the most prone to cold injury^{16,31}. It is common practice among thermal comfort studies to monitor the temperature of the big toe and relate it to cold and pain sensations, as it is the first part of the foot to reach critical conditions in cold environments³⁴. An important factor explaining this effect is the fact that the big toe is generally isolated from the others, having a greater surface area exposed to cold and less blood flow. Although the manikin in the present work had all five toes fused together, the big toe was more pronounced than the others. It had more surface area exposed to its surroundings, which may explain why the model can simulate the behavior of a real human foot quite accurately.

4.3 Time-to-pain, Time-to-numbness and Steady-state cooling speed

Other relevant thermal parameters can be extracted from the temperature-time chart generated from manikin tests, such as:

- the time needed for specific foot areas to cool down to a certain temperature, namely the pain ($15\text{ }^{\circ}\text{C}^{55}$, TTP, "Time To Pain") and numbness ($7\text{ }^{\circ}\text{C}^{51}$, TTN, "Time To Numbness") thresholds;
- the foot areas with the highest steady-state cooling speed.

The former information would be definitely useful in drafting recommendations for use and specifying the maximum time allowed in the cold while wearing a given shoe. Of course, further studies are needed for establishing the correct correlations between the cooling time of the foot manikin and that of a human foot in a real cold environment. In addition, it should not be forgotten that the manikin only simulates dry heat loss and, because it does not have a gait simulator, does not consider the pumping effect produced during physical foot movement. These strong approximations would almost certainly lead to an overestimation of the heat insulation assessments and should be addressed in further studies.

On the other hand, knowing the steady-state cooling rate of each area of the foot would allow a better understanding of the cold-related pain sensation felt when the skin temperature drops below 15°C , providing insight into the areas most affected by rapid cooling and, therefore, acute thermal discomfort.

Figure 4.6 shows the time it takes for each sensor (excluding sensor n. 11) to detect a temperature below (a) $15\text{ }^{\circ}\text{C}$ and (b) $7\text{ }^{\circ}\text{C}$ from the time the manikin is placed in the freezer. Once again it is clear that the toes are the parts of the foot most affected by cold exposure, reaching the threshold of pain and numbness before any other area, with the big toe proving to be the most sensitive of all.

The TTN values seem to be more homogeneous than TTPs. This is especially true for the sensors located on the top of the foot (n. 3-4-5-6-7), which gradually approach values more similar to those measured by sensors n. 1-9 (leg).

Considering absolute values, the TTP chart suggests that wearing only a liner and a wool sock would allow a person stationary in extreme cold to tolerate it for about 9 minutes (without directly touching any cold surface and ignoring the effects of vasoregulation), after which the lower toe would begin to feel pain. After 36 minutes from the start, the big toe would go numb, and shortly thereafter the same fate would befall the other toes. Of course, these remain entirely rough and inaccurate estimates and are intended for illustrative purposes only.

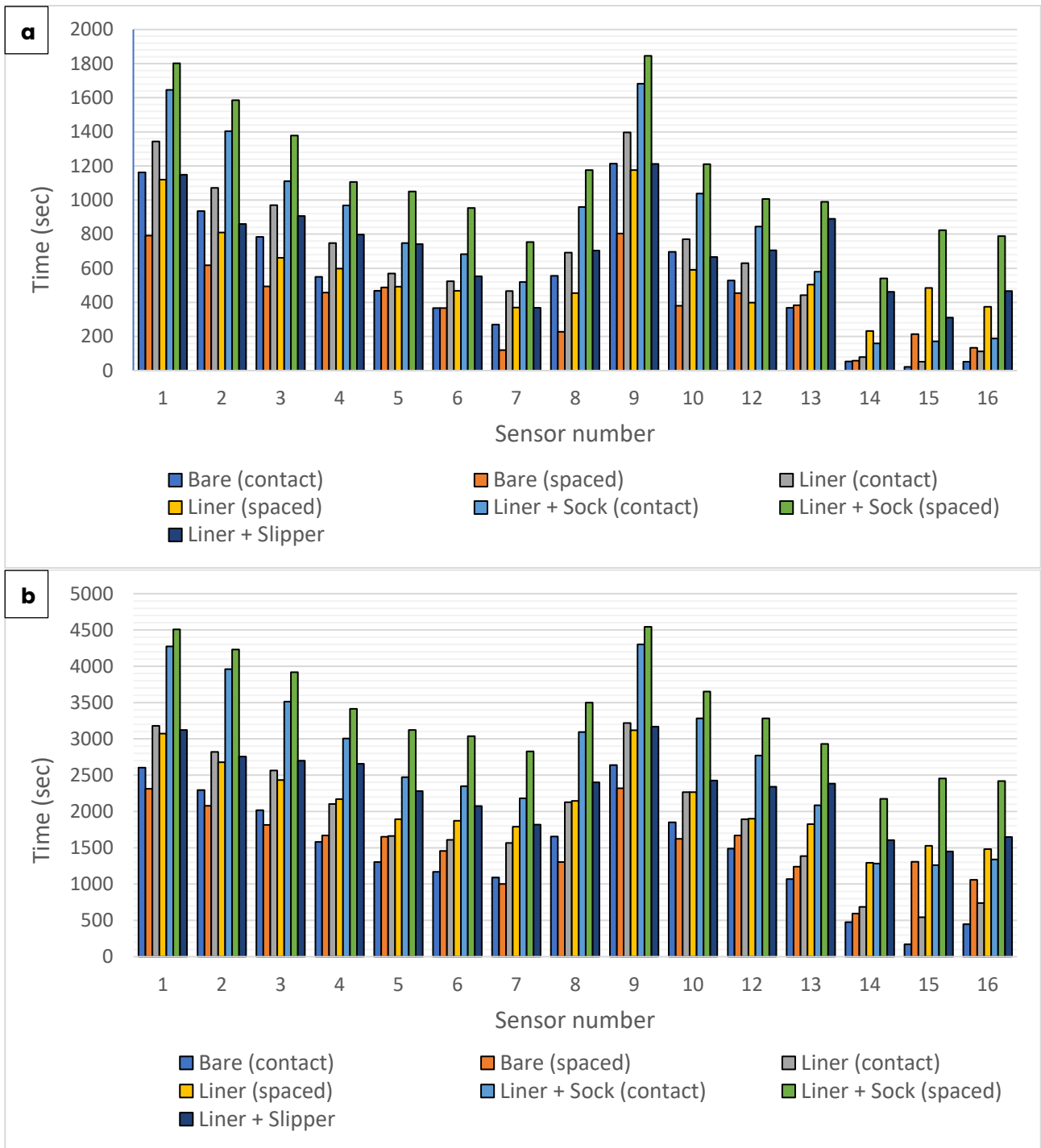


Figure 4.6 Time-to-pain (a) and Time-to-numbness (b) for each sensor position across all tests.

Figure 4.7 shows the computed “steady-state cooling rate” (when the heat transfer rate between the shell and the environment becomes constant) of every functioning sensor across all the tests. On the y-axis is the cooling rate and on the x-axis is the sensor number. Cooling rates were calculated by linearly interpolating the temperature-time curves in their steady-state cooling segment,

extracting the derivative from the slope of the function and considering only its absolute value.

The results indicate that the sensors on the top and bottom of the toes experienced the highest cooling rates, although they are probably still underestimated for the "contact" conditions, since in these cases the temperature followed an exponential decay, and the steady-state region was fuzzy or absent. Comparing the "contact" tests with the "spaced" tests with the same footwear configuration, it is evident that the sensors on the foot sole area experienced faster cooling in the former conditions, again confirming previous results and demonstrating that the manikin is able to discriminate between different levels of cold protection in different parts of the foot.

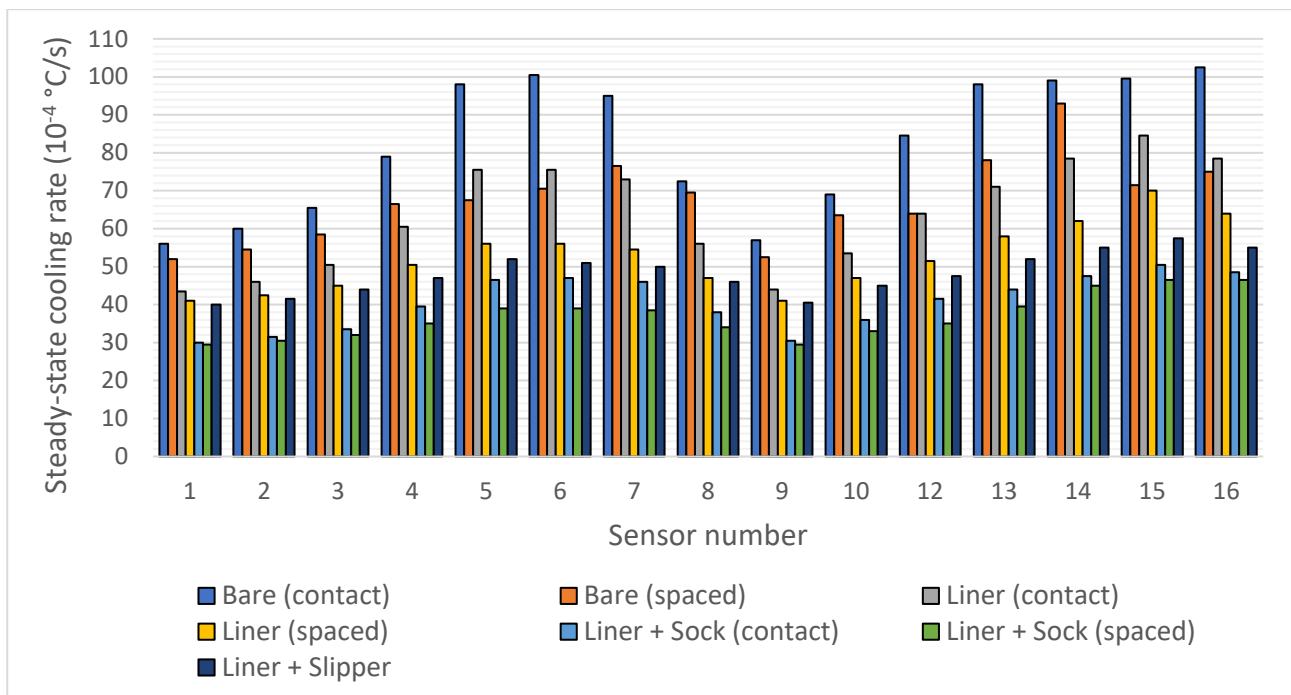


Figure 4.7 Steady-state cooling rates for each sensor position across all tests.

Lastly, having found that the toes are the most sensitive parts of the foot to cold exposure, with the big toe being the most critical among all, it was decided to superimpose all the cooling curves for sensors n. 7 (upper big toe) and n. 14 (lower big toe) to evaluate the differences in their trends. From Figure 4.8a, it can be seen that after the acclimation phase, the upper toe generally stabilizes its rate of heat loss, while the lower toe (Figure 4.8b) never does, with the exception of the spaced "Liner + Sock" configuration. The cooling trends of the lower toe are simply exponential, indicating that this part is even more sensitive to cold than the upper one. The reason for this is that the sole of the foot is generally in indirect contact with cold surfaces, so although the shoe sole (or wooden spacers, for that matter)

provide some thermal insulation, it still suffers most from exposure to cold. Another key difference between Figures 4.8a and 4.8b is found in the 0-4 °C range. The upper toe seems to be affected by the rearrangement of water molecules that precedes freezing, signaled by the sudden drop in temperature around 4 °C, while the lower toe does not show the same trend. This could be related to the fact that the lower toe cools down faster, thus not giving time for water molecules to reorganize into the hexagonal lattice structure typical of ice. The temperature of ~ 0 °C is then reached gradually, with no sudden changes, allowing molecule restructuring (freezing) to begin at that point. Ultimately, it is worth noting that when the lower toe is protected from direct contact with cold surfaces by the slipper, its steady-state cooling rate is more aligned with that of the upper toe than any other test condition.

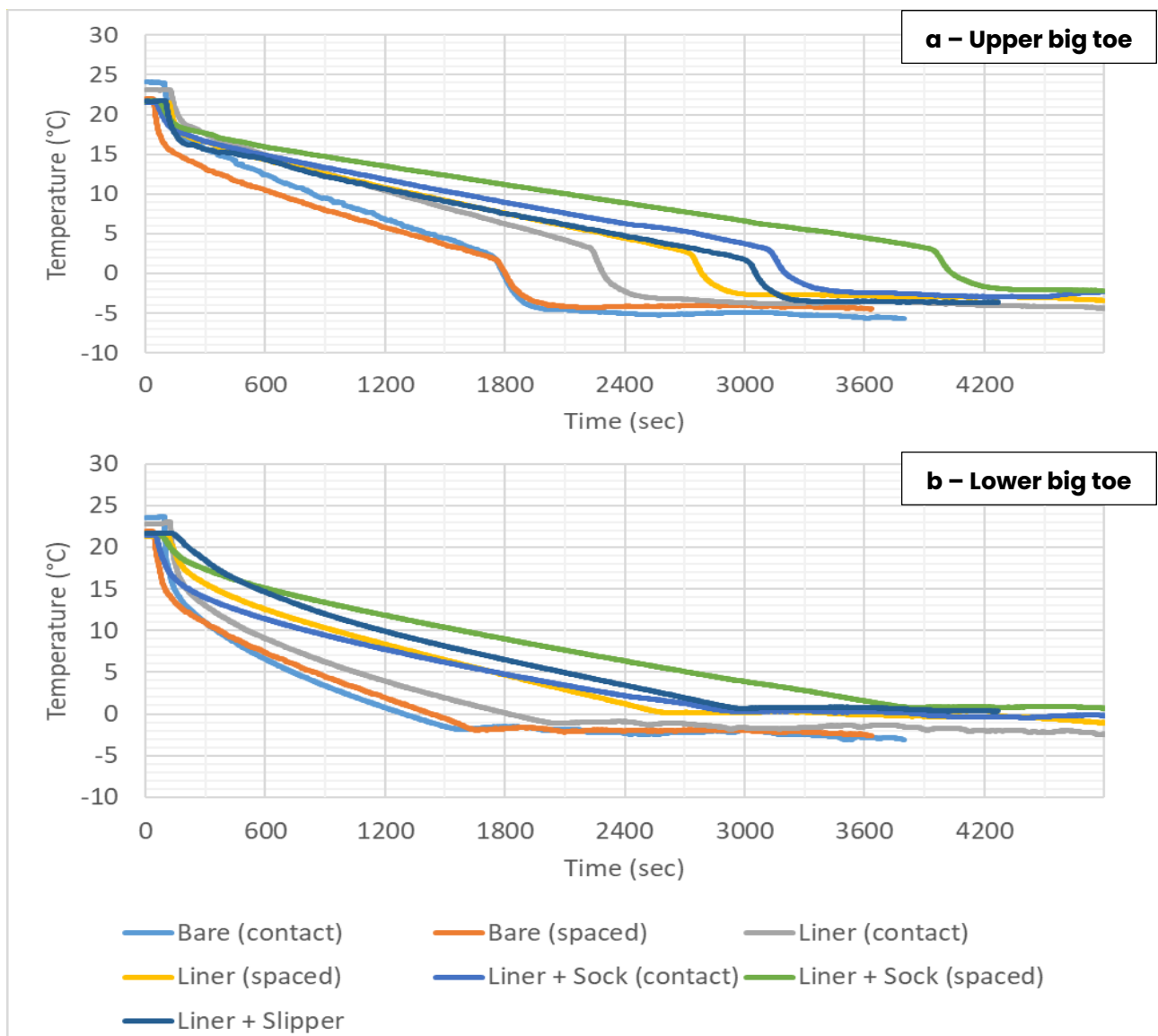


Figure 4.8 Temperature-time graphs of sensors n. 7 (a, upper big toe) and n. 14 (b, lower big toe) for each configuration tested.

4.4 Personal experience and Future developments

Developing a 3D-printed thermal foot manikin system has proven to be a complex process, involving tasks of different nature and requiring a variety of engineering skills and knowledge in material science, additive manufacturing, CAD modeling, electronics systems and software programming. Despite the difficulties encountered during this process, the present work has shown that making a thermal manikin according to this approach is within the reach of any research laboratory specializing in the study of thermal comfort. As mentioned above, this model can already have an impact on the way thermal insulation of footwear is currently evaluated. It can help make more precise usage recommendations, supporting both manufacturers and end users in making and choosing the correct shoes for specific weather conditions.

Compared to EN ISO 20344 current standard method for footwear cold protection, manikin tests provide more detailed and diverse information. The results can be easily linked to measurements on human subjects and correlations with thermal sensations can be established. As some scholars have suggested¹⁶, manikin tests should replace the current standard for footwear, but more comparative tests using different models and sweat simulation techniques are needed to standardize the method.

This 3D-printed manikin could have a potential advantage, compared to existing thermal foot models²¹, thanks to its passive heating nature and the continuous cooling testing. Kalev Kuklane¹⁶ claims, in fact, that “the insulation values from thermal foot measurements [at constant temperature and with power modulation] are well correlated with the insulation measurements on human subjects”, but “if the demand for total and local thermal comfort is not followed, then an uncertain factor influences the results showing higher insulation measured on human subjects than on thermal model”. This implies that testing footwear in cold environments could lead to great inaccuracies, if done with the classic approach of keeping the manikin at constant temperature with power modulation. Although the present work shows no conclusive evidence of this error not affecting the 3D-printed manikin, one must remember that feet in cold suffer from significant vasoconstriction, which severely limits blood flow and thus heat supply. Consequently, as long as the tests are static, the manikin of the present work might behave more like a human foot in a cold environment than the state-of-the-art actively heated, power-controlled thermal foot models.

A final benefit to note is that additive manufacturing enables rapid and inexpensive prototyping, improving the replicability and reproducibility of tests in

any laboratory with the appropriate equipment. For the same amount of time spent, a larger number of versions of a manikin can be made with 3D printing, achieving improvements faster and for less money.

However, many aspects of the manikin have to be refined if one aims to use it for these purposes. Defects found in the first version of the system and how they can be avoided if one were to take the project back in hand and build a second version will now be discussed in detail.

First, the manikin's most obvious and impactful flaw is its current shape, which makes it impossible to fit into any closed shoe. The forefoot design, in particular, did not take into account the compression that a real foot undergoes when inserted into a shoe, significantly reducing its volume, an effect that cannot be reproduced by the manikin's rigid polyamide shell. Personal experience has suggested that the only way the current model can fit into a size 42.5 EU shoe is to make a custom-made sample shoe with an enlarged forefoot, but this route is unnecessarily laborious and expensive. Therefore, it seems inevitable to return to the modeling stage and modify the 3D shape of the foot so that it can fit the shoe in which it is inserted.

Although this redesign would allow the manikin to ideally fit any shoe, there would still remain a problem related to insertion: when a person wants to put on a shoe, he or she usually rotates the ankle so as to extend the foot, and upon entering the shoe, the ankle rotates in the opposite direction until it returns to the starting position. This action cannot be reproduced by the current version of the model; in fact, attempts at insertion have shown that the sides of the shoe tab need to be peeled back to accommodate the manikin, which is unable to flex and extend. This would also be an unnecessary waste of time and resources, as the shoe would be ruined and test preparation would take longer than necessary, not to mention that the tongue would have to be taped to the rest of the shoe to restore its original properties, e.g., waterproofing or the special thermal insulation of some types of boots, potentially interfering with correct measurements.

One possible solution would be to slice the shell model at ankle level with a 30–40° inclined plane, printing two separate parts instead of one and joining them only when the first one is already inserted into the shoe. Of course, many questions would arise, such as: how is the waterproofing of the shell preserved? Should the water inside the two parts communicate through a hole? Or should the two compartments be watertight with respect to each other? And how would these changes affect the cooling of different parts of the foot? Future studies should try to answer these questions to choose the best solution for the "fit problem."

Another thing to be checked in the next version of the foot manikin will be to

provide the sensors with better protection against fast temperature changes, which were probably the cause of the failure of sensor n. 11 (lower heel). Being in direct contact with the freezer floor in the first test, the device may have been disconnected from the system due to thermal contraction of the wires and subsequent breakage at the soldering point.

4.4.1 Tests for manikin-foot comparison

Human testing for a direct comparison between the real and surrogate foot was one of the goals that was not achieved during this work. Future studies will need to address whether the behavior of the manikin in cold environments is similar to that of a human foot and, if not, what the differences are and to what extent they affect the cooling of different parts of the model.

For this purpose, a sensorized sock is already under development. To facilitate comparison and make the results as relevant as possible, the sock system aims to look (and function) identical to that of the manikin: 16 temperature sensors embedded in the fabric of the sock, connected to two switches and placed at approximately the same locations as the surrogate model, would monitor the cooling of the human foot in real time. Ideally, the thermal foot manikin and the person wearing the sensorized sock should be tested simultaneously, so that data can all be collected and analyzed together by the same program, while also avoiding large changes in environmental conditions between tests. The initial water temperature inside the manikin shell is a parameter that should be discussed in future studies and probably refined in a trial-and-error approach until the best match is found with the cooling of a human foot.

Figure 4.9 shows the model of the box that will house the two switches connected to the sensors on one side and the interface device on the other. This box should be strapped to the thigh of the person wearing the sensorized sock, so as to contain the length of the wires and preserve the integrity of the data. The curved shape of the box was modeled following the curvature of the author's thigh to achieve the best possible fit, and the back is hollowed out to make room for a belt. A prototype has already been 3D-printed and is ready to be used.

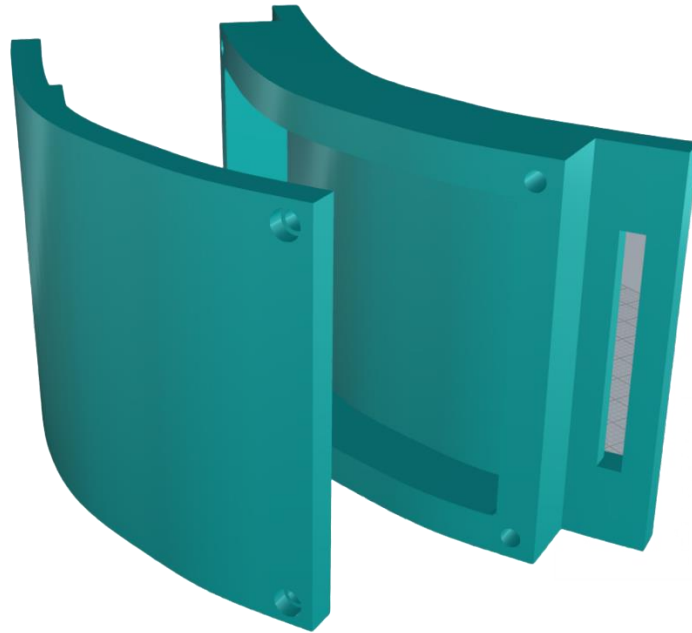


Figure 4.9 Board box model made in Rhino 3D.

4.4.2 Water recirculation and Active heaters

During the discussion, much emphasis was placed on the fact that the manikin was passively heated, thus unable to maintain its temperature in a cold environment. This led to the development of a test procedure that involved continuous cooling of the foot and subsequent analysis of the temperature-time curve of each sensor.

One potential improvement that could completely change how this system works is the addition of an active heat source to the manikin. This would allow the system to undergo constant temperature testing, in which the energy provided to maintain thermal equilibrium would be an indicator of the thermal insulation provided to the foot. The manikin would then behave more like existing thermal foot models, but with the advantage of being easily and economically reproducible through additive manufacturing.

Two possibilities for active heating were discussed. The first, based on what is already used in existing manikins, is electric heaters. They can be easily and finely controlled and would eliminate the need for filling the shell with water, but they are expensive and must be adequately protected from direct contact with cold or humid surfaces. In addition, a polyamide manikin would probably not be suitable, as polymers have low thermal conductivity. To avoid temperature inhomogeneity, the shell would have to be made of metal, exponentially increasing the cost of additive manufacturing.

The second option would be to integrate a water recirculation system inside the existing manikin shell, with a hot water source providing heat to the foot and a cold sink collecting the cooled water leaving the foot after losing heat to the environment through the shell. By knowing the water flow rate and measuring the temperature difference between the hot source and the cold sink, one could calculate the heat loss and relate it to the thermal insulation provided by the footwear "worn" by the dummy. Of course, such a system requires that the hot source and cold sink be well insulated to avoid unwanted heat loss and some preliminary tests to estimate the heat loss from the barefoot manikin (to be subtracted from the heat loss calculated in the following footwear tests). Compared with electric heaters, the water recirculation approach would certainly be more labor intensive and give less accurate results, but overall, it would help to keep system costs down tremendously.

Conclusions

A passively heated foot manikin has been developed with the aim of determining thermal insulation of footwear. After an initial design and modeling phase, the manikin's polyamide shell was 3D-printed with SLS technology, cleaned from inside dust particles, and 16 holes were drilled to accommodate the temperature sensors. Through the use of two analog switches, signals from the sensors were channeled to an interface device and then sent to the laptop where a LabVIEW program was running. Freezer tests were performed at (-40 ± 1) °C and cooling curves from 15 out of the 16 sensors were analyzed, since sensor n. 11 (lower heel) stopped working during the first measurements.

Results show that toes are the part of the foot most affected by cold exposure, with the big toe being the most sensitive of all. Although the manikin had all toes "fused" together, this result is coherent with findings from human studies that indicate the big toe as the most critical part of the foot in cold environments³⁴. This suggests that the big toe temperature should be considered as the limiting factor for thermal comfort in future standard methods. Moreover, if lower and upper toe temperatures are compared, the first is usually cooler than the latter.

An innovative approach to thermal insulation values was discussed, making use of the cooling time to a temperature 10 °C lower than the starting temperature and comparing it with that imposed by the standard EN ISO 20344 test methodology. Following this route could provide manufacturers with useful information on the cold protection at different points of the shoe to improve the thermal properties of their products. In addition, by knowing the time it takes for a part of the foot to reach the threshold temperatures for pain and numbness, recommendations for use and maximum allowable time in the cold could be accurately formulated and final users could be directly informed.

The present work was not error-free. Large approximations have been made from the beginning, including simplification of the model shape, neglect of sweat influence on insulation and completely passive heating (not considering any heat supply from blood circulation). Additionally, unforeseen events occurred, such as the failure of sensor n. 11 and the impossible fitting of the foot manikin inside any close shoe. This means that the project has wide room for improvement, and future studies can pick up where this one left off to continue the work.

References

1. Havenith, G. Interaction of clothing and thermoregulation. *Exogenous Dermatology* vol. 1 (2002).
2. Havenith, G. Heat balance when wearing protective clothing. in *Annals of Occupational Hygiene* vol. 43 (1999).
3. Parsons, K. C. Human thermal environments. in *Human Thermal Environments* (2010). doi:10.4324/9780203302620_chapter_1.
4. Laskowski, M. B. Fundamentals of neurophysiology, 2nd edition. By Robert F. Schmidt, 339 pp, illus, Sprznger-Verlag, New York, NY, 1978. \$14.80. *Muscle Nerve* **3**, (1980).
5. Enander, A. E. Effects of thermal stress on human performance. *Scand. J. Work. Environ. Heal.* **15**, (1989).
6. Vincent, M. J. & Tipton, M. J. The effects of cold immersion and hand protection on grip strength. *Aviat. Sp. Environ. Med.* **59**, (1988).
7. Enander, A. Performance and sensory aspects of work in cold environments: A review. *Ergonomics* **27**, (1984).
8. McIntyre, D. A., Griffiths, I. D. & Griffiths, I. D. The Effects of Added Clothing on Warmth and Comfort in Cool Conditions. *Ergonomics* **18**, (1975).
9. Williamson, D. K., Chrenko, F. A. & Hamley, E. J. A study of exposure to cold in cold stores. *Appl. Ergon.* **15**, (1984).
10. Holmér, I. TLV in cold environments. *J. Therm. Biol.* **18**, (1993).
11. Howaan, E. & Oakley, N. The design and function of military footwear: A review following experiences in the south atlantic. *Ergonomics* **27**, (1984).
12. LOVE, L. H. Heat loss and blood flow of the feet under hot and cold conditions. *J. Appl. Physiol.* **1**, (1948).
13. Endrusick, T. L., Santee, W. R., DiRaimo, D. A., Blanchard, L. A. & Gonzalez, R. R. Physiological responses while wearing protective footwear in a cold-wet environment. in *ASTM Special Technical Publication* (1992). doi:10.1520/stp19186s.
14. Enander, A., Ljungberg, A. & Holmer, I. Effects of work in cold stores on man. *Scand. J. Work. Environ. Heal.* **5**, (1979).
15. Luczak, H. Work under extreme conditions. *Ergonomics* **34**, (1991).
16. Kuklane, K. Footwear for cold environments - thermal properties, performance and testing. *Div. Ind. Ergon.* (1999).
17. McCaig, R. H. & Gooderson, C. Y. Ergonomic and physiological aspects of military operations in a cold wet climate. *Ergonomics* **29**, (1986).

18. Harirchi, I., Arvin, A., Vash, J. H. & Zafarmand, V. Frostbite: Incidence and predisposing factors in mountaineers. *Br. J. Sports Med.* **39**, (2005).
19. Bergquist, K. & Abeysekera, J. Ergonomic aspects of safety shoes worn in the cold climate. in *3rd Pan-Pacific Conference on Occupational Ergonomics* (1994).
20. Bergquist, K. & Holmér, I. A method for dynamic measurement of the resistance to dry heat exchange by footwear. *Appl. Ergon.* **28**, (1997).
21. Lu, Y., Kuklane, K. & Gao, C. Types of thermal manikin. in *Manikins for Textile Evaluation* (2017). doi:10.1016/B978-0-08-100909-3.00002-9.
22. Che, H., Nigg, B. M. & de Koning, J. Relationship between plantar pressure distribution under the foot and insole comfort. *Clin. Biomech.* **9**, (1994).
23. Au, E. Y. L. & Goonetilleke, R. S. A qualitative study on the comfort and fit of ladies' dress shoes. *Appl. Ergon.* **38**, (2007).
24. González, J. ., Alcantara, E., Bataller, A. & Garcia, A. . Physiological and Subjective Evaluation of Footwear Thermal Response Over Time. in *Proceedings of the 5th Symposium on Footwear Biomechanics* (2001).
25. Luximon, A. & Luximon, Y. Shoe-last design innovation for better shoe fitting. *Comput. Ind.* **60**, (2009).
26. Koptyug, A. & Bäckström, M. Body Part Surrogates for Medicine, Comfort and Safety Applications. in *Advances in 3D Printing* (2023). doi:10.5772/intechopen.110119.
27. Arezes, P. M., Neves, M. M., Teixeira, S. F., Leão, C. P. & Cunha, J. L. Testing thermal comfort of trekking boots: An objective and subjective evaluation. *Appl. Ergon.* **44**, (2013).
28. Holmér, I. Thermal manikin history and applications. *Eur. J. Appl. Physiol.* **92**, (2004).
29. Melikov, A. Breathing thermal manikins for indoor environment assessment: Important characteristics and requirements. *Eur. J. Appl. Physiol.* **92**, (2004).
30. Babič, M., Lenarčič, J., Žlajpah, L., Taylor, N. A. S. & Mekjavić, I. B. A device for simulating the thermoregulatory responses of the foot: Estimation of footwear insulation and evaporative resistance. *Stroj. Vestnik/Journal Mech. Eng.* **54**, (2008).
31. Kuklane, K. & Kaced, Y. Footwear for cold weather conditions. in *Handbook of Footwear Design and Manufacture* (2021). doi:10.1016/b978-0-12-821606-4.00003-x.
32. Kuklane, K., Afanasieva, R., Burmistrova, O., Bessonova, N. & Holmér, I. Determination of heat loss from the feet and insulation of the footwear. *Int. J. Occup. Saf. Ergon.* **5**, (1999).
33. Ducharme, M. B. & Brooks, C. J. The effect of wave motion on dry suit

- insulation and the responses to cold water immersion. *Aviat. Sp. Environ. Med.* **69**, (1998).
34. Kuklane, K. The use of footwear insulation values measured on a thermal foot model. *Int. J. Occup. Saf. Ergon.* **10**, (2004).
 35. Kuklane, K., Geng, Q. & Holmér, I. Effect of footwear insulation on thermal responses in the cold. *Int. J. Occup. Saf. Ergon.* **4**, (1998).
 36. Geng, Q. Hand Cooling, Protection and Performance in Cold Environment. *Dr. Thesis, Lulea Univ. Technol.* (2001).
 37. Tochihara, Y., Ohnaka, T., Tuzuki, K. & Nagai, Y. Effects of repeated exposures to severely cold environments on thermal responses of humans. *Ergonomics* **38**, (1995).
 38. Wang, Y., Mu, L. & He, Y. Thermogram-based estimation of foot arterial blood flow using neural networks. *Appl. Math. Mech. (English Ed.)* **44**, (2023).
 39. Wang, Y. P., Cheng, R. H., He, Y. & Mu, L. Z. Thermal Analysis of Blood Flow Alterations in Human Hand and Foot Based on Vascular-Porous Media Model. *Front. Bioeng. Biotechnol.* **9**, (2022).
 40. Sudha, B. G., Umadevi, V. & Shivaram, J. M. Thermal image acquisition and segmentation of human foot. in *2017 4th International Conference on Signal Processing and Integrated Networks, SPIN 2017* (2017). doi:10.1109/SPIN.2017.8049920.
 41. Bougrine, A., Harba, R., Canals, R., Ledee, R. & Jabloun, M. On the segmentation of plantar foot thermal images with deep learning. in *European Signal Processing Conference vols 2019-September* (2019).
 42. Zolet, C. M. L. S., Ulbricht, L., Romaneli, E. F. R. & Neves, E. B. Thermal Asymmetries and Mean Foot Temperature. in *Proceedings of the Annual International Conference of the IEEE Engineering in Medicine and Biology Society, EMBS* (2019). doi:10.1109/EMBC.2019.8857378.
 43. PENNES, H. H. Analysis of tissue and arterial blood temperatures in the resting human forearm. *J. Appl. Physiol.* **1**, (1948).
 44. Copetti, M. I. M., Durany, J., Fernández, J. R. & Poceiro, L. Numerical analysis and simulation of a bio-thermal model for the human foot. *Appl. Math. Comput.* **305**, (2017).
 45. Mekjavic, I. B., Korosec, B. A., Tomsic, M. & Golja, P. Phase Change Material in Hiking Boots Does Not Minimise the Risk of Cold Injury. in *Prevention of Cold Injuries. RTO-MP-HFM-126* (2005).
 46. Bogerd, C. P., Brühwiler, P. A. & Rossi, R. M. Heat loss and moisture retention variations of boot membranes and sock fabrics: A foot manikin study. *Int. J. Ind. Ergon.* **42**, (2012).
 47. Lella's foot from Thingiverse. <https://www.thingiverse.com/thing:4938904>.

48. Nike EU Size. https://img.nike.com.hk/resources/sizcart/mens-shoe-sizing-chart_en.html.
49. AIM Sweden. <https://aimsweden.com/>.
50. Human Studio. <https://human.biodigital.com/>.
51. Kuklane, K. *et al.* Interlaboratory tests on thermal foot models. *Therm. Environ. Lab. EAT Rep.* (2003).
52. Proceedings of the International Conference on Environmental Ergonomics. in *International Conference on Environmental Ergonomics* 617 (2009).
53. Leens, F. An introduction to I2C and SPI protocols. *IEEE Instrumentation and Measurement Magazine* vol. 12 (2009).
54. Sensirion STS40 Specifications. <https://sensirion.com/products/catalog/STS40-DIS/>.
55. Kuklane, K. Protection of feet in cold exposure. *Industrial Health* vol. 47 (2009).
56. Sahagian, M. E. & Goff, H. D. Fundamental Aspects of the Freezing Process. in *Freezing Effects on Food Quality* (2019). doi:10.1201/9780203755495-1.
57. Auerbach, D. Supercooling and the Mpemba effect: When hot water freezes quicker than cold. *Am. J. Phys.* **63**, (1995).
58. Feuillebois, F., Lasek, A., Creisméas, P., Pigeonneau, F. & Szaniawski, A. Freezing of a subcooled liquid droplet. *J. Colloid Interface Sci.* **169**, (1995).